Structural Characterization of Adsorbed Helical and Beta-Sheet Peptides

Newton Thangadurai Samuel

A dissertation submitted in partial fulfillment of the
requirements for the degree of

Doctor of Philosophy

University of Washington

2005

Program Authorized to Offer Degree: Department of Chemical Engineering

University of Washington
Graduate School

This is to certify that I have examined this copy of a doctoral dissertation by

Newton Thangadurai Samuel

and have found that it is complete and satisfactory in all respects,
and that any and all revisions required by the final
examining committee have been made.

Chair of Supervisory Committee:

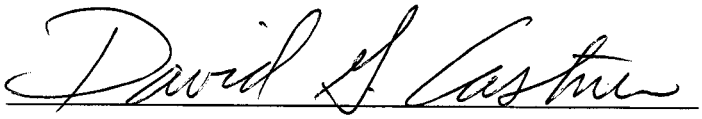

David G. Castner

Reading Committee:

David G. Castner

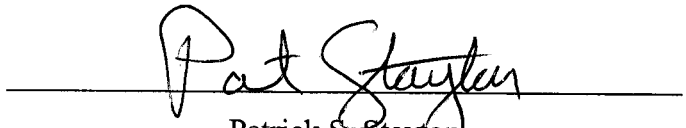

Patrick S. Stayton

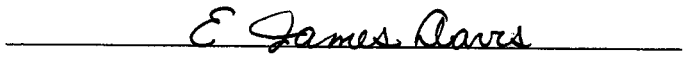

E. James Davis

Date: Aug 8, 2005

In presenting this dissertation in partial fulfillment of the requirements for the doctoral degree at the University of Washington, I agree that the Library shall make its copies freely available for inspection. I further agree that extensive copying of the dissertation is allowable only for scholarly purposes, consistent with "fair use" as prescribed in the U.S. Copyright Law. Requests for copying or reproduction of this dissertation may be referred to Proquest Information and Learning, 300 North Zeeb Road, Ann Arbor, MI 48106-1346, to whom the author has granted "the right to reproduce and sell (a) copies of the manuscript in microform and/or (b) printed copies of the manuscript made from microform."

Signature T. Neal Samuel

Date Aug. 10, 2005

University of Washington

Abstract

Structural Characterization of Adsorbed Helical and Beta-Sheet Peptides

Newton Samuel

Chair of the Supervisory Committee:
Professor David G. Castner
Department of Chemical Engineering

Adsorbed peptides on surfaces have potential applications in the fields of biomaterials, tissue engineering, peptide microarrays and nanobiotechnology. The surface region, the "biomolecular interface" between a material and the biological environment, plays a crucial role in these applications. As a result, characterization of adsorbed peptide structure, especially with respect to identity, concentration, spatial distribution, conformation and orientation, is important. The present research employs NEXAFS (near-edge X-ray absorption fine structure spectroscopy) and SFG (sum frequency generation spectroscopy) to provide information about the adsorbed peptide structure. Soft X-ray NEXAFS is a synchrotron-based technique which typically utilizes polarized X-rays to interrogate surfaces under ultra-high vacuum conditions. SFG is a non-linear optical technique which utilizes a combination of a fixed visible and a tunable infrared laser beams to generate a surface-vibrational spectrum of surface species. SFG has the added advantage of being able to directly analyze the surface-structure at the solid-liquid interface.

The main goals of the present research were twofold: characterize the structure of adsorbed peptides (1) *ex situ* using soft X-ray NEXAFS, and (2) *in situ* using non-linear

laser spectroscopy (SFG). Achieving the former goal involved first developing a comprehensive characterization of the carbon, nitrogen and oxygen *k*-edge NEXAFS spectra for amino acids, and then using a series of helical and β-sheet peptides to demonstrate the sensitivity of polarization-dependent NEXAFS to secondary structure of adsorbed peptides. Characterizing the structure of adsorbed peptides *in situ* using SFG involved developing a model system to probe the solid-liquid interface *in situ*; demonstrating the ability to probe the molecular interactions and adsorbed secondary structure; following the time-dependent ordering of the adsorbed peptides; and establishing the ability to obtain high-resolution peptide-surface interactions *in situ*. The results from the present research establish SFG and NEXAFS as powerful techniques for chemical and structural characterization of surfaces and biomolecules immobilized onto those surfaces.

TABLE OF CONTENTS

LIST OF FIGURES

LIST OF TABLES

ACKNOWLEDGEMENTS

This project represents the collective effort of several people – both direct and indirect. I personally thank all of you for your assistance, enthusiasm and friendship.

First and foremost, I am grateful for my advisor, Prof. Dave Castner, for all his support, and being a wonderful mentor during the last five years. I always felt recharged and motivated, whenever I got a chance to talk with him about my research.

I would like to thank my committee members – Dr. Buddy Ratner, Dr. James Davis, Dr. Patrick Stayton and Dr. James Hermanson, for their time and valuable guidance; especially, Dr. Davis and Dr. Hermanson, for kindly agreeing to be my committee members during the last stages of my Ph.D.

I have had the wonderful opportunity to know several people in the NESAC/BIO group over the last five years; particularly, I would like to thank my initial mentors – Dr. Sally McArthur, Dr. Matt Wagner and Dr. Lara Gamble, for their patience and getting me up-to-speed during the initial years. They also set high standards to emulate and for being wonderful people. Dr. Daniel Fischer, Dr. Zugen Fu, Winston Ciridon, Dr. Daniel Graham, Dr. Heather Canavan, Dr. Roger Michel, Dr. Stephanie Bryant, Lizzy Mayorga, Chi-Ying Lee, Jim Hull, Deborah Leech-Scampavia, Dr. Esmaeel Naeemi, Glenda Deatherage, Jason Hwang, and other Castner and Ratner group members, are gratefully acknowledged for their assistance and friendship. Mady Lund is personally thanked for all her excellent administrative support during the last five years.

Dr. Keith McCrea is personally thanked for giving the opportunity to work with him. I am always amazed by his insatiable enthusiasm and creativity. I will certainly treasure the experience to collaborate and learn from him.

Members in Dr. Stayton and Dr. Drobny group especially, Dr. Riki Goobes, Dr. Gill Goobes, Vinodh Raghunathan, Liz Louie and Jennifer Popham, are thanked for their help with the peptide synthesis, collaborations and being great people to work.

All the staff members in the Chemical Engineering department are personally thanked for their excellent support, and making it a pleasure to work in the department.

All the members of our gang (Ani, Ajay, Niranjan, Sudhip, Kundan, Sunil, Sam, Dinesh, Pat, Vasanth, and Gaurav) are gratefully thanked for making my stay in Seattle enjoyable and fun. Gary and his family are thanked for their friendship and support during the last five years.

I would like to thank Brookhaven National lab for giving me access to the U7-A beamline. In addition, Polymer Technology Group, Berkeley, for granting access and support to use their Sum Frequency Generation experimental setup.

I would like to thank all the funding sources for the opportunity to conduct research. The research was supported generously by the following grants: NESAC/BIO (NIH Grant EB-002027), NSF Grant DMR-0110505 and NIH Grant EB-001473.

Finally, I would like to thank my parents for their never-ending love and support; and my brother's family, for their inspiration, wisdom and kind support.

DEDICATION

To my family and all the wonderful teachers in my life

1 : INTRODUCTION

1.1 General and Motivation

Significant research has been devoted towards reducing the foreign body response for implant devices[1-3]. The primary methodology adopted towards countering the above ubiquitous problem has been to control the initial protein adsorption onto these devices. Various approaches such as non-fouling surfaces and bio-functionalized surfaces have been investigated to mitigate the above problem. Similarly, in the area of bio-diagnostics the challenge is to use immobilized probe molecules to uniquely sense an analyte present in a complex biological milieu[4]. Usually the analyte interaction with the probe molecules is mediated by specific interactions such as hydrophobic, shape of the molecule, hydrogen bonding, electrostatic, etc.

The surface region mediates the above diverse events and underscores the importance of biomolecules at interfaces. Hence, characterization of biomolecules on surfaces is important in a wide range of applications such as medical devices, diagnostics, tissue engineering and biomimetic materials. The important questions to be addressed are the: identity, concentration, spatial distribution, conformation and orientation of surface bound biomolecules. To understand the above complex interactions it is essential to develop appropriate model systems which are easier to interpret and more tractable to study.

Realizing the importance of characterizing and manipulating biomolecules on surfaces, the new concept of "biological surface science" was proposed[5,6]. The fundamental premise is that the surface region mediates the different diverse biological interactions. By specifically controlling the surface region, subsequent events might be controlled. For example, by specifically controlling the biomolecule attachment to the surface, subsequent downstream events such as the interaction of the surface with other cells/proteins can be controlled. Numerous examples of engineering complex surfaces are present in the literature[7-18]. However, to characterize these complex engineered surfaces requires the development of specialized tools. For example, an approach to

develop non-fouling surfaces requires the use of tools to detect low amounts (often in the pico-mole range) of adsorbed protein.

Good model systems are important for characterizing complex biomolecules. Hence the importance of characterizing simple systems such as amino acids, nucleic acids, lipids at surfaces was pointed out[5]. These simple building blocks form the basis of all living organisms. Eventually the knowledge gained from these model studies could be used to characterize tissues *in vitro* and finally *in vivo*. Though it is a challenging goal, it is important to systematically climb the complexity scale.

The major themes explored as part of this proposal are: molecular orientation, secondary structure and biomolecule-surface interactions. The ability to obtain the above information through surface-specific tools is demonstrated for the relatively simple case of peptides on surfaces. Knowledge gained from this present proposal should be helpful in characterizing more complex biological assemblies at surfaces using these surface-specific tools.

1.2 Specific Aims

The main goal of the thesis was to characterize the adsorbed peptide structure with soft X-ray absorption NEXAFS and non-linear laser spectroscopy (SFG). The key objectives to achieve this goal are:

Specific Aim 1: NEXAFS and ToF-SIMS characterization of poly(amino acids)

Specific Aim 2: Characterize the X-ray absorption behavior of nucleic acids and the molecular-orientation of surface-bound DNA oligomers

Specific Aim 3: NEXAFS characterization of adsorbed peptide structure

Specific Aim 4: In situ Sum Frequency Generation of adsorbed peptide structure

Specific Aim 5: Time-dependent SFG characterization of adsorbed alpha-helical peptide

Specific Aim 6: Probing locally peptide-surface interactions: Deuterium labeling experiments

1.3 Importance of characterizing adsorbed peptides

The major thrust behind this research has been to characterize the surface-structure of adsorbed peptides. There are several reasons for addressing this problem

- Peptides represent lower levels of chemical complexity compared to proteins.
- The peptides employed in the present study are chemically and structurally well-defined, simplifying interpretation of the NEXAFS and SFG data.
- NEXAFS and SFG represent powerful techniques for structural characterization of biomolecules due to their inherent surface sensitivity and chemical specificity. However, these techniques are constrained by the availability of good model systems to fully realize their potential. The present proposal establishes the ability to obtain useful surface-structure information with SFG and NEXAFS.
- Immobilization of bioactive peptides onto surfaces is an area of considerable interest in a range of research areas such as tissue engineering, diagnostics, affinity separations, and cell-culture technologies. The key element to retaining the biological specificity of the immobilized peptides is to preserve their structure.
- Though surface-modification of materials is routinely done by several techniques onto "real" hydrophobic polymeric substrates, the scheme employed in this present approach represents true molecular-level modification of "real" hydrophobic polymeric substrates.

1.4 Organization of the dissertation

Chapter one presents the motivation for the research, overview of the dissertation, and also explains the major analytical tools used in the present thesis

Chapter two provides a summary of the key experimental methods common to the different sections of the dissertation.

Chapter three discusses the characterization of polyamino acids with NEXAFS and ToF-SIMS. The results from this chapter will be submitted for publication in *Surface and Interface Analysis*.

Chapter four describes the X-ray absorption characteristics of nucleic acids and also the ability to probe molecular-orientation with NEXAFS. Results from this chapter will be submitted for publication in *J. of Electron Spectroscopy and Related Phenomenon.*

Chapter five describes the sensitivity of polarization-dependent NEXAFS to secondary structure and also identifies peptides with unique adsorbed secondary structure. Results from this chapter will be submitted for publication in *Langmuir.*

Chapter six discusses an in situ approach to characterize the adsorbed secondary structure with SFG. The results from this chapter will be submitted for publication in *J. of American Chemical Society.*

Chapter seven builds on previous results by characterizing the time-dependent evolution of the surface structure.

Chapter eight summarizes the approaches to probe peptide-surface interactions locally and introduces unique deuterium labeling experiments. The results from this chapter will be submitted for publication in *Physical Chemistry Chemical Physics.*

Chapter nine summarizes the key conclusions from the present thesis, and proposes future plans for extending the applicability and understanding of NEXAFS and SFG.

Appendix one is the collection of the mass spectrum of all the different synthetic peptides discussed in the dissertation.

1.5 Analytical techniques used in this proposal

1.5.1 Time-of-flight Secondary Ion Mass Spectrometry (ToF-SIMS)

ToF-SIMS experiment involves bombarding the sample surface with highly energetic, positively charged primary ions. The bombardment results in emission of secondary particles from the sample surface. These secondary particles are predominantly neutral in charge. However, the secondary particles also contain charged atoms, molecular fragments and molecular ions. The secondary ions are extracted by suitable application of a positive/negative potential and mass analyzed using a time-of-flight detector. Under static conditions (total ion dose<10^{13} ions/cm^2) the resulting mass spectrum is characteristic of the surface chemistry with extreme surface-sensitivity (10-20 Å). The major advantages of ToF-SIMS are surface sensitivity, molecular specificity, and excellent mass resolution. Detailed reviews of SIMS are available[19-22].

A partial list of the different information obtained from a SIMS experiment include identification of solid materials, spatial distribution of surface chemical species, characterization of molecular weight distribution in polymers, identification of surface contaminants, composition of surface species, characterization of surface modification of materials, and detecting molecular orientation and conformation[23-29]. Though ToF-SIMS is not a quantitative technique, when coupled with XPS they can be powerful tools towards quantifying and identifying surface structures.

1.5.2 X-ray Photoelectron Spectroscopy (XPS)

X-ray Photoelectron Spectroscopy (XPS), also commonly known as Electron Spectroscopy for Chemical Analysis (ESCA), is one of the most commonly used surface analysis technique. XPS is uniquely sensitive to all the elements in the periodic table (except hydrogen and helium) and quantitative in nature. It is primarily a core-level spectroscopic technique, which uses energetic x-rays to eject core-level electrons from a sample of interest. The kinetic energy of the electrons emitted from the sample is analyzed. The binding energy of the different electrons can be uniquely determined from Einstein's equation,

$E_{kin} = h\nu - E_b - \phi_{sp}$

where, E_{kin} is the kinetic energy of the outgoing photoelectrons measured by the energy analyzer, $h\nu$ is the energy of the incoming radiation (usually monochromatic Al Kα 1486.6 eV), and ϕ_{sp} is the work function of the spectrometer. Since the E_{kin}, $h\nu$ and ϕ_{sp} are known, the binding energy (E_b) can be determined.

Different elements produce core photoelectrons with characteristic binding energies. In addition, for a particular core photoelectron, the binding energy shifts according to the chemical environment of the particular element. By appropriately normalizing the different elements with their individual absorption cross-section, quantitative surface composition information can be obtained. Excellent reviews on XPS and its application to practical problems are available[30,31].

1.5.3 Near-edge x-ray absorption Fine Structure spectroscopy (NEXAFS)

NEXAFS or X-ray absorption near edge structure (XANES) is a core-level spectroscopy technique which uses tunable, polarized x-rays from a synchrotron source to probe the structure of materials[32]. Similar to XPS, NEXAFS can detect different elements in the periodic table. However, NEXAFS experiments are typically only be done at a synchrotron. A synchrotron source is a facility wherein highly energetic particles traveling near the speed of light are made to travel in a circular path. Due to constant acceleration when they travel in a curved path they emit radiation which spans the infrared, UV and x-ray region. The soft x-ray region is comprised of photons with energy in the range of 250-1000 eV. This region includes the core-level excitation of elements of interest for this study: carbon (285 eV), nitrogen (400 eV) and oxygen (535 eV).

The NEXAFS region usually represents the first 20-30 eV from the energy where the x-ray absorption starts (edge-jump). The region beyond the near-edge region is the extended x-ray absorption fine structure region (EXAFS), which can give bond length information. The near-edge structure around the edge-jump is sensitive to the bonding

environment of the element. In addition, orientation of the different bonds can be obtained because of the polarized nature of the incoming radiation.

When x-rays of sufficient energy are employed, they cause core-level transitions in the different elements. For example, at 285 eV carbon starts absorbing x-rays which causes the removal of the electron from the C 1s level. The atom responds to this excitation in several ways – it could eject an Auger electron or emit a photon due to the relaxation of an electron at a higher energy level to occupy the initial core-level vacancy. For low atomic number elements the probability of an Auger emission is higher. When Auger electrons and photoelectrons are used to follow the x-ray absorption, it gives surface sensitivity to the technique because of the strong attenuation of low-energy electrons by materials. Following the x-ray absorption by detecting the fluorescent photon is more effective at probing buried interfaces or the bulk of the material. Another method for analyzing x-ray absorption is by following the x-ray attenuation of a thin sample in the transmission mode.

Two approaches are employed to follow the x-ray absorption of the sample in the electron emission mode. In the total electron yield, all the emitted electrons (Auger, photoelectron and secondary electron) from the sample are collected and detected. In the partial electron yield mode (PEY), a small negative bias is applied to the detector to cut off the secondary electron emission from the sample. The PEY mode is normally used because it results in a better signal-to-noise ratio and surface sensitivity[32].

Polarization-dependent experiments are performed by changing the polar angle between the incoming x-rays and the sample surface. Hence the electric field vector of the incoming x-rays is changed in relation to the surface for different polar angles of the incoming x-rays. When the incoming x-rays are normal to the sample surface (normal incidence), the electric vector is parallel to the sample surface and probes bonds oriented in the surface plane of the sample. At glancing incidence the incoming x-rays are incident at 20 degrees from the sample surface. At this angle of incidence, the electric field vector has a near-normal orientation and couples strongly into σ bonds normal to the

sample surface. Usually the near-edge structure of the sample is recorded at these two different angles of incidence. The edge-jumps are normalized to unity, which ensures that the concentration of the element, the decrease in the beam current with time and the detector efficiency are all normalized to unity. This procedure allows a comparison of the x-ray absorption of the sample due to the orientation of the different bonds at these two different angles of incidence. The peak intensities can be fitted and quantitative information about the orientation of the different bonds can be obtained. Spectra of reference compounds are usually recorded at the magic angle (55 deg), which is the angle of incidence when the polarization effects are minimal.

The near-edge structure is sensitive to different chemical environments. Hence one of the major applications of NEXAFS has been fingerprinting different chemical species[33-37]. The structures of organic monolayers on surfaces have also been extensively investigated with polarization-dependent NEXAFS spectroscopy[38-41]. Recently, there has been a great interest in the near-edge structure of amino acids and nucleic acids at the carbon, nitrogen and oxygen *k*-edges[34,37,42-47]. NEXAFS has also been extensively applied to problems in catalysis[48-50]. Polymers have also been extensively investigated with NEXAFS[33,51-56]. Another emerging application of NEXAFS spectroscopy is imaging with very high spatial resolution (around 40 nm)[56-59]. Because of the chemical sensitivity of NEXAFS, it enables chemical speciation at high spatial resolution.

1.5.4 Sum frequency generation spectroscopy (SFG)

IR-Visible Sum Frequency generation (SFG) is fast emerging as a premier method for analyzing biomedically-relevant surfaces. SFG has the unique advantage of being a chemically specific probe and can be used to interrogate a wide range of interfaces under different conditions. SFG should not be confused with second-harmonic generation (SHG), which is a related technique. In SHG a single incoming beam of light is focused on the sample surface and the outgoing light at twice the incoming frequency is detected. SFG and SHG are non-linear optical techniques which typically only generate signals at interfaces. Usually the bulk of a material does not generate a SFG signal because it is

disordered (polymers and other related materials) or has inversion symmetry (metals). However, at an interface where there is a break in inversion symmetry or a material can re-structure to minimize its free energy, order can be induced resulting in the interface being SFG active.[60-62]

The ability to observe sum frequency generation is only possible with the advent of modern intense and pulsed lasers. Light from a diffused source (not a laser) does not produce observable SFG because these sources are governed by linear optics. Simply stated, the induced dipole in the medium due to the incoming electric field of the incoming radiation is given by,

$$\hat{P}^1 = \varepsilon_0 \chi^{(1)} \hat{E}(r)\cos(\omega t)$$

Where $\hat{P}^1$ is the first-order polarization of the material, $\chi^{(1)}$ is the linear susceptibility of the medium, analogous to polarizability α for condensed phases, $\hat{E}(r)$ represents the electric vector of the light source, ω is the frequency of the incoming light, ε_o is the permittivity of free space and *t* stands for time.

The above equation shows that for simple materials irradiated with diffused light sources the outgoing light would have same form as the incoming light.

However, when two incoming intense light beams from lasers are overlapped onto a medium, the induced polarization ($\hat{P}$) has the following form,

$$\hat{P} = \hat{P}^{(1)} + \hat{P}^{(2)} + \hat{P}^{(3)} + ...$$

The above expression shows that the induced polarization has higher-order contributions ($\hat{P}^{(2)}, \hat{P}^{(3)}, \ldots$). The higher-order contributions are responsible for the non-linear optical effects observed.

The second-order polarization of the material is given by,

$$\hat{P}^{(2)} = \varepsilon_0 \chi^{(2)} : \hat{E}_1(r)\hat{E}_2(r)\cos\omega_1 t \cos\omega_2 t$$

Where, $\chi^{(2)}$ is the second-order (non-linear) susceptibility of the medium, $\hat{E}_1(r)$ and $\hat{E}_2(r)$ represent the electric field of the incoming two light source and ω_1 and ω_2 represent their frequencies.

The above expression for $\hat{P}^{(2)}$ could be re-written as,

$$\hat{P}^{(2)} = \tfrac{1}{2}\varepsilon_0 \chi^{(2)} : \hat{E}_1(r)\hat{E}_2(r)[\cos(\omega_1 + \omega_2)t + \cos(\omega_1 - \omega_2)t]$$

The above expression shows that the outgoing light can equal the sum and the difference of the two incoming light beams.

The intensity of the light coming out at the sum of the frequencies is given by,

$$I(\omega_1 + \omega_2) \propto \left|\chi^{(2)}\right|^2 I(\omega_1) I(\omega_2)$$

As the intensities of the incoming beams of light are fixed, this expression shows that the sum frequency generation measures the second-order nonlinear optical susceptibility ($\chi^{(2)}$) of the medium.

In general, $\chi^{(2)}$ has a more complex form because of the contribution from the substrate surface non-linearity. The measured $\chi^{(2)}$ could be expressed as,

$$\chi^{(2)} = \chi_R{}^{(2)} + \chi_{NR}{}^{(2)}$$

Where, $\chi_{NR}{}^{(2)}$ represents the non-resonant contribution to $\chi^{(2)}$ from the substrate surface and $\chi_R{}^{(2)}$ represents the resonant contribution to the overall response. Usually $\chi_{NR}{}^{(2)}$ is independent of the frequency except for metal surfaces. The resonant contribution represents the situation where the incoming tunable IR radiation is in resonance with the vibrational band of one of the surface species. This could be modeled as a lorentzian with the following functional form,

$$\chi_R{}^{(2)} = \sum_q \frac{A_q}{\omega_{IR} - \omega_q + i\Gamma_q}$$

Where, A_q, ω_q, Γ_q represent the strength, resonant frequency and damping coefficient for the q^{th} vibrational mode and ω_{IR} represents the frequency of the tunable IR radiation.

The first studies of probing the solid-liquid interface were demonstrated by Guyot-Sionnest et. al. in 1988[63]. This experiment demonstrated the surface-sensitivity of SFG and also the ability to probe the solid-liquid interface. Some of the earlier studies were devoted towards characterizing silane monolayers on silica. SFG has been used to characterize various monolayers on solid surfaces[64-66].

Recently, Wang et. al. demonstrated through a series of experiments that the SFG signal was obtained from the polymer-air/water interface and not from the polymer/substrate interface[67]. This allowed selective probing of the surface-structure of the polymer interface in a variety of environments. Another equally explored system is the structure of water at the solid surface[68-77]. Using a series of experiments, Du et. al.[71] were able to probe the structure of the water next to a solid surface. They demonstrated the strong ordering of the water molecules in the form of ice-like structure on a hydrophobic surface resulting in an extended hydrogen-bonded state.

Some of the major applications of SFG include characterizing surfactants at solid surfaces[78], understanding the adsorption of protein at the solid-liquid interface as well as the air-water interface[79-82], characterization of the surface structures of biomedically relevant polymers[62], and polymer re-structuring in different environments[67,83-85]. The ability to observe the amide I signals (vibrational bands from C=O stretching) in SFG for adsorbed protein monolayers was demonstrated recently by Wang et. al.[86] Observation of amide I signals opens a whole new possibility of obtaining secondary-structural information at solid surfaces. A doubly-resonant SFG experimental method was demonstrated for the first time recently by Rashke et. al.[87] In this experimental approach both the incoming visible and the infrared are near a surface electronic or vibrational transition. The outgoing SFG signal is hence double-resonant enhanced. The above approach was shown to have dramatic enhancement in the SFG signal and improved sensitivity.

The use of isotopically-labeled biomolecules to probe the biomolecule-surface interactions has also been demonstrated[88]. Isotopic labeling is routinely done in NMR experiments to obtain hi-resolution structural information of biomolecules in solution. Several stable nuclei such as C^{13}, N^{15}, and D are available. In addition, the labeled molecules are stable in solution and do not exchange rapidly with the natural nuclei. The labeling strategies result in selective shifting of the peaks in the SFG spectrum and

molecules can be probed at the level of individual residues. Labeling strategies represent an opportunity to obtain more detailed structural information about biomolecules.

1.5.5 Solid-state NMR (ssNMR)

Solid-state NMR is a bulk sensitive technique. Only recently the technique has been applied to problems related to the surface-structure of adsorbed peptides on different surfaces[89]. In NMR, two nuclei can interact through space through an induced magnetic field that interacts with the nearby spin. This effect is called the dipolar coupling effects. In normal solution NMR experiments coupling between different nuclei average to zero because of random orientations and are not observed. However, in the solid state NMR these effects can be observed if the other interactions are averaged out[90]. Using the average Hamiltonian theory and through the usage of appropriate pulse sequences, useful information can be gleaned through dipolar coupling effects between NMR active nuclei[89-91]. By isotopically enriching certain nuclei in the backbone, information about the distances between the nuclei, the local secondary structure and dynamics of the labeled nuclei can be obtained.

The above methods has been applied to investigate the adsorbed structure of peptides and their dynamics on hydroxyapatite[92-94]. They have also been used to obtain secondary-structural information of adsorbed peptides onto hydrophobic substrates[95].

2 : Experimental Methods

2.1 Substrates

Gold-coated silicon pieces

Silicon wafers were obtained from Silicon Valley Microelectronics, Inc. They were cut into 1cmx1cm pieces. The cut silicon pieces were later cleaned by sequentially sonicating twice in methylene chloride, acetone and methanol. The cleaned silicon pieces were then blown dry with nitrogen and taken for gold deposition. Cleaned silicon pieces were coated by electron beam evaporation at pressures below $1x10^{-6}$ torr, first with a titanium adhesive layer ~100 Å thick and then with ~ 1000 Å of gold.

SFG substrates

Circular, 9.53 mm thick CaF_2 windows were obtained from ISP Optics and circular, 6 mm thick quartz windows were obtained from Esco products. Quartz windows were used to acquire SFG spectra in the CH, NH and OH regions. Calcium fluoride windows were used to acquire SFG spectra in the amide region because the quartz windows absorb significant amounts of the incoming IR radiation in the amide region. The CaF_2 windows were cleaned by sonicating them in methanol for 10 minutes followed by blowing dry with nitrogen. The quartz windows were cleaned by sonicating them sequentially in DI water, methanol, acetone, and methylene chloride for 5 minutes each followed by blowing dry with nitrogen. To create hydrophobic substrates, thin fluorocarbon films were deposited onto the substrates from a hexafluoropropylene RF glow discharge (RFGD), as described in the next paragraph.

Radio Frequency Glow Discharge Deposition (RFGD)

The fluorocarbon films were deposited from a hexafluoropropylene RFGD using a home-built, inductively-coupled RF reactor described in detail elsewhere[96]. Cleaned SFG windows were placed in the glow region of the reactor. They were initially etched at an argon pressure of 150 mTorr for 5min with an input power of 40W. A fluorocarbon film was then deposited onto the windows using an input power of 80W for 1min followed by

an input power of 20W for 4 min. The fluorocarbon films were quenched for 5 min under flowing hexafluoropropylene monomer with the RF power turned off. The RFGD-deposited films were thin enough to avoid any significant attenuation of the laser beams used in the SFG experiments. Cleaned silicon pieces (Silicon Valley Microelectronics, Inc.) placed near the windows were also coated. These coated silicon pieces were then later analyzed by x-ray photoelectron spectroscopy (XPS) to determine the composition of the fluorocarbon films.

2.2 Peptide Synthesis

All the peptides were prepared on an Applied Biosystems automated synthesizer (ABI 433A) using MBHA (p-Methyl-Benzhydrylamine) resin. The 9-fluoroenylmethoxy-carbonyl (Fmoc) protected amino acids and the resin were purchased from Anaspec, Inc. The peptides were cleaved from the resin using 95% trifluoroacetic acid with 2.5% triisopropylsilane and 2.5% water. The crude peptides were purified using a Waters reversed-phase high pressure liquid chromatography (HPLC) C-18 column using a water/acetonitrile solvent system containing 0.1% trifluoroacetic acid. The purity and integrity of the peptides were analyzed with electrospray mass spectrometry.

2.3 Preparation of Fmoc labeled deuterated-leucine

Deuterium labeled leucine was purchased from Cambridge Isotopes. FMOC-O-Su was obtained from EMD Biosciences. The leucines were Fmoc labeled by the following procedure. First 2.25mmol of the unprotected leucine was dissolved in 20ml of warm 5% Na_2CO_3 solution. Then 2.25mmol of the FMOC-O-Su was dissolved in 5ml of dioxane. The above solution was later mixed with the solution of the unprotected leucine in Na_2CO_3 solution prepared earlier and stirred for 24hrs at room temperature. After 24hrs the solution was diluted with 20ml of water and extracted three times with ethyl ether. The aqueous layer was adjusted to pH=2 using concentrated HCl. The solution turned turbid. This solution was then extracted with ethyl acetate solution. The ethyl acetate solution was then taken and the ethyl acetate removed with a rotovap. The final traces of the ethyl acetate were removed by vacuum drying. A small amount of the solid

was dissolved in methanol and analyzed by ESI mass spectrometry. The ESI mass spectrum for the Fmoc labeled protected leucine is shown in appendix I. This confirms the synthesis of the Fmoc labeled protected leucine.

2.4 Peptide Adsorption

Phosphate buffered saline (PBS, pH=7.4) was obtained from FischerBiotech. The samples for XPS analysis were prepared by placing 1cm x 1cm pieces of the fluorocarbon coated silicon pieces in 20μg/ml of the peptide solution in PBS. The sample with the peptide solution was held in 1.5ml polystyrene cups for 2hrs. The samples were then washed with DI water and blown dry with nitrogen prior to XPS analysis. The buffers for the pH-dependent XPS experiments were prepared by adding 1N HCl to the PBS buffer solution to adjust their pH to the desired value (pH=2).

A Teflon cell was used for the *in situ* SFG experiments. The fluorocarbon coated or the uncoated quartz windows were immersed in a 20μg/ml solution of the peptide in PBS buffer. The visible and the tunable IR radiation were then focused onto the side of the window in contact with the fluid and the outgoing SFG signal was collected and detected. Some of the windows with the adsorbed peptides were removed from the liquid cell, washed with the buffer and allowed to air-dry. They were later analyzed by focusing the visible and the tunable IR radiation onto the side with the adsorbed peptide. Details regarding doing peptide adsorption avoiding the air-water interface and through the air-water interface are described in Chapter 7.

2.5 X-ray Photoelectron Spectroscopy

All XPS spectra were taken on a Surface Science Instruments S-probe spectrometer. This instrument has a monochromatized Al Kα X-ray source and a low energy electron flood gun for charge neutralization. X-ray spot size for these acquisitions was ~ 800μm. Pressure in the analytical chamber during spectral acquisition was less than 5×10^{-9} Torr. The analyzer pass energy for the survey spectra (composition) was 150 eV and for high resolution C1s spectra was 50 eV. The take-off angle (the angle between the sample

normal and the input axis of the analyzer lens) was 55° (55 degree take-of angle ≈ 50 Å sampling depth). The Service Physics ESCAVB Graphics Viewer program was used to determine peak areas, to calculate the elemental compositions from peak areas and to peak fit the high resolution spectra. Further details about the XPS analysis procedures have been published elsewhere[31,97,98].

2.6 Time-of-flight Secondary Ion Mass Spectrometry

ToF-SIMS experiments were done using a PHI Model 7200 Reflectron time-of-flight secondary ion mass spectrometer (Physical Electronics, Eden Prairie, MN) using an 8 keV Cs^+ primary ion source. The spectra were acquired under static conditions where the primary ion dose is less than 10^{12} ions/cm^2 over an area of 200um x 200um. A pulsed low-energy electron flood gun was used for charge neutralization. The mass resolution ($m/\Delta m$) at the $C_2H_3^+$ (m/z = 27) and C_2H^- (m/z = 25) peaks were typically above 4000 and 3000 in the positive ion and negative ion spectra, respectively. Positive and negative ion ToF-SIMS spectra were calibrated to the CH_3^+, $C_2H_3^+$, $C_3H_5^+$, and $C_7H_7^+$ peaks and CH^-, CN^-, and CNO^- peaks, respectively. Further details about the ToF-SIMS analysis procedures have been published elsewhere[22,28,99].

2.7 Near-Edge X-ray Absorption Fine Structure

The NEXAFS experiments were done at the National Synchrotron Light Source (NSLS) U7-A beamline at Brookhaven National Laboratory. The beamline uses a ~85% polarized, high intensity beam and a monochromator with 600 l/mm grating for the carbon *k*-edge, producing a full-width at half-maximum (FWHM) resolution of ~0.15eV. The monochromator energy scale was calibrated using the absorption peaks in the Io grid spectra for the carbon and oxygen edges. The nitrogen edge was calibrated to the intense π* amide feature of poly(glycine) at 401.6 eV. The NEXAFS spectra were normalized with the signal from an *in situ* gold coated 90% transmission grid placed in the path of the x-rays. Partial electron yield (PEY) was monitored using a channeltron with a negatively applied bias voltage to monitor the Auger and photoelectron yield from the sample. The pre-edge was subtracted from the spectra using a linear background and the

spectra were normalized to unit absorption jump height. The reference spectra were acquired at an angle of 55 deg where the polarization effects were minimal. An electron flood gun was employed to prevent charging of electrically insulating samples. The orientation of the molecules was probed by acquiring the spectra at the normal as well as glancing angles of incidence. At normal incidence, the direction of the incoming X-rays is normal to the sample surface. At glancing incidence, the incoming X-rays are at 20 deg to the sample surface. At these angles, the electric vector of the incoming polarized radiation makes different angles with the surface normal. The difference spectra were obtained by first normalizing the spectra at normal and glancing incidences to unit absorption edge jump height. The spectrum at glancing incidence was subtracted from the spectrum at normal incidence to remove the isotropic components. A disordered system does not show any peaks in the difference spectra. A strong orientation of bonds from strong directional alignment of the molecules shows intensities corresponding to that particular transition in the difference spectra.

2.8 Sum Frequency Generation

Radiation with a wavelength of 1064nm was generated from a Nd:YAG laser system from EKSPLA. This laser has a pulse width of 20 pico-seconds and operates at a repetition rate of 20 Hz. The 1064nm radiation was input into an optical parametric generator/amplifier (OPG/OPA) from Laser Vision, US and frequency doubled to 532nm. The portion of this radiation that was used as the constant wavelength visible radiation in the SFG experiments was focused onto the sample surface at an angle of approximately 60 degrees. The remaining portion of the 532nm radiation was used to generate the tunable IR radiation (1000-4000cm^{-1}) for the SFG experiments. The tunable IR radiation was overlapped at the sample surface in time and space with the visible radiation. The outgoing radiation was collected using focusing mirrors, passed through filters to remove any reflected visible and IR radiation, then sent through a monochromator with the resulting SFG signal detected by a photomultiplier tube. Enough scans were acquired to obtain spectra with a good signal to noise ratio. A parallel signal of reflected IR radiation from the mirror was used to normalize the amide spectra by removing the features in

those spectra arising from absorption by the crystals. The amide region spectra were calibrated using the peak at 1606cm^{-1} and the spectra in the CH regions were calibrated using the peak at 2850cm^{-1} in the transmission spectra of polystyrene[100]. The SFG spectra in this study were acquired with the ssp polarization combination (s polarized SFG, s polarized visible and p polarized IR) or ppp polarization.

3 : NEXAFS and ToF-SIMS Characterization of Poly(amino acids)

The near-edge x-ray absorption fine structure (NEXAFS) spectra of poly(amino acids) at the carbon, nitrogen and oxygen *k*-edges and their time-of-flight secondary ion mass spectrometry (ToF-SIMS) fragmentation patterns are investigated in this study. The poly(amino acid) NEXAFS spectra at the *k*-edges closely resemble the spectra of the corresponding monomeric amino acids and most of the peaks in the poly(amino acid) spectra could be assigned to specific transitions based on these earlier monomeric amino acid studies. All the poly(amino acids) exhibited NEXAFS peaks corresponding to $\pi^*_{C=O}$ and σ^*_{C-C} resonances in the carbon spectra with intense π^* and broad σ^* resonances in both the nitrogen and oxygen spectra. Peaks corresponding to $\pi^*_{C=C}$, $\pi^*_{C=N}$, π^*_{C-OH}, σ^*_{C-N} and the C-H Rydberg resonances were also observed in some of the poly(amino acid) carbon *k*-edge spectra. The ToF-SIMS data from the poly(amino acids) indicate that several peaks in the fragmentation pattern originate from successive breaking of bonds the side chains. A comprehensive listing of positive ion fragments from the poly(amino acids) is provided, which will provide additional ways to identify individual amino acid residues in protein ToF-SIMS spectra. In addition, the ToF-SIMS spectra from a sequence of well-defined peptides indicate that the secondary ion yield scales well with the molecular composition of the amino acid residues, indicating with appropriate sensitivity factors ToF-SIMS can used in some applications for quantitative analysis of the amino acids in peptides.

3.1 Introduction

Interfaces play an important role in a wide range of research areas from biomaterials to semiconductors. Recently, the importance of characterizing simple biological building blocks, then systematically increasing the complexity of the samples was highlighted as part of the biological surface science model[6,101] that uses the information obtained from surface spectroscopies to solve important biological surface and interface problems. The present study of the poly(amino acids) provides important information needed to interpret the results obtained from more complex biological samples. Poly(amino acids), because each polymer only contains a single amino acid, represent versatile model systems of

proteins, which contain up to twenty different amino acids. For example, poly(amino acids) have been used to elucidate the secondary structures and physico-chemical characterization of proteins[102-106]. Near-edge x-ray absorption fine structure (NEXAFS) and time-of-flight secondary ion mass spectrometry (ToF-SIMS) are two techniques that are used to use characterize protein films. This study provides a detailed studies of poly(amino acids) with NEXAFS and ToF-SIMS. The results from these studies will allow more detailed interpretation of NEXAFS and ToF-SIMS protein spectra.

NEXAFS is a core-level spectroscopy technique[32]. The incoming tunable X-rays excite a core photoelectron to an unoccupied molecular orbital. Then the atom with the core hole relaxes by emitting either an Auger electron or a fluorescent photon. In the partial electron yield mode (detection of Auger, photo and high energy secondary electrons) NEXAFS is highly surface sensitive and provides electronic and structural information about the outer 5nm of the surface. The various peaks (resonances) in the near-edge region can be assigned to excitations of electrons from core level to anti-bonding orbitals. NEXAFS can be used for elemental and chemical bond identification, fingerprinting materials, determining electronic states and analyzing the orientation of molecules[32].

The application of NEXAFS spectroscopy to biological samples is relatively limited[34,36,37,42-45]. Boese et al[34] published the first NEXAFS spectra of individual monomeric amino acids at the carbon *k*-edge. They demonstrated that the near-edge is sensitive to the different amino acids and the observed resonances could be assigned to characteristic bonds in the amino acids. Previous studies have explored the application of NEXAFS to different polymers[33,35,51,107-110]. The origin of resonances in the NEXAFS spectra, especially in the carbon *k*-edge spectra, is fairly well understood and has been assigned based on different *ab initio* calculation methods[43,45,47]. Recently, Crain et. al. applied NEXAFS to probe the orientation of self-assembled double-stranded DNA oligomers on gold surfaces. They were able to determine the orientation of the DNA strands based on the polarization dependence of nitrogen *k*-edge spectra[111].

In ToF-SIMS a beam of highly energetic primary ions is focused onto a solid substrate. The sputtered secondary ions are collected and mass analysed. In the static regime, the molecular secondary ions are highly surface-sensitive (1-2nm) and provide information about the molecular surface structure of the material being analyzed. Mantus et. al.[112] showed the ability to characterize poly(amino acids) and adsorbed protein films using SIMS. Recently, the ability to characterize different adsorbed protein films[113], conformational changes[114], multi-component protein films[115] and orientation of adsorbed proteins[116] were demonstrated. These results establish ToF-SIMS as a powerful tool for characterizing adsorbed protein films.

In this study the NEXAFS spectra of poly(amino acids) were recorded at the carbon, nitrogen and oxygen *k*-edges. The peaks present in these spectra were assigned to characteristic bonds based on earlier quantum mechanical calculations for monomeric amino acids[37,43,45]. The present study extends the early NEXAFS experiments on monomeric amino acids by obtaining a more comprehensive set of carbon, nitrogen and oxygen *k*-edge spectra from amino acid homopolymers containing peptide bonds. In addition, it also addresses the assignment of the amide π^* feature in the amino acid nitrogen *k*-edge, which has been the subject of some disagreemnt in previous studies[42,43]. Previous SIMS studies on the poly(amino acids) have been done with both quadrapole and ToF instruments[112,117,118]. The present ToF-SIMS study provides a more extensive assignment of the positive ion fragments from the poly(amino acids) and a more comprehensive list of these fragments. All samples in this study were also characterized by x-ray photoelectron spectroscopy (XPS).

3.2 Experimental Methods

3.2.1 Substrates

Silicon wafers were obtained from Silicon Valley Microelectronics, Inc. They were cut into 1cmx1cm pieces. The cut silicon pieces were later cleaned by sequentially sonicating twice in methylene chloride, acetone, and methanol. The cleaned silicon pieces were then blown dry with nitrogen. Some of the cleaned silicon pieces were coated by electron

beam evaporation at pressures below $1x10^{-6}$ torr, first with a titanium adhesive layer ~100 Å thick and then with ~ 1000 Å overlayer of gold.

3.2.2 Peptide Synthesis

The following list of peptides were synthesized:

LKα Ac – LKKLLKLLKKLLKL – NH_2

LKβ Ac – LKLKLKLKL – NH_2

LK310 Ac – LLKLLKLLKLLKL – NH_2

Where L stands for Leucine and K stands for Lysine.

All the peptides used were synthesized on an automated synthesizer using MBHA resin. The 9-fluoroenylmethoxycarbonyl (Fmoc) protected amino acids and the resin were purchased from Anaspec, Inc. The peptides were cleaved from the resin using a solution of 95% trifluoroacetic acid with 2.5% triisopropylsilane and 2.5% water. The crude peptides were purified using a reverse-phase HPLC C-18 column with a water/acetonitrile solvent system containing 0.1% trifluoroacetic acid. The composition of the peptides was checked with electrospray mass spectrometry[119].

3.2.3 Poly(amino acid) and Peptide sample preparation

All the chemicals were purchased from the Sigma Chemical Co. Poly(lysine), poly(arginine), poly(aspartic acid) and poly(glutamic acid) were dissolved in de-ionized (DI) water (Resistivity > 18Mohm.cm). Poly(tyrosine) was dissolved in ethanol. Poly(histidine), Poly(aspargine) and poly(proline) were dissolved in formic acid. Poly(serine) and tryptophan could not be dissolved in any solvent. They were compacted as a thin layer of powder onto the surface of pliable indium disks (AESAR, Seabrook, NH). The remaining poly(amino acids) were dissolved in trifluoroacetic acid (TFA). Poly(phenylalanine) also could not be dissolved in any solvent. Hence, a tetramer of phenylalanine which readily dissolved in TFA was used. All solution concentrations were 1mg/ml. Thin films for the poly(amino acids) were prepared by spin-casting 40µl of solution onto cleaned silicon wafer pieces at 1500rpm for 45sec. Some thick film

samples were also prepared by pipetting 20μl of solution onto the silicon substrate and allowing the solvent to evaporate. Poly(aspartic acid) and glutamic acid exhibited intense sodium signals in ToF-SIMS and XPS since they are sodium salts. For the ToF-SIMS experiments they were desalted using Alltech desalting columns and then deposited as thin films. All samples were stored under nitrogen prior to analysis. Poly(cysteine) and poly(glutamine) were not analyzed because they were not commercially available.

To prepare the peptide films gold-coated silicon pieces were first immersed in a 1mM solution of a carboxy-terminated alkane thiol for 1day at room temperature. The structure of the carboxy-terminated thiol was: $HS - (CH_2)_{15} - COOH$. The samples were then copiously washed with ethanol and placed in a 20μg/ml peptide solution in phosphate buffer (pH 7.4) for 2hrs. After washing copiously with DI water the samples were blown dry with nitrogen and analyzed with ToF-SIMS.

3.2.4 Near-Edge X-ray Absorption Fine Structure

The NEXAFS experiments were done at the National Synchrotron Light Source (NSLS) U7-A beamline at Brookhaven National Laboratory. The beamline uses an ~85% polarized, high intensity beam and a monochromator with 600 line/mm grating that produces a full-width at half-maximum (FWHM) energy resolution at the carbon *k*-edge of ~0.15eV. The energy for each spectrum was calibrated using the absorption peaks in the corresponding Io grid spectrum. The energy of these peaks were calibrated to the π^* peak of highly oriented graphite at 285.35eV[120]. The NEXAFS spectra were normalized with the signal from an *in situ,* gold-coated 90% transmission grid placed in the path of the incoming x-rays. Partial electron yield (PEY) was monitored using a channeltron with a negatively applied bias voltage of –150V to monitor the Auger and photoelectron yield from the sample. The spectra were acquired with surface of the sample at an angle of 55 deg with respect to the incident x-ray beam. At this angle the polarization effects are minimized. A typical spectrum required about 10min to acquire. The pre-edge was subtracted from the spectra using a linear background and the spectra normalized to unit absorption jump height.

3.2.5 Time-of-flight Secondary Ion Mass Spectrometry

ToF-SIMS experiments were done using a PHI Model 7200 Reflectron time-of-flight secondary ion mass spectrometer (Physical Electronics, Eden Prairie, MN) using an 8 keV Cs^+ primary ion source. The spectra were acquired over an area of 200um x 200um under static conditions where the primary ion dose was kept less than 10^{12} ions/cm^2. A pulsed low-energy electron flood gun was used for charge neutralization. The mass resolutions ($m/\Delta m$) at the $C_2H_3^+$ (m/z = 27) and C_2H^- (m/z = 25) peaks were typically above 4000 and 3000 in the positive ion and negative ion spectra, respectively. Positive and negative ion ToF-SIMS spectra were calibrated to the CH_3^+, $C_2H_3^+$, $C_3H_5^+$ and $C_7H_7^+$ peaks and CH^-, CN^- and CNO^- peaks, respectively. Further details about the ToF-SIMS analysis procedures have been reported previously[22,98].

3.2.6 X-ray photoelectron Spectroscopy

All XPS data were taken on a Surface Science Instruments X-probe spectrometer. This instrument has a monochromatized Al Kα X-ray source and a low energy electron flood gun for charge neutralization. X-ray spot size for these acquisitions was 800μm x 800μm. Pressure in the analytical chamber during spectral acquisition was less than 5 x 10^{-9} Torr. The analyzer pass energy for the survey spectra (composition) was 150 eV and for the high-resolution C1s spectra was 50 eV. The take-off angle (the angle between the sample normal and the input axis of the analyzer lens) was 55° (55 degree take-of angle ≈ 50 Å sampling depth). The surface composition of the different samples was determined from the survey scans. Further details about the XPS analysis procedures have been reported previously[97,98,121].

3.3 Results and discussion

3.3.1 XPS

The poly(amino acid) samples were characterized by XPS. Due to its quantitative nature, XPS can be used to optimize sample preparation by showing which conditions produce the experimental composition that is most consistent with the expected theoretical composition. Table 3.1 lists the chemical structures of the different poly(amino acid) samples employed in this study. The elemental composition of the different poly(amino acid) samples determined by XPS are listed in Table 3.2 and are comparable to an earlier XPS investigation of poly(amino acid) samples[122]. Some of the samples showed small amounts of fluorine (<2%). A few of the samples showed a silicon signal from the underlying substrate. ToF-SIMS experiments confirmed the silicon signal was from the substrate and not adventitious polysiloxane contamination. For samples that had a silicon signal, the substrate contribution to the elemental composition was removed based on the atomic ratios measured on a silicon control sample. It is apparent from Table 3.2 that the XPS determined elemental compositions of the different poly(amino acids) were similar to their expected theoretical compositions. A few of the samples showed excess amounts of carbon (>10%). This is likely due to the presence of adventitious carbon contamination. Nearly all the samples showed excellent agreement between experimentally measured and the theoretically expected nitrogen to oxygen ratios.

3.3.2 NEXAFS carbon k-edge

Figure 3.2 shows the carbon *k*-edge spectra of some selected poly(amino acids) spin-cast onto silicon. The major peaks of interest common to all the poly(amino acids) are the sharp $\pi^*_{C=O}$ peak at 288.1eV and the broad peak near 292eV due to the σ^*_{C-C} resonance[42,43,45]. The position of the $\pi^*_{C=O}$ peak is shifted from its position in the monomeric amino acids because of the presence of the amide bond[43]. In addition, it is broadened and shifted to 288.6 eV in poly(glutamic acid) because of the contribution from the carboxyl π^* features from the side chain acid group. These assignments are in agreement with the recent work done at the carbon *k*-edge for the monomeric amino

acids[43]. Some of the poly(amino acids) exhibit a small peak at 285eV. This is due to adventious carbon contamination on the silicon substrates, as detected in the XPS experiments. Similar contamination issues were also observed in other recent studies[42]. The poly(amino acids) with methylene groups in the side chain such as poly(leucine) and poly(isoleucine) have a pronounced shoulder at 287.5eV. The added intensity at this energy for these poly(amino acids) can be attributed to the Rydberg C-H resonance seen in hydrocarbon chains[32]. The poly(tyrosine) spectrum has a distinct peak near 287 eV, which can be assigned to a $\pi^*_{C\text{-}OH}$ resonance from the presence of the C-O bond in the tyrosine side chain ring.[43] Poly(leucine) and poly(isoleucine) are isomers but only poly(leucine) exhibits a noticeable peak at 289.3eV, possibly due to the $\sigma^*_{C\text{-}N}$ resonance. Previous studies on monomeric amino acids did not seem to show this pronounced enhancement of the $\sigma^*_{C\text{-}N}$ resonance in the leucine spectra[34,45]. ToF-SIMS and XPS experiments did not detect any contaminants that could be responsible for this peak.

Poly(histidine) represents a unique amino acid because of the presence of the double-bonded nitrogen in the ring. Consequently, it shows a peak at 286.6eV having contributions from the $\pi^*_{N\text{-}C=N}$ and $\pi^*_{N\text{-}\underline{C}=C}$ carbon atoms. Poly(arginine) shows an intense $\pi^*_{C=N}$ resonance, as reported earlier for the monomeric amino acids[34,45]. The $\pi^*_{C=N}$ peak in poly(arginine) is shifted to a higher value of 289eV because the carbon is bonded to three nitrogen atoms[45]. The spectra of amino acids with side chain aromatic groups (eg. poly(phenylalanine) and tyrosine) are characterized by intense peaks at 285eV from the $\pi^*_{C=C}$ resonance.

3.3.3 NEXAFS nitrogen k-edge

Nitrogen in proteins and peptides occupy an unique position in the peptide backbone since it is part of the peptide bond that links together the different amino acids. This peptide or amide bond has a partial double bond character due to resonance stabilization of the N-C=O structure. In addition, nitrogen atoms are also present in the side-chains of some of the amino acids (arginine, tryptophan, histidine and asparagine). However, only

the NEXAFS nitrogen *k*-edge spectra of glycine has been previously studied[42,43]. In this study we report the nitrogen *k*-edge spectra for 17 different poly(amino acids).

Figures 3.2 (a) and (b) present the nitrogen *k*-edge spectra of the poly(amino acids). In these spectra of poly(amino acids) there are four features of interest. The π^* resonance observed between 401.0 to 401.8eV is due to the partial double bond character of the amide nitrogen. This resonance is also observed in gas-phase electron energy loss spectroscopy (EELS) of urea and urea-based derivatives, which have a similar structure to the amide unit[123]. Recently, there has been a controversy regarding the origin of this particular peak[12,14]. All the poly(amino acids) examined in our study exhibit an intense π^* resonance near 401.5 eV, suggesting this peak originates from the amide nitrogens in the peptide backbone. For most of the poly(amino acids) this π^* feature is located at 401.5eV. For poly(aspartic acid) and glutamic acid it shifts down to 401eV. For poly(arginine), and poly(tryptophan) it shifts up to 401.8eV. The small shoulder at 403eV apparent in some of the poly(amino acid) spectra is probably due to the Rydberg resonance of the N-H bonds. This feature is also observed in studies of oriented glycine and ammonia on single crystal surfaces[46]. The two broad features at 406eV and 412eV are due to σ^* resonances. Based on earlier studies on oriented glycine[46] and *ab initio* calculations[43] the peak at 406eV can be assigned to $\sigma^*_{C\text{-}N}$ and $\sigma^*_{N\text{-}H}$ resonances while the peak at 412eV can be assigned to the σ^*_{CONH} resonance.

Poly(histidine) has an additional pronounced π^* resonance at 399.8eV. This is assigned to the $\pi^*_{C=N}$ from the double-bonded nitrogen in the ring. Similar features have also been seen in other studies of pyridine, nucleic acids and imidazole[44,124,125]. Poly(proline), where the amide nitrogen is located in a ring structure, exhibits a low energy resonance at 398.8eV. Care was taken to ensure this peak was not due to any beam damage feature (see the next paragraph for a discussion of the x-ray induced peak that occurs at 398.7eV.)

Figure 3.3 shows the effect of exposing the poly(threonine) to the X-ray beam. The nitrogen *k*-edge data were acquired as repeated scans at the same spot on the sample.

With increasing x-ray exposure, an additional feature at 398.7eV is observed. This peak increases in magnitude with increasing X-ray exposure. This peak was assigned to the formation of new species created by exposure of the poly(amino acid)s to X-rays, not to any specific bond in the undamaged poly(amino acid) samples. The appearance of this peak after 10 minutes of X-ray exposure was also observed with the other poly(amino acids) and proteins (data not shown).

3.3.4 NEXAFS oxygen k-edge

Figure 3.4 shows some representative oxygen *k*-edge spectra of the poly(amino acids). Oxygen primarily resides in the backbone of peptides and proteins, although some amino acid residues also have oxygen atoms in their side-chains (tyrosine, asparagine, serine, aspartic acid and glutamic acid). The spectra of poly(glycine) is illustrative of the oxygen *k*-edge spectra for most of the poly(amino acids). The sharp peak at 531.8 eV is assigned to the π^* feature from the amide oxygen atom. Studies with glycine monolayers[46], monomeric amino acids[37,43] also show similar features. The π^* feature in poly(glutamic acid) and poly(aspartic acid) is shifted to 532.4eV (poly(aspartic acid) data not shown), indicative of the contribution from the side-chain carboxyl group. Recent calculations have observed similar shifts in the position of the π^* feature[43,126]. The broad features seen at 539eV and 547eV are assigned to the transition of the O1s electrons to σ^* states associated with the C=O bond. Similar features are also seen in the spectrum of 2,5-diketopiperazine which has C=O groups[42].

3.3.5 Fragmentation of poly(amino acids) in ToF-SIMS

Under static conditions, the ToF-SIMS spectrum is sensitive to the surface chemical structure of the material being analyzed. Previous studies have shown how fragments from the poly(amino acids) are related to the structure of each amino acid present in proteins[112,113,118]. A pathway was identified in these studies that produced immonium ions and fragments of the immonium ions. These ions are characteristic of the individual amino acid residues since the immonium ion contains the side chain (R)[112]. The present

study identifies additional fragment pathways (e.g., side chain fragments) of amino acid residues and develops a more comprehensive set of peaks for identifying the fragments from the poly(amino acids). The motivation for identifying this more extensive set of secondary ions is because many of the fragments from the amino acids overlap in mass, either among themselves or with fragments from organic substrates. Thus, the more fragments that can be uniquely assigned to specific amino acids, the easier protein and unknown compounds can be identified.

Figure 3.5 shows the positive ToF-SIMS spectra of poly(tyrosine). A set of peaks in this spectrum can be assigned to successive fragmentation of the side-chain ($R=C_7H_7O$, R-CH, R-O, etc.). The side-chain of tyrosine contains an oxygen atom, permitting easy identification of the side-chain fragments. The fragmentation from the amino acids with hydrophobic side-chains also exhibited a systematic series of fragments from the side-chains (R). For example R, $R\text{-}H_2$, $R\text{-}CH_2$, etc. were observed in the poly(leucine) positive ion spectrum. For some poly(amino acids) the entire amino acid residues (M) are also detected as M-H or M+H ions. Typically the most intense peak in the poly(amino acid) spectra is from the immonium ions ($^+NH_2{=}CH\text{-}R$), as previously reported[112]. Several peaks in the poly(tyrosine) spectrum can be identified that are related to the immonium ion (I) or the monomer amino acid residue of poly(tyrosine) (I, M-H, M-NH, etc.). In addition, there are other peaks in the poly(amino acid) spectra that can be assigned to a specific amino acid residue. For example, poly(alanine) and poly(methionine) have peaks with a molecular composition of RCH_2CO^+. All the other poly(amino acids) except glycine, proline, argininine, lysine, serine, aspartic and glutamic acid, have peaks with a molecular composition of $RCCO^+$.

Table 3.3 lists in detail the different fragments observed for each of the poly(amino acids). The peaks included in this table are related to the amino acid chemical structure (M=amino acid monomer, R=amino acid side chain, and I=amino acid ammonium ion). Many of these individual peaks reported have related peaks which differ by the addition or subtraction of hydrogen atoms (e.g., loss of H from adjacent carbon atoms). These additional peaks are not included in Table 3.3. The most intense peaks are usually from

the ions that are most stable with a positive charge (e.g., the immonium ions). Many of the peaks listed in Table 3.3 have been reported previously[112,113,118]. The complete set of spectra for fifteen of these homopolymers have been published elsewhere[118].

3.3.6 Effect of amino acid molecular composition on secondary ion yield

To determine if the order of the amino acids present in the primary sequence affects their secondary ion yield, three different LK peptides with different amino acid compositions, secondary structures and sequences were examined. These peptides were absorbed onto carboxy-teminated self-assembled monolayers (SAMs). It is likely that the LK peptides adsorb onto the negatively charged SAM surfaces through their positively charged lysine residues. The reason for choosing this system is that peptides should adsorb as a monolayer in a similar orientation on the carboxy-terminated SAMs, so any sampling depth effects should be minimized.

Figure 3.6 shows the representative ToF-SIMS spectra for two different peptides (LK310and LKα) adsorbed onto the SAM surface. The composition of the lysine and leucine residues in the two peptides varies significantly. It is apparent that the peaks at m/z=84 and m/z=86, attributed to the lysine and leucine residues, show large differences in their relative intensities. To quantify these differences, the ratio of the 84 to 86 peak areas was determined. This experimental ratio was then normalized by dividing it by the theoretical lysine to leucine ratio of the individual peptides. The normalized ratio for all the three peptides is very similar, as shown in Table 3.4. This normalized ratio represents the lys/leu (K/L) ratio of a peptide containing equal amounts of lysine and leucine residues. This proves that the secondary ion yield on the carboxyl terminated SAMs is not significantly affected by the positions of the individual residues in the primary peptide sequence. It also shows the relative ratio of the lysine to leucine peak areas scales with the molecular composition of the different LK peptides. The reason the LK310 ratio differs slightly from the other LK peptide ratios is because the LK310 peptide has a higher concentration of leucine residues. Since leucine also contributes

some intensity to the peak at m/z=84 (86-2H), this peak has a higher leucine contribution in the LK310 spectrum.

The above results are consistent with the observation by Wagner et. al.[113] that the intensity pattern of the amino acid fragments in protein ToF-SIMS spectra is related to the amino acid composition of the proteins. However, for large proteins where the size of the protein is significantly greater than the ToF-SIMS sampling depth, the location of the amino acid residues in the three dimensional protein structure also needs to be accounted for[99]. This is especially true for samples where the hydrated structure of the protein is preserved for ultra-high vacuum ToF-SIMS analysis[114,127].

3.4 Conclusions

The major findings of this study are:

- The partial electron yield NEXAFS spectra at the carbon, nitrogen and oxygen *k*-edges exhibit a range of features that can be uniquely assigned to specific transitions ($\pi^*_{C=O}$, $\pi^*_{C=C}$, $\pi^*_{C=N}$, σ^*_{C-N}, σ^*_{C-C}, etc.) based on earlier studies of monomeric amino acids obtained in the transmission mode. In particular a sharp, strong π^* peak from the amide group in the peptide bond backbone is present in the carbon, nitrogen and oxygen *k*-edges of all poly(amino acid) spectra.
- The nitrogen *k*-edge data of the poly(amino acids) support the assignment of the peak at 401.5eV to the π^* amide bond.
- The positive ion poly(amino acids) ToF-SIMS spectra contain unique fragments from the monomeric repeat units, side chains and immoniuim ions of the amino acid residues.
- A comprehensive set of positive ion fragments from the poly(amino acid) spectra has been prepared for use in interpreting ToF-SIMS peptide and protein spectra.
- The ToF-SIMS spectra from LK peptides with different molecular compositions show that the secondary ion yields of the leucine and lysine fragments scale with the molecular composition of the peptides.

3.5 Credits

Financial support from NESAC/BIO (NIH Grant EB-002027), NSF Grant DMR-0110505 and NIH Grant EB-001473 are gratefully acknowledged. The NEXAFS studies were performed at the NSLS U7A beamline, Brookhaven National Laboratory, which is supported by the DOE. Lara Gamble, Dan Graham and Zugen Fu are thanked for extensive discussions and technical assistance. Certain commercial names are identified for purposes of example or clarity; such identification does not indicate endorsement by the National Institute of Standards and Technology.

Table 3.1 Chemical Structures of the poly(amino acids).

Poly(Glycine) (GLY)	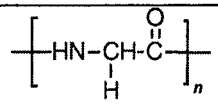
Poly(Alanine) (ALA)	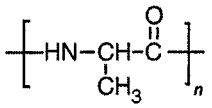
Poly(Proline) (PRO)	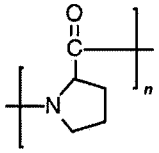
Poly(Valine) (VAL)	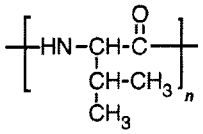
Poly(Leucine) (LEU)	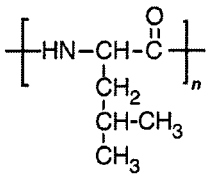
Poly(Isoleucine) (ILE)	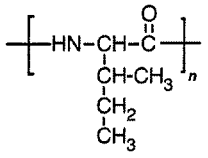
$(Phenylalanine)_4$ (PHE)	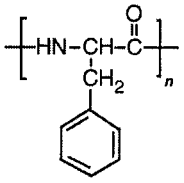
Poly(Tyrosine) (TYR)	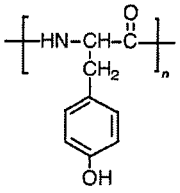

Table 3.1 (continued)

Poly(Tryptophan) (TRP)	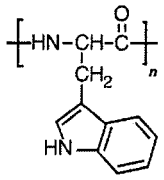
Poly(Histidine) (HIS)	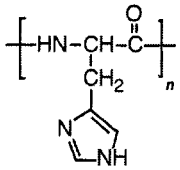
Poly(Arginine) (ARG)	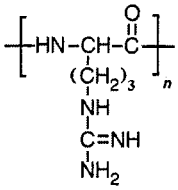
Poly(Lysine) (LYS)	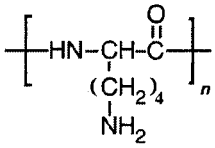
Poly(Asparagine) (ASN)	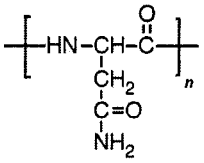
Poly(Threonine) (THR)	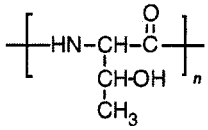
Poly(Serine) (SER)	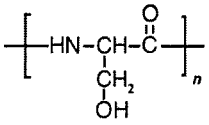
Poly(Aspartic acid) (ASP)	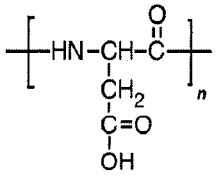

Table 3.1 (continued)

Poly(Glutamic acid) (GLU)	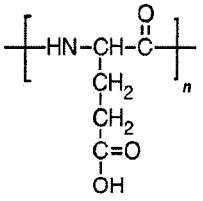
Poly(Methionine) (MET)	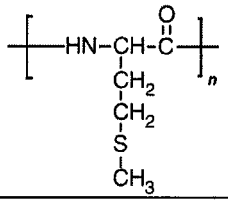

Table 3.2 XPS determined and theoretical (in brackets) elemental compositions of the poly(amino acid) samples. For samples where silicon from the underlying substrate was detected, the substrate contributions were removed based on the observed elemental ratios for a control silicon sample. Each elemental composition represents the average from two analysis spots on each sample.

Poly(amino acids)	C(1s)	N(1s)	O(1s)	N/O
Poly(Glycine) [*, †]	55.9 (50)	21.0 (25)	23.1 (25)	0.9 (1.0)
Poly(Alanine)	64.8 (60)	18.3 (20)	17.1 (20)	1.1 (1.0)
Poly(Proline)	74.3 (71.4)	12.2 (14.3)	13.5 (14.3)	0.9 (1.0)
Poly(Valine) [*, †]	73.8 (71.4)	12.1 (14.3)	14.1 (14.3)	0.9 (1.0)
Poly(Leucine) [*, †]	73.5 (75)	13.7 (12.5)	12.8 (12.5)	1.1 (1.0)
Poly(Isoleucine) [†]	77.6 (75)	10.8 (12.5)	11.6 (12.5)	0.9 (1.0)
$(Phe)_4$ [*, †]	80.7 (81.8)	9.2 (9.1)	10.1 (9.1)	0.9 (1.0)
Poly(Tyrosine) [†]	76.6 (75)	7.9 (8.3)	15.5 (16.7)	0.5 (0.5)
Poly(Tryptophan)	79.4 (78.6)	13.0 (14.3)	7.6 (7.1)	1.7 (2.0)
Poly(Histidine)	60.2 (60)	23.5 (30)	16.4 (10)	1.4 (3.0)
Poly(Arginine) [*, ‡]	62.1 (54.5)	29.8 (36.4)	8.1 (9.1)	3.7 (4.0)
Poly(Lysine) [‡]	78.4 (66.7)	14.3 (22.2)	7.3 (11.1)	2.0 (2.0)
Poly(Asparagine)	59.6 (50)	16.1 (25)	24.3 (25)	0.7 (1.0)

Table 3.2 (continued)

Poly(Threonine)	61.4 (57.1)	11.3 (14.3)	27.3 (28.6)	0.4 (0.5)
Poly(Aspartic acid)[*, ‡]	58.8 (50)	10.4 (12.5)	30.8 (37.5)	0.3 (0.3)
Poly(Glutamic acid)[*, ‡]	60.1 (55.6)	10.1 (11.1)	29.8 (33.3)	0.3 (0.3)

	C(1s)	N(1s)	O(1s)	S(2p)	N/O
Poly(Methionine)[*, †]	64.5 (62.5)	11.2 (12.5)	12.2 (12.5)	12.1 (12.5)	0.9 (1)

[*] samples with small amounts of fluorine detected (<2%)
[†] samples with silicon detected (~ 5%)
[‡] samples with silicon detected (~25%)

Table 3.3 Summary of the major positive ions observed in the poly(amino acids) ToF-SIMS spectra. Assignments are given in terms of the fragment chemical formula, mass, type (M, I, R, etc.) and relative intensity. The listed fragments have approximately 5% or higher intensity relative to the most intense peak (usually the immonium ion). Generally hydrocarbon peaks below 50 m/z were not included unless they are from hydrocarbon containing amino acids such as leucine etc.

Poly(amino acid)	Fragment(m/z)	Relative Intensity
Poly(glycine) M=C_2H_3NO I= CH_4N R=H	CH_4N (30.03) = I C_2H_4NO (58.03) = M+H $C_2H_7N_2O$ (75.06) = M+H_4N	1.00 0.05 0.04
Poly(alanine) M=C_3H_5NO I= C_2H_6N R=CH_3	CH_4N (30.03) C_2H_6N (44.05) = I C_3H_5O (57.03) = M-N C_3H_4NO (70.03) = M-H C_3H_6NO (72.05) = M+H	0.77 1.00 0.16 0.13 0.22
Poly(valine) M=C_5H_9NO I= $C_4H_{10}N$ R=C_3H_7	CH_4N (30.03) C_3H_7 (43.05) = R C_4H_7 (55.05) = R+CH C_4H_8N (70.07) = I-H_2 $C_4H_{10}N$ (72.08) = I C_5H_7O (83.05) = M-H_2N C_5H_8NO (98.06) = M-H $C_5H_{10}NO$ (100.08) = M+H	0.10 0.20 0.28 0.20 1.00 0.21 0.04 0.04
Poly(proline) M=C_5H_7NO I= $C_5H_{10}N$ R=C_4H_7N	CH_4N (30.03) C_3H_6N (56.05) = R-CH C_4H_6N (68.05) = I-H_2 C_4H_8N (70.06) = I C_5H_6N (80.05) = M-HO C_6H_8N (94.07) = M+CH-O C_5H_8NO (98.06) = M+H	0.10 0.09 0.43 1.00 0.11 0.09 0.13
Poly(leucine) M=$C_6H_{11}NO$ I= $C_5H_{12}N$ R=C_4H_9	CH_4N (30.03) C_3H_7 (43.05) = R-CH_2 C_4H_9 (57.07) = R C_5H_9 (69.07) = R+C $C_5H_{10}N$ (84.08) = I-H_2 $C_5H_{12}N$ (86.09) = I $C_5H_{13}N$ (87.10) = I+H C_6H_9O (97.06) = M-H_2N	0.19 0.31 0.04 0.07 0.17 1.00 0.13 0.09

Table 3.3 (continued)

Poly(Isoleucine) M=$C_6H_{11}NO$ I= $C_5H_{12}N$ R=C_4H_9	CH_4N (30.03) C_3H_7 (43.05) = R-CH_2 C_4H_9 (57.07) = R C_5H_9 (69.07) = R+C $C_5H_{10}N$ (84.08) = I-H_2 $C_5H_{12}N$ (86.09) = I $C_5H_{13}N$ (87.10) = I+H C_6H_9O (97.06) = M-H_2N	0.17 0.22 0.12 0.19 0.20 1.00 0.09 0.15
Poly(threonine) M=$C_4H_7NO_2$ I= C_3H_8NO R=C_2H_5O	CH_4N (30.03) C_2H_5O (45.03) = R C_3H_6N (54.05) = I-H_2O C_3H_7N (57.06) = I-HO C_4H_5O (69.03) = R+C_2 C_3H_6NO (72.04) = I-H_2 C_3H_8NO (74.06) = I $C_4H_6O_2$ (86.04) = M-HN $C_4H_8NO_2$ (102.05) = M+H	0.40 0.33 1.00 0.60 0.76 0.20 0.20 1.00 0.11 0.06
Poly(serine) M=$C_3H_5NO_2$ I= C_2H_6NO R=CH_3O	CH_4N (30.03) CH_3O (31.02) = R C_2H_3O (43.02) = R+C C_3H_3O (55.02) = R+C_2 C_2H_6NO (60.04) = I	0.14 0.06 0.19 0.15 1.00
Poly(Asparagine) M=$C_4H_6N_2O_2$ I= $C_3H_7N_2O$ R=C_2H_4NO	CH_4N (30.03) CH_2NO (44.01) = R-CH_2 C_2H_5NO (59.04) = R-H C_3H_4NO (70.03) = I C_3H_6NO (72.04) = I+H_2 $C_3H_7N_2O$ (87.05) = M+H-CO $C_4H_4NO_2$ (98.02) = M-H_2N $C_4H_7N_2O_2$ (115.05) = M+H	0.19 0.46 0.28 1.00 0.37 0.40 0.42 0.06
Poly(lysine) M=$C_6H_{12}N_2O$ I= $C_5H_{13}N_2$ R=$C_4H_{10}N$	CH_4N (30.03) C_2H_6N (44.05) = R-C_2H_4 C_2H_7N (45.06) = R-C_2H_3 C_3H_6N (56.05) = R-CH_4 C_4H_8N (70.07) = R-H_2 C_5H_8N (82.08) = I-H_2 $C_5H_{10}N$ (84.08) = I	1.00 0.24 0.24 0.82 0.17 0.14 1.00

Table 3.3 (continued)

Poly(Histidine) M=$C_6H_7N_3O$ I= $C_5H_8N_3$ R=$C_4H_5N_2$	CH_4N (30.03) $C_3H_5N_2$ (69.04) = R-C $C_4H_5N_2$ (81.04) = R $C_4H_6N_2$ (82.05) = R+H $C_5H_8N_2$ (94.05) = R+CH_3 $C_5H_8N_3$ (110.07) = I $C_6H_5N_2O$ (121.04) = M-H_2N $C_6H_6N_3O$ (136.05) = M-H	0.42 1.00 0.57 0.51 0.14 0.59 0.11 0.06
Poly(Arginine) M=$C_6H_{12}N_4O$ I= $C_5H_{13}N_4$ R=$C_4H_{10}N_3$	CH_4N (30.03) CH_3N_2 (43.03) = R-C_3H_7 CH_5N_3 (59.05) = R-C_3H_5 C_4H_8N (70.06) = R-H_2N_2 $C_2H_7N_3$ (73.06) = R-C_2H_3 $C_3H_9N_3$ (87.08) = R-CH $C_4H_{10}N_3$ (100.08) = R $C_5H_{10}N_3$ (112.08) = R+C $C_5H_{11}N_4$ (127.09) = I+H_2	0.55 0.84 0.75 1.00 0.47 0.16 0.12 0.06 0.03
$(Phe)_4$ M=C_9H_9NO I= $C_8H_{10}N$ R=C_7H_7	CH_4N (30.03) C_6H_5 (77.04) = R C_7H_7 (91.05) = R C_8H_8 (104.06) = R $C_8H_{10}N$ (120.08) = I C_9H_7O (131.05) = M-H_2N C_9H_8NO (146.06) = M-H	0.07 0.15 0.53 0.21 1.00 0.25 0.56
Poly(Tyrosine) M=$C_9H_9NO_2$ I= $C_8H_{10}NO$ R=C_7H_7O	CH_4N (30.03) C_7H_7 (91.05) = R-O C_6H_6O (94.04) = R-CH C_7H_7O (107.05) = R C_8H_8O (120.05) = R+CH $C_8H_{10}NO$ (136.07) = I $C_9H_7O_2$ (147.04) = M-H_2N $C_9H_8NO_2$ (162.05) = M-H	0.07 0.20 0.06 0.70 0.17 1.00 0.33 0.05
Poly(Tryptophan) M=$C_{11}H_{10}N_2O$ I= $C_{10}H_{11}N_2$ R=C_9H_8N	C_8H_6N (117.06) = R+CH_2 C_9H_8N (130.06) = R C_9H_9N (131.06) = R+H $C_{10}H_9N$ (143.07) = R+CH $C_{10}H_{11}N_2$ (159.09) = I $C_{11}H_8NO$ (170.06) = M-H_2N	0.10 1.00 0.12 0.08 0.26 0.15

Table 3.3 (continued)

Poly(Aspartic acid) M=$C_4H_5NO_3$ I= $C_3H_6NO_2$ R=$C_2H_3O_2$	CH_4N (30.03) C_2H_3O (43.02) = R-O C_3H_3O (55.02) = I-H_3NO $C_3H_6NO_2$ (88.04) = I	0.50 0.73 0.95 1.00
Poly(Glutamic acid) M=$C_5H_7NO_3$ I= $C_4H_8NO_2$ R=$C_3H_5O_2$	CH_4N (30.03) C_3H_3O (55.02) = R-H_2O C_4H_6NO (84.04) = I-H_2O $C_4H_8NO_2$ (102.06) = I	0.25 0.82 1.00 0.94
Poly(methionine) M=C_5H_9NOS I= $C_4H_{10}NS$ R=C_3H_7S	CH_4N (30.03) C_2H_5S (61.01) = R-CH_2 C_3H_7S (75.03) = R C_4H_9S (89.04) = R+CH_2 C_4H_8NS (102.04) = I-H_2 $C_4H_{10}NS$ (104.05) = I C_5H_9SO (117.04) = M-N	0.16 1.00 0.14 0.07 0.10 0.34 0.26

Table 3.4 The ToF-SIMS secondary ion yields of the m/z=84 and 86 fragments from the LK peptides adsorbed onto carboxyl terminated SAM surfaces.

	LK α	LK 310	LK β
Experimental Lys/Leu ratio (A)	1.45±0.01	0.808±0.01	1.56±0.03
Theoretical Lys/Leu ratio (B)	0.75	0.44	0.8
A/B	1.93±0.01	1.82±0.02	1.95±0.03

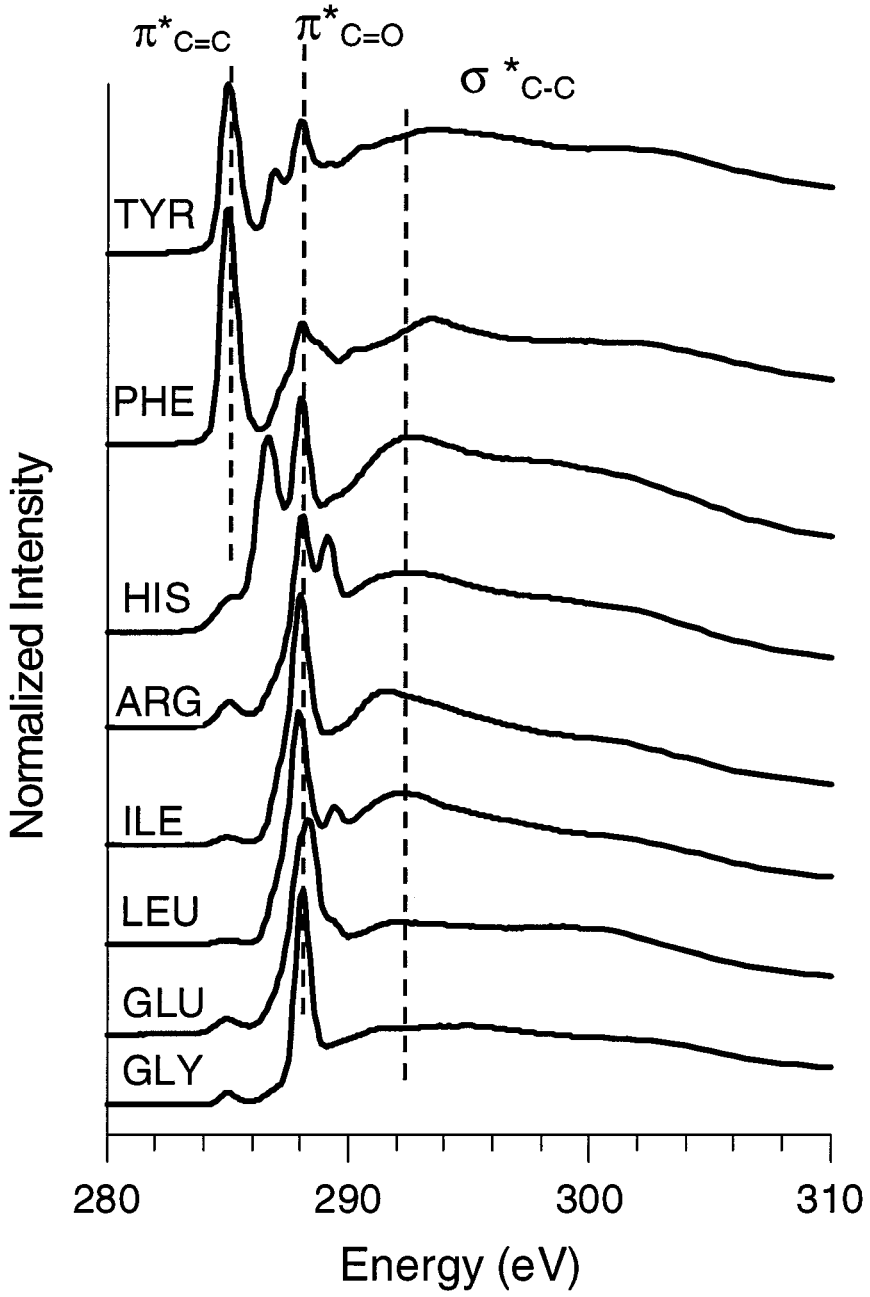

Figure 3.1 The partial electron yield carbon *k*-edge NEXAFS spectra of selected poly(amino acids).

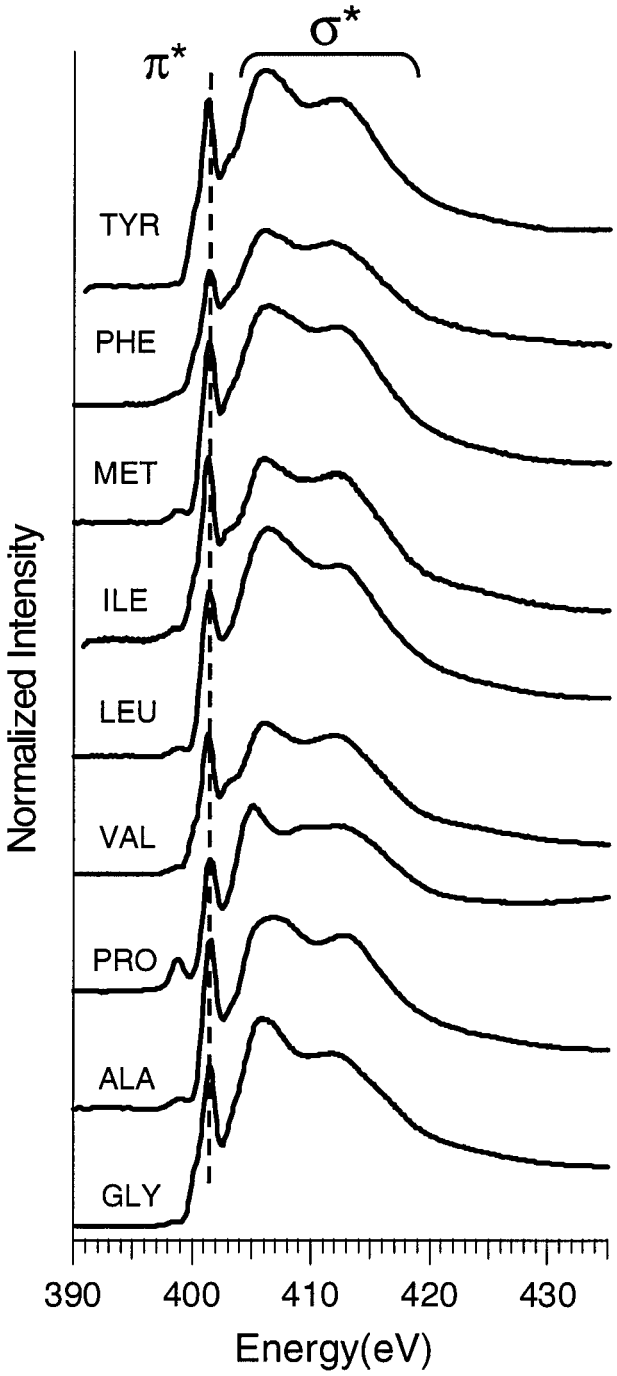

Figure 3.2 (a) The partial electron yield nitrogen k-edge NEXAFS spectra of the poly(amino acids).

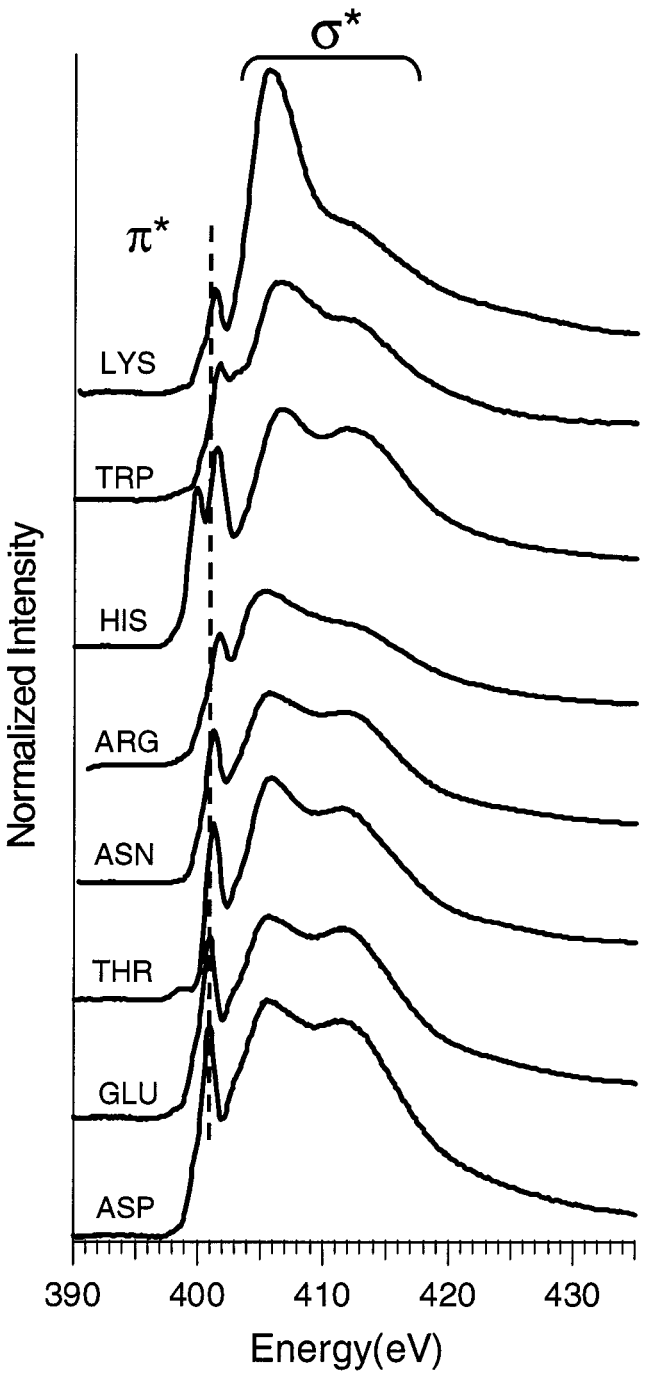

Figure 3.2 (b) The partial electron yield nitrogen *k*-edge NEXAFS spectra of the poly(amino acids).

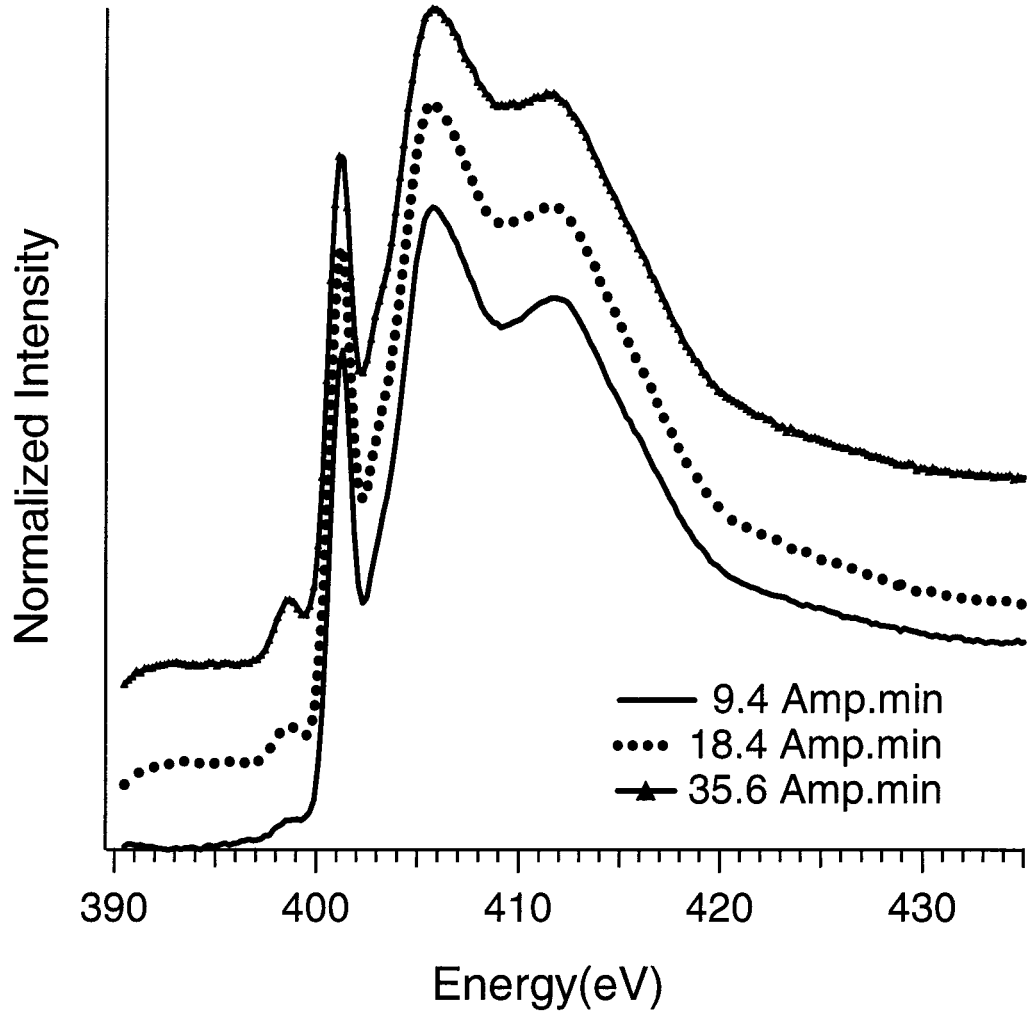

Figure 3.3 Successive nitrogen k-edge spectral scans at the same sample location showing the effect of soft-x-ray irradiation on poly(threonine). The peak near 399 eV increases in intensity with increasing x-ray exposure.

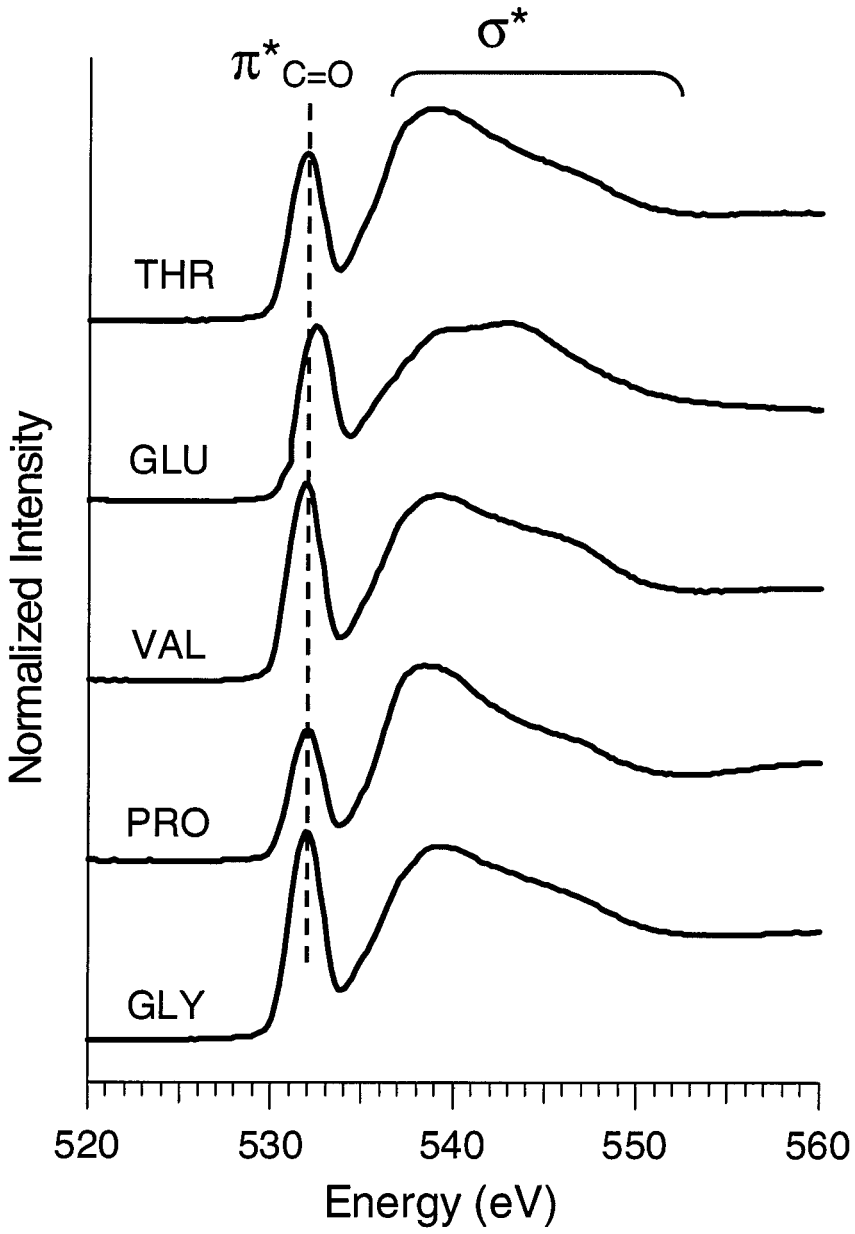

Figure 3.4 The partial electron yield oxygen k-edge NEXAFS spectra of selected poly(amino acids).

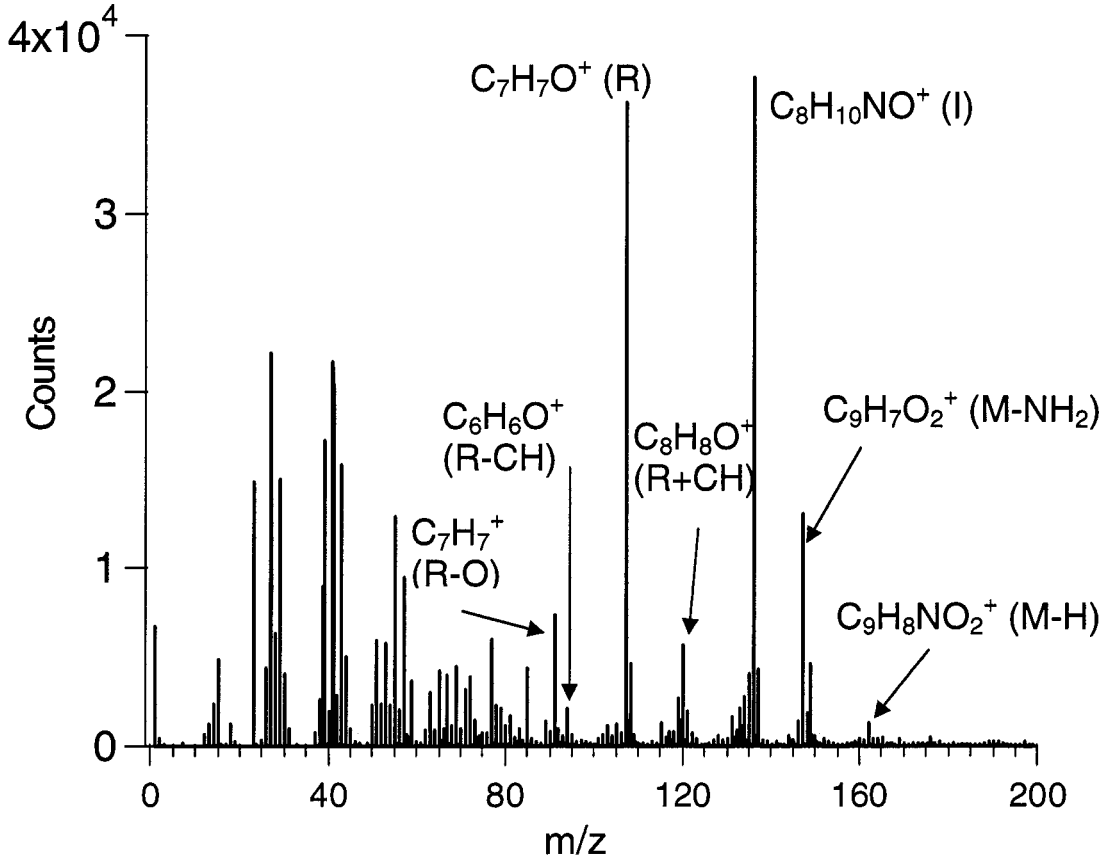

Figure 3.5 The positive ion ToF-SIMS spectrum of poly(tyrosine). The major peaks in the spectrum can be assigned to fragments from the monomer repeat unit (M), ammonium ion (I) and side-chain (R) groups of poly(tyrosine).

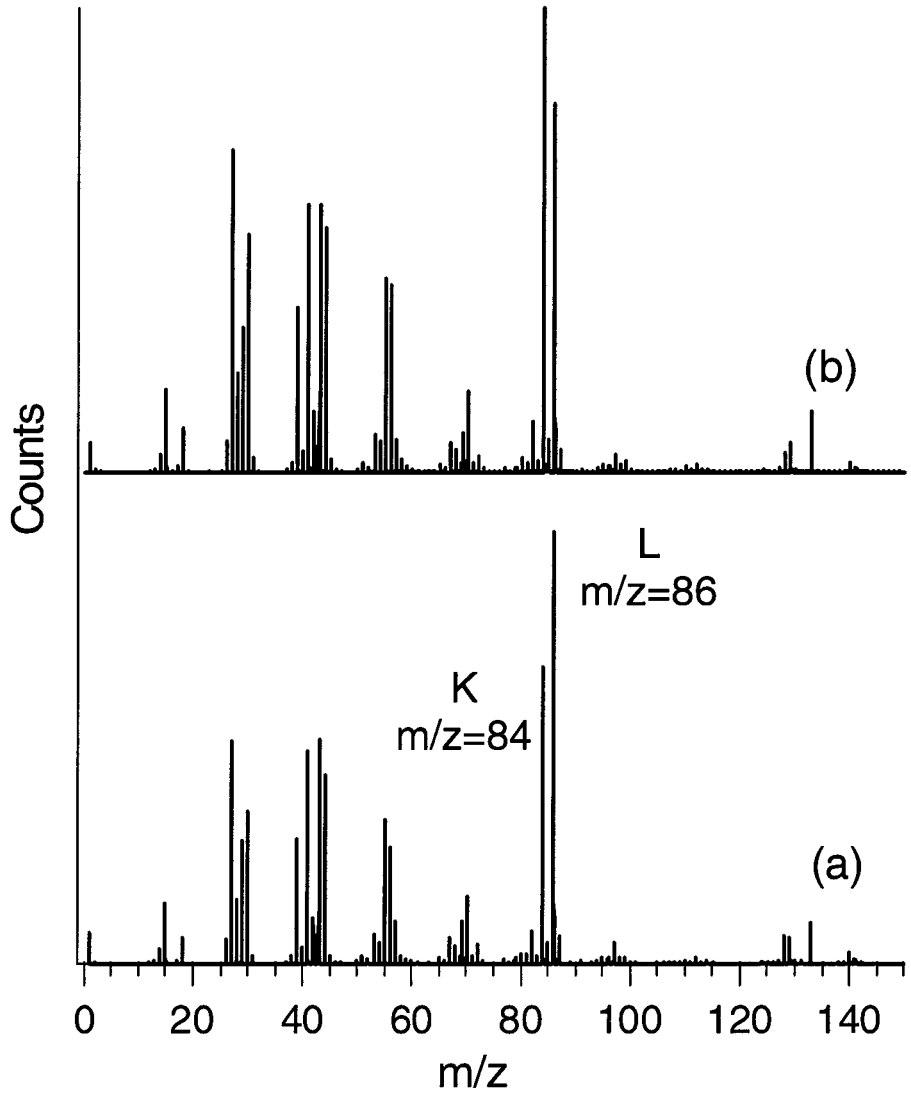

Figure 3.6 The positive ion ToF-SIMS spectra of the (a) LK310 and (b) LKα peptides adsorbed onto carboxy-terminated self-assembled monolayers. The peaks at m/z=84 and 86 originate primarily from the lysine and leucine amino acid residues.

4 : NEXAFS Characterization of DNA Components and Molecular-Orientation of Surface-Bound DNA Oligomers

Single stranded DNA oligomers (ssDNA) immobilized onto solid surfaces forms the basis for several biotechnological applications such as DNA microarrays, affinity separations, and biosensors. The surface structure of the surface-bound oligomers is expected to significantly influence their biological activity and interactions with the environment. In this study near-edge x-ray absorption fine structure spectroscopy (NEXAFS) is used to characterize the components of DNA (nucleobases, nucleotides and nucleosides) and the orientation information of surface-bound ssDNA. The *k*-edges of carbon, nitrogen and oxygen have spectra with features that are characteristic of the different chemical species present in the nucleobases of DNA. The effect of addition of the DNA sugar and phosphate components on the NEXAFS *k*-edge spectra was also investigated. The polarization-dependent nitrogen *k*-edge NEXAFS data show significant changes for different orientations of surface bound ssDNA. These results show NEXAFS is a powerful, non-destructive technique for chemical and structural characterization of surface-bound DNA oligomers.

4.1 Introduction

Immobilizing of single-stranded DNA oligomers (ssDNA) onto solid surfaces and characterizing their molecular organization on the surface (packing density, orientation, etc.) is important for applications such as diagnostics, DNA microarrays etc[4,5,128-137]. There are several different schemes that have been used to immobilize ssDNA onto a surface[138-146]. These different approaches can cause the ssDNA molecules to be immobilized onto the surface with different surface structures. For example, DNA physically immobilized onto poly(lysine) coated surfaces would be expected to lie flat on the surface due to strong interaction between the negatively charged phosphate backbone and the positively charged lysine groups[147]. Specific immobilization through thiol linkers attached to their 3' or 5' ends of the DNA oligomer is expected to result in a more upright orientation[148-154]. The different orientations resulting from the different immobilization methods could have significant influence on the hybridization efficiency of ssDNA.

Hence, information about the structure of immobilized ssDNA would be invaluable for optimizing the performance of DNA microarrays and other applications using surface-bound oligomers.

Various tools have been employed to characterize the immobilization of ssDNA to gold surfaces with a short alkanethiol linker and the subsequent hybridization with complement DNA. These tools include X-ray Photoelectron Spectroscopy (XPS)[139,155], radiolabeling[139], neutron reflectivity[156], Surface Plasmon Resonance (SPR)[148], Atomic Force Microscopy (AFM)[157], and more recently FTIR[149]. The results from these characterization experiments provide information about the structure of surface immobilized ssDNA. Based on XPS[139,155], neutron reflectivity[156] and electrophoretic measurement[151], thiolated ssDNA has been proposed to initially bind to the surface through the nitrogen groups in the bases, then become more upright with the addition of additional molecules.

The first part of the paper describes the near-edge structure at the carbon, nitrogen and oxygen *k*-edges of the different DNA components (nucleobases, nucleotides and nucleosides). The present study extends the earlier experiments[36,44,158,159] characterizing the near-edge structure of the DNA bases by systematically examining the effect observed in the NEXAFS spectra when DNA sugar and phosphate groups are added to the nucleobases. All the samples were prepared by the same procedure used in a previous Time-of-Flight Secondary Ion Mass Spectrometry (ToF-SIMS) and XPS study[160]. The latter part of the paper demonstrates the ability to probe different molecular orientations of the surface immobilized ssDNA . The ability to obtain information about molecular orientation is demonstrated by using ssDNA sequences that adopt different orientations on the surface.

4.2 Experimental Methods

4.2.1 Preparation of the reference samples

Nucleobases (adenine, cytosine, guanine, thymine, uracil), nucleosides--nucleobase plus one sugar--(2'-deoxyadenosine, 2'-deoxycytidine, 2'-deoxyguanosine, thymidine, 2'-deoxyuridine) and the nucleotides--base plus sugar plus phosphate--(2'-deoxyadenosine 5'-monophosphate, 2'-deoxycytidine 5'-monophosphate, 2'-deoxyguanosine 5'-monophosphate, thymidine 5'-monophosphate and 2'-deoxyuridine 5'-monophosphate) were purchased from Sigma Chemical (St. Louis, MO) and were used as received. Indium shot was obtained from AESAR (Seabrook, NH). Small pieces of Indium shot (~2 mm radius) were cut with a scalpel to expose fresh metal surfaces, then pressed into disks of ~5mm radius. The DNA powders were compacted into the surface of the indium disks. Because of the pliable nature of indium, the powders were easily compacted into the metal and provide a stable and smooth surface for analysis. All the samples were stored under nitrogen in petri dishes until analysis.

4.2.2 Gold substrate preparation

Gold-coated silicon wafers were used as substrate material for DNA immobilization. Silicon wafers (Silicon Valley Microelectronics, Inc., San Jose) were diced into 10 mm x 10 mm squares and cleaned by sequential sonication in DI water, methylene chloride, acetone, and methanol for 5 min, two times in each solvent. Substrates were coated by electron beam evaporation of a 100 Å titanium adhesive layer followed by a 1000 Å gold layer (99.99%) at pressures below 1 x 10^{-6} Torr.

4.2.3 Adsorption of the DNA oligomers

The HPLC purified synthetic ssDNA oligomers were obtained from Trilink Biotechnologies. All the oligos were stored under 25mM Tris at pH=7.4. The sequences for the different oligomers were:

polydT-SH 5' – HS – $(CH_2)_6$ – $(dT)_{16}$ – 3'

polydA 5' – $(dA)_{16}$ – 3'

where, dA = deoxyadenosine and dT = deoxythymidine.

The adsorption experiments were done at room temperature from 1 μM solutions in TE buffer (10mM Tris, 1mM EDTA and 1M NaCl at pH=7.0) for time periods up to 24 hours. The samples were then washed copiously with DI water (Resistivity > 18Mohm.cm) and stored in petri dishes under nitrogen until analysis.

4.2.4 X-ray Photoelectron Spectroscopy

All XPS spectra were taken on a Surface Science Instruments S-probe spectrometer. This instrument has a monochromatized Al Kα x-ray source, hemispherical analyzer, multi-channel detector and a low energy electron flood gun for charge neutralization. X-ray spot size for these acquisitions was 800μm x 800μm. Pressure in the analytical chamber during spectral acquisition was less than 5 x 10^{-9} Torr. The analyzer pass energy for the survey spectra (composition) was 150 eV and for high resolution C1s spectra was 50 eV. The take-off angle (the angle between the sample normal and the input axis of the analyzer lens) was 55° (a 55° take-off angle corresponds to a ~ 50 Å sampling depth). The Service Physics ESCAVB Graphics Viewer program was used to determine peak areas, to calculate the elemental compositions from peak areas, and to peak fit the high resolution spectra.

4.2.5 Near-Edge X-ray Absorption Fine Structure (NEXAFS)

The NEXAFS experiments were done at the National Synchrotron Light Source (NSLS), NIST U7-A beamline. The beamline uses a ~85% polarized, high intensity beam and a monochromator with 600 l/mm grating that provides a full-width at half-maximum (FWHM) resolution of ~0.15eV at the carbon *k-edge*. The monochromator energy scale was calibrated by setting the C(1s) $\rightarrow \pi^*$ transition in the graphite carbon *k*-edge NEXAFS spectrum to 285.35 eV[120]. Partial electron yield (PEY) was monitored using a channeltron with a negatively applied bias voltage to monitor the Auger and photoelectron yield from the sample. The NEXAFS spectra were normalized with the

signal (Io) from an *in situ* gold coated 90% transmission grid placed in the path of the x-rays, to account for changes in the incoming x-ray intensity with time and energy.

The data for the reference bases was collected with the bias voltage maintained at -150 V for the carbon *k*-edge spectrum, -280 V for the nitrogen *k*-edge spectrum and -390 V for the oxygen *k*-edge spectrum. The higher bias voltage for the nitrogen and the oxygen *k*-edges was used to reduce the Auger yield from the carbon and the nitrogen atoms. For all the spectra, the pre-edge was subtracted using a linear background and then the difference in the signal 40 eV above and below the first resonance was normalized to unit absorption jump height. The reference spectra of the different nucleobases, nucleosides and nucleotides were acquired at an angle of 55 deg where the polarization effects were expected to be minimal. An electron flood gun operating in constant current mode with electron energy of 10 eV and an emission current of 60 μAmp was employed to prevent charging of the substrates.

The nitrogen *k*-edge spectra for polydT-SH and polydA were collected with a detector bias voltage of -360 V. This removed the carbon Auger signal and the Au 4d photoelectrons, and resulting in a more straightforward background subtraction of the partial electron yield data in the nitrogen *k*-edge region. A small dip was detected around 427 eV due to the second harmonic peak of the nickel line. The presence of the nickel likely arises from contamination in the beamline optics and is detected only when the detector bias is around -360 V. For lower values of the grid bias, a higher electron yield signal is obtained, and this feature is no longer prominent. Polarization-dependent experiments to probe the orientation of the immobilized ssDNA was done by monitoring the NEXAFS spectra at various polar angles (the angle between the incoming x-rays and the sample surface). At normal incidence the direction of the incoming x-rays is normal to the sample surface and at glancing incidence the incoming x-rays are 20 deg from the sample surface. A disordered system does not show any polarization-dependence (change in NEXAFS peak intensities with changing incidence angle of the x-rays) because of random distribution of the molecular orientations. However, as the directional

alignment of the molecules in the overlayer increases the polarization-dependence of the NEXAFS spectra will increase.

The possible effect of x-ray irradiation on the ssDNA oligomers was examined by repeated exposure to x-rays. No significant changes in the nitrogen *k*-edge spectra were observed in repeated scans, indicating the ssDNA samples were stable under the x-ray flux used to acquire the NEXAFS spectra (data not shown). This is unlike peptides and proteins, which show additional beam damage features in the nitrogen *k-edge* spectra in repeated scans[161].

4.3 Results and Discussion

4.3.1 Carbon k-edge of the DNA bases

The structures of the different DNA nucleobases are shown in Table 4.1. The carbon *k*-edge NEXAFS spectra of these nucleobases are shown in Figure 4.1. As can be seen from the spectra in Figure 4.1, the different nucleobases could be distinguished based on their characteristic carbon *k*-edge spectra (except thymine and uracil, which only differ by replacement of a hydrogen atom in uracil with a methyl group in thymine). Using results from previous studies on amino acids and polymers, the major peaks in the spectrum of thymine and uracil can be uniquely assigned to the functional groups present in these nucleobases. For example, the peak at 288.1eV is assigned to a transition to the π^* orbital of the O=C-NH group (π^*_{CONH}). This assignment is based on the work done recently showing how the π^*_{CO} peak shifts with addition of different groups[126]. The π^*_{CO} peak normally appears at 286.6 eV, but is shifted to 288.1 eV when a nitrogen is attached to the carbonyl group. Similarly, the peak shifts further to 289.4 eV when two nitrogens are attached to the carbonyl group. Thus, the peak at 289.4 eV in the thymine and uracil spectra can be assigned to the π^*_{HNCONH} peak. The peak at 285 eV is assigned to $\pi^*_{C=C}$ species, similar to the features found in NEXAFS spectra of polymers[32] and amino acids[45] containing double-bonded and aromatic carbon atoms. The peak at 286 eV is assigned to a $\pi^*_{C=C-N}$ species based on the assignments for the amino acids[45]. This building block approach to interpreting the peaks found in the NEXAFS spectra is

successful in explaining the many features in NEXAFS spectra, provided there is not extensive delocalization in the structure resulting in new electronic states[32]. The spectrum of polymers and amino acids has been explained using the building block approach[32,33,43,45].

Adenine has a double ring structure that contains carbon, nitrogen and hydrogen atoms. A small $\pi^*_{C=C}$ peak is observed at 285 eV. The two strong peaks near 286.5 and 287.5 are from the C-N_x species in the adenine structure. Guanosine has a similar two ring structure to adenine. The two differences between these nucleobases is the location of the amine group on the 6-member ring and the addition of a carbonyl group in guanosine (see Table 4.1). These changes do not change the location of the C-N peak at 286.5 in the guanosine spectrum, but does result in an unresolved doublet near 288.5 eV. Part of the intensity of this doublet is due to a π^*_{CONH} peak. The structure of cytosine is similar to that of uracil. The only difference is one of the carbonyl groups in uracil have been replaced by an amine group in cytosine (see Table 4.1). This replacement does not change the energies of the $\pi^*_{C=C}$ and $\pi^*_{C=C-N}$ peaks, but does slightly lower the energy of the π^*_{HNCONH} peak. The cytosine spectrum also has a peak near 287.5 eV. Based on the fact three nucleobases with amine groups attached to ring structures (adenine, cytosine, and guanosine) all have peaks in their NEXAFS spectrum near 287 eV is likely this peak is due to a transition to the π^* orbital of the C-NH_x group. However, because of the extended aromatic structure of adenine, cytosine and guanosine, rigorous quantum mechanical calculations are needed to to confirm the peak assignments for their NEXAFS spectra. It has been recently shown that *ab initio* calculations are capable of capturing the different π^* features in NEXAFS spectra arising from different carbon species[158].

4.3.2 DNA bases Nitrogen k-edge

The nitrogen in the DNA resides in the nucleobases. Hence, the nitrogen *k*-edge spectra can be used to selectively probe the nucleobase structure in immobilized ssDNA. The nitrogen *k*-edge NEXAFS spectra shown in Figure 4.2 for the five nucleobases can be divided into two regions. Peaks due to transitions to π^* orbitals are located around 400

eV and peaks due to transitions to σ* orbitals are located above 405 eV. These assignments are based on recent quantum mechanical calculations and experimental studies[44,162]. The peak positions for the π* orbitals for the nucleobases are listed in Table 4.2. Similar to the carbon *k*-edge spectra, the nitrogen *k*-edge spectra exhibit differences among the five nucleobases. The π* peaks in the thymine and uracil spectra is near 401 eV, consistent with the fact that all nitrogen atoms in these two nucleobases are located next to carbonyl groups. The major π* peak for adenine, which has no carbonyl groups, is located near 399 eV, consistent with the location of the nitrogen π* peak in other biomolecules that have nitrogen atoms present in a ring structure (e.g., the amino acid histidine)[45,107,161]. The remaining two nucleobases, guanosine and cytosine, have nitrogen groups both adjacent and removed from carbonyl groups (see Table 4.1). These two nucleobases have unresolved doublet π* peaks in the 399 to 401 eV energy range (see Table 4.2 for the exact energy positions), consistent with the type of nitrogen species in guanosine and cytosine.

4.3.3 DNA bases Oxygen k-edge

The oxygen *k*-edge NEXAFS spectra of the five nucleobases are shown in Figure 4.3. Recent quantum mechanical calculations have shown the π* peak for carbonyl species ($\pi^*_{C=O}$) is located near 532 eV and σ* peaks for oxygen species are located above 535 eV[44]. The peak positions in Figure 3 are consistent with these assignments. All nucleobases except adenine have a strong $\pi^*_{C=O}$ peak near 532 eV and σ* peaks above 535 eV. The relative intensities and positions of the σ* peak vary slightly among the nucleobases, as expected from their slightly different structures. Thymine shows a slight splitting of the π^*_{CO} peak compared to the other nucleobases. Uracil does not show an apparent splitting of the π^*_{CO} because of the lower energy resolution at the oxygen *k*-edge. The position of the π^*_{CO} is shifted to 532.5 eV for cytosine. Similar trends have been reported earlier [44,126]. As expected, the oxygen k-edge NEXAFS spectrum of adenine does not show any signal since it does not contain oxygen (data not shown).

4.3.4 Effect of addition of different DNA constituents in their NEXAFS spectra

DNA is made up of the different nucleobases, each attached to a ribose sugar and a phosphate group (see Figure 4.4). Thymine is used as a typical case to show the effect on the carbon *k*-edge NEXAFS spectra of adding the sugar and phosphate groups (Figure 4.5). The NEXAFS carbon *k*-edge spectra of the thymine nucleotide (thymidine 5'-monophosphate) were not collected because of excess carbon contamination in the sample (similar problems were observed with the XPS characterization results[160]). For this reason, the spectrum of polydT-SH (24hrs) is used to represent the effect of addition of the phosphate group. The major peaks expected from the thymine π^* features are present in all three spectra, but their intensities vary as the sugar and phosphate groups are added. With the addition of the sugar to the base, a new peak at 288.6 eV is observed, which is attributed to the σ^* peak from the carbon atoms attached to the oxygen in the sugar unit[32]. Upon addition of the sugar, enhanced intensities are also seen in the σ^* peaks from the C-C and the C-O bonds in the region beyond 290 eV. PolydT-SH shows similar spectrum to the thymine nucleoside spectra. This is expected since the phosphate group does not contain any carbon atoms. Similar trends were seen for the other nucleobases upon addition of the sugar in the carbon *k*-edge region (data not shown).

Using guanine as a typical example, the effect of adding the sugar and phosphate groups to a nucleobase on nitrogen *k*-edge NEXAFS spectra is shown in Figure 4.6. Since neither the sugar or phosphate groups contain nitrogen, no large changes are expected. This is the case for the σ^* region above 405 eV. However, the addition of sugar and the phosphate groups did have a noticeable effect in the π^* region of the spectrum. This effect is most apparent for guanine, which shows shifts in the position of the π^* peaks (see Table 4.2). However, detailed calculations are needed to understand the origin of the shift in the π^* peak positions. Adenine also shows some shifting in the position of the second π^* peak around 401.5 eV (see Table 4.2). Thymine and uracil do not show large changes in the position of their π^* peak with the addition of the sugar and phosphate groups (see Table 4.2).

The effect on the oxygen *k*-edge NEXAFS thymine spectrum from adding the sugar and phosphate groups is shown in Figure 4.7. The major change is a significant reduction in the $\pi^*_{C=O}$ intensity relative to the σ^* intensities. This is expected since the oxygen species in the sugar and phosphate groups should only contribute intensity in the σ^* region. The spectrum of a sodium phosphate salt is shown to provide an example of the oxygen *k*-edge spectra of the phosphate group. With the addition of the sugar and phosphate groups, the thymine spectrum becomes more characteristic of the phosphate group.

4.3.5 Probing the Molecular-Orientation of surface-bound DNA oligomers

To determine the ability of NEXAFS to probe the orientation of surface-bound ssDNA, two different oligomers which adopt different surface structures on gold surfaces were selected for investigation. The first was polydT-SH, which should attach to the surface through the thiol groups and is expected to adopt a more upright structure. The second was polydA, which should attach to the surface through interactions with nitrogen groups in the nucleobases and is expected to adopt a more flat orientation. Recent results from several studies point to the different molecular orientations adopted by specifically (through thiol) and non-specifically (through the side-chain bases) immobilized ssDNA oligomers[148-154]. In particular, polydA was immobilized non-specifically because of the amine groups in the nucleobases interacting with the gold surface[148,149]. In contrast, polydT-SH would be primarily immobilized through the thiol groups because of the low affinity of its nucleobases to the gold surface[149]. Hence, we hypothesize that the two immobilized ssDNA molecules on gold surfaces should exhibit different polarization-dependent NEXAFS spectra characteristic of their different interactions and structures on gold surfaces.

The elemental surface compositions of the different oligomers adsorbed onto gold surfaces are listed in Table 4.3. All the elements from the ssDNA oligomers are detected, except sulfur from polydT-SH. Sulfur is not detected because of its low concentration in polydT-SH (S atomic percent = 0.3 %) and its attenuation by the immobilized ssDNA

overlayer. The XPS determined P/N and O/N elemental ratios for polydT-SH agree well with the theoretical ratios expected from the stoichiometry of the polydT-SH (Table 4.4). The agreement between the XPS and theoretical P/N and O/N ratios is not as good for polydA. For both ssDNA oligomers the amount of carbon determined by XPS was greater than the amount expected from their stoichiometries (see Table 4.4), indicating the presence of some hydrocarbon contamination on these samples. The carbon concentration did decrease for polydT-SH at the 24 hr assembly time; indicating as more ssDNA oligomers are immobilized onto the surface, the residual carbon contamination is removed from the gold surface (data not shown). The XPS gold concentration for the 24 hr assembly of polydT-SH was half the value of the gold concentration for the 24 hr assembly of polydA. The differences in the gold concentrations indicate the polydT-SH overlayer was thicker or more dense than the polydA overlayer. This is consistent with a more upright surface-structure of polydT-SH on gold compared to polydA.

Figure 4.8 shows the polarization-dependent nitrogen *k*-edge spectra of the two ssDNA oligomers immobilized onto gold. The π^* region of the polydT-SH spectrum exhibits enhanced intensity at glancing x-ray incidence. In contrast, the π^* region of the polydA spectrum exhibits enhanced intensity at normal x-ray incidence. Since the electric field vector of the incident x-ray beam is parallel to the surface at normal incidence this means on gold surfaces polydT-SH stands more upright structure with the plane of the nucleobases relatively parallel to the surface while polydA lies flat on the surface with the plane of the nucleobases relatively perpendicular to the surface (see the idealized schematic in Figure 4.9). Similar trends were observed with surface-bound double-stranded DNA oligomers[111] and surface-bound single-stranded peptide nucleic acids[163] on gold surfaces. This result is also consistent with previous studies that show polydT-SH binds mostly through the thiol group and polydA binds mostly through the nucleobases[148-150]. However, the amount of polarization-dependent in the nitogen *k*-edge spectra of both ssDNA samples is relatively small. This is suggestive of disorder in the ssDNA monolayers.

4.4 Conclusions

The major conclusions from the present study are

- NEXAFS spectra at the carbon *k*, nitrogen *k* and oxygen *k*-edges of the DNA nucleobases exhibit a range of features that can be assigned to specific species in the nucleobases.
- The carbon *k* and oxygen *k*-edge NEXAFS spectra show significant differences with the addition of the sugar and phosphate components of DNA. The nitrogen *k*-edge NEXAFS spectra of adenine and guanine show noticeable shifts in the peak positions of the π^* peaks upon addition of the sugar and phosphate groups.
- Polarization-dependent NEXAFS experiments demonstrate the ability to probe different molecular orientations adopted by polydT-SH and polydA on gold surfaces.

4.5 Credits

Financial support from NESAC/BIO (NIH Grant EB-002027) and NIH Grant EB-001473 are gratefully acknowledged. Dr. Zugen Fu is gratefully acknowledged for his help with the experiments and discussion. Members of the NESAC/BIO group are thanked for their helpful discussions and suggestions. The NEXAFS studies were performed at the NSLS, Brookhaven National Laboratory, which is supported by the DOE, Division of Materials Science and Division of Chemical Sciences. Certain commercial names are identified for purposes of example or clarity; such identification does not indicate endorsement by the National Institute of Standards and Technology.

Table 4.1 Chemical structures of the DNA nucleobases.

Adenine (A)	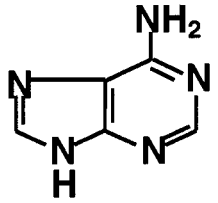
Cytosine (C)	
Thymine (T)	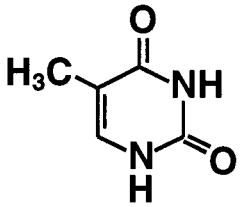
Guanosine (G)	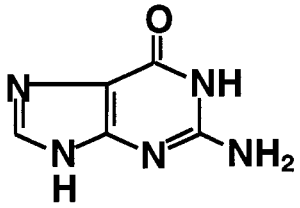
Uracil (U)	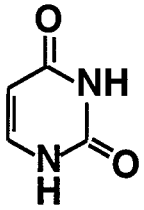

Table 4.2 Peak positions of the prominent π^* features in the nitrogen k-edge NEXAFS spectra for DNA nucleobases, nucleotides, and nucleosides.

	π^*_1 (eV)	π^*_2 (eV)
A	399.3	401.2
C	399.0	400.2
T	401.2	-
G	399.9	400.7
U	401.0	-
A+S	399.4	401.7
C+S	399.0	400.1
T+S	401.0	-
G+S	399.9	401.6
U+S	401.0	-
A+S+P	399.4	401.2
C+S+P	399.9	400.8
T+S+P	401.3	-
G+S+P	399.8	401.0
U+S+P	401.3	-

A = Adenine, T = Thymine, C = Cytosine, G = Guanine, U = Uracil,
S = Sugar, and P = Phosphate group.

Table 4.3 Elemental composition determined by XPS for the ssDNA oligomers adsorbed onto gold surfaces from TE buffer for 24 hrs.

Atomic Percentages ± standard deviation

	C1s	N(1s)	O(1s)	P(2p)	S(2p)	Au(4f)
PolydT-SH (24hrs)	46.8±1.1	6.7±1.0	24.8±0.2	2.9±0.6	0.0	18.8±0.3
PolydA (24hrs)	40.0±1.8	7.8±0.5	15.4±0.4	1.2±0.2	0.0	35.5±1.2

Table 4.4 Theoretical elemental compositions of the DNA oligomers vs the XPS-determined elemental compositions without including gold.

	C1s	N(1s)	O(1s)	P(2p)	S(2p)	P/N	C/N	O/N
PolydT-SH (24hrs)	57.7±1.2	8.2±1.3	30.5±0.3	3.6±0.7	0.0	0.4	7.0	3.7
PolydT-SH (theoretical)	50.9	9.5	34.3	5.0	0.3	0.5	5.4	3.6
PolydA (24hrs)	62.1±1.7	12.1±1.0	23.9±0.6	1.8±0.3	0.0	0.15	5.1	2.0
PolydA (theoretical)	47.6	23.8	23.8	4.8	0.0	0.2	2.0	1.0

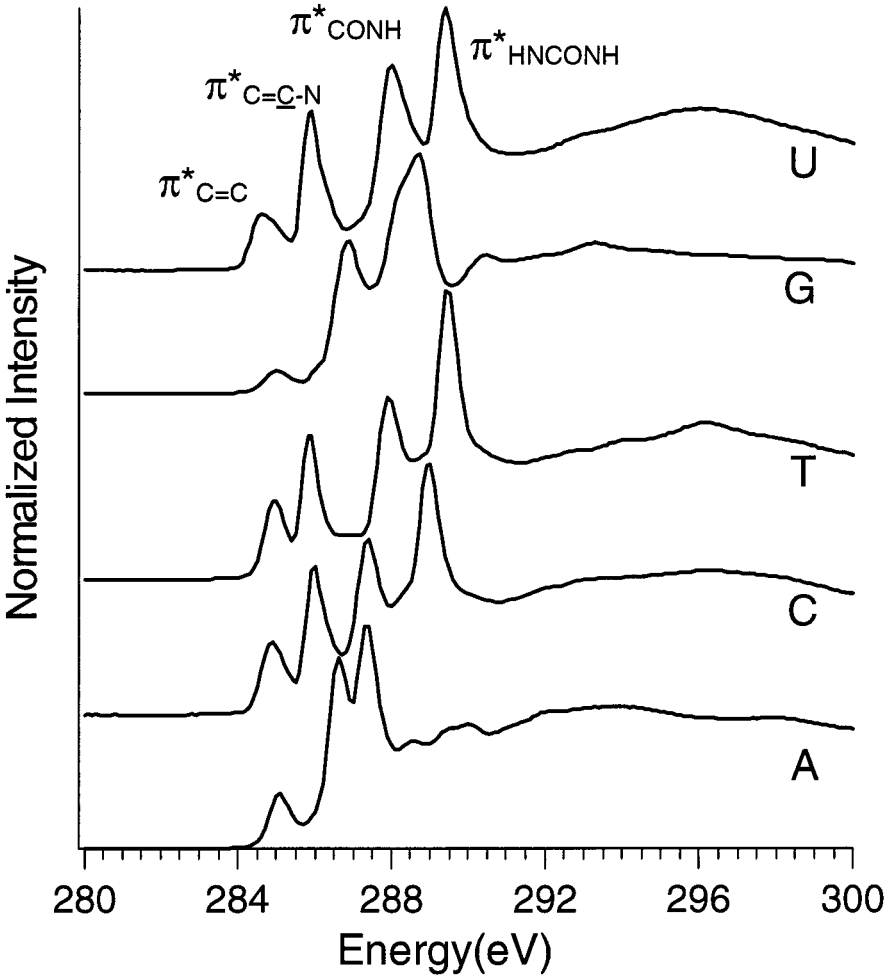

Figure 4.1 Carbon k-edge NEXAFS spectra of DNA nucleobases.

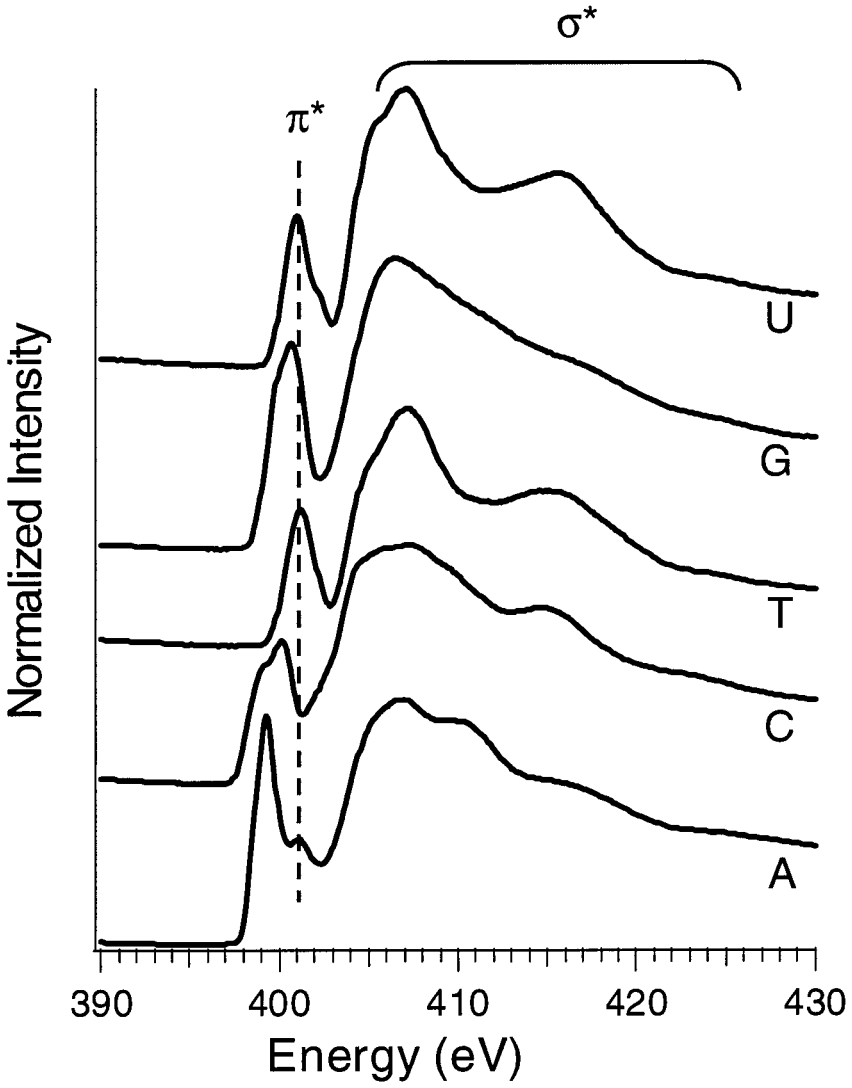

Figure 4.2 Nitrogen k-edge NEXAFS spectra of DNA nucleobases.

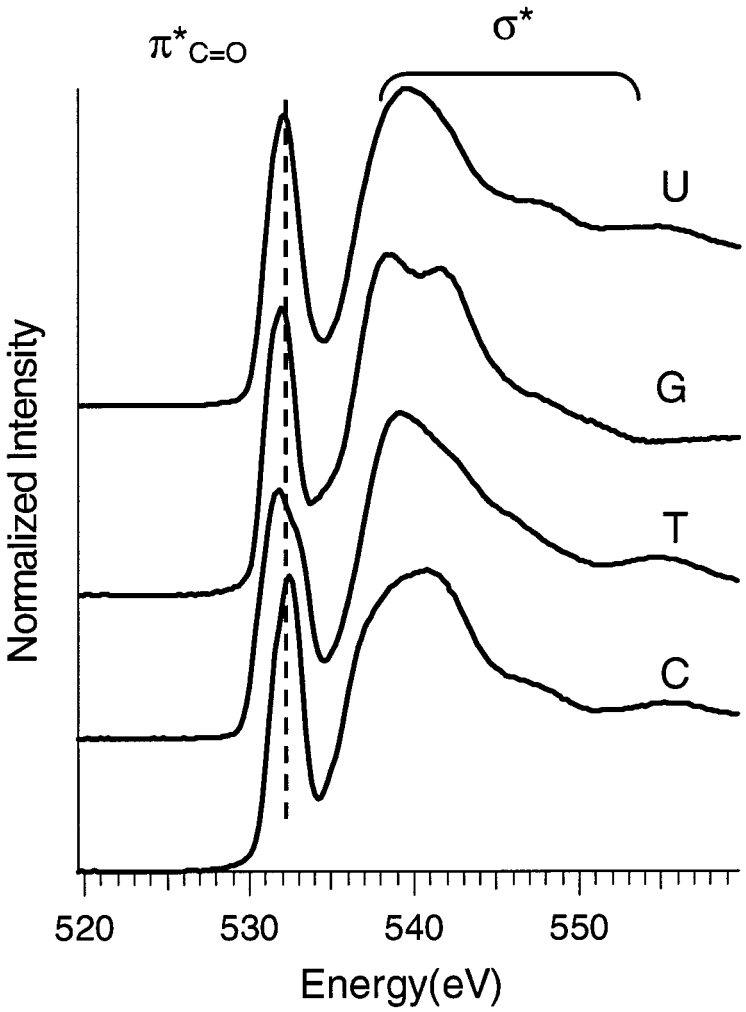

Figure 4.3 Oxygen k-edge NEXAFS spectra of DNA nucleobases.

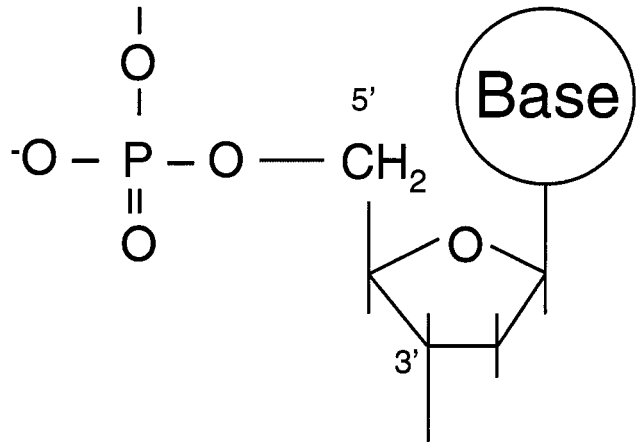

Figure 4.4 Schematic representing the chemical structure of DNA with its nucleobase, sugar and phosphate components.

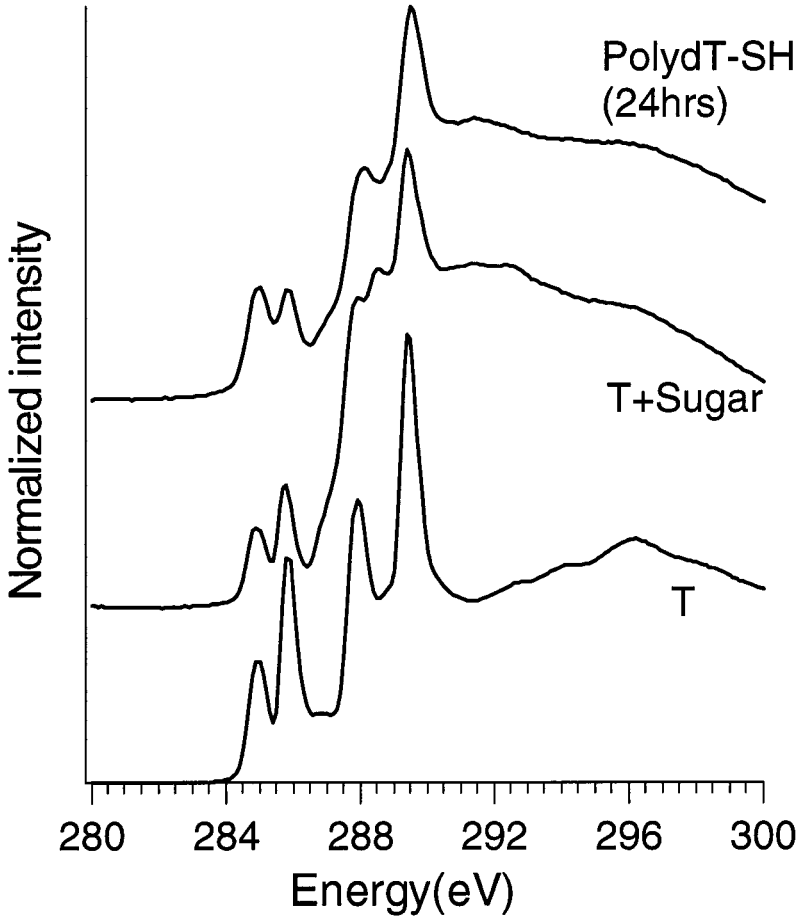

Figure 4.5 The effect on the carbon k-edge NEXAFS spectra from adding the sugar and phosphate groups of DNA to thymine (T).

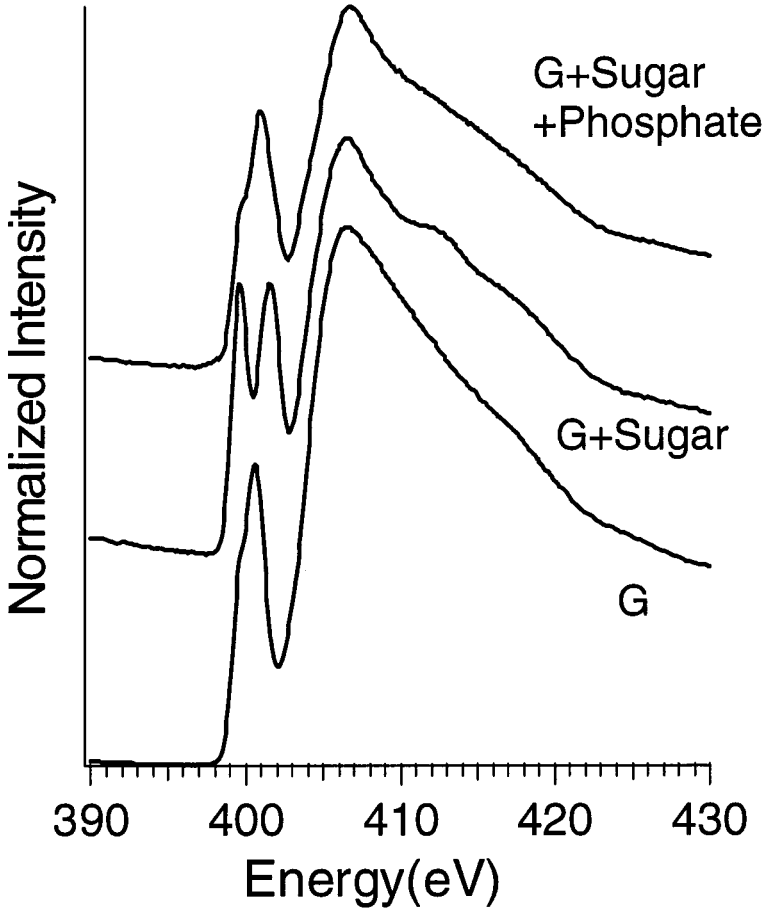

Figure 4.6 The effect on the nitrogen k-edge NEXAFS spectra from adding the sugar and phosphate groups of DNA to guanine (G).

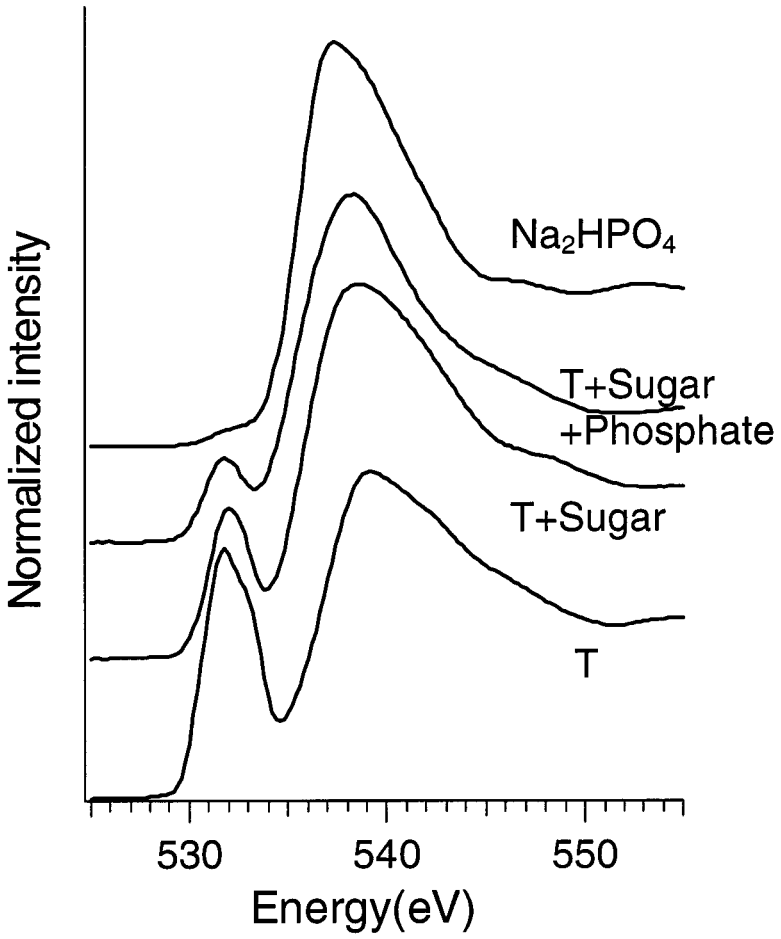

Figure 4.7 The effect on the oxygen k-edge NEXAFS spectra from adding the sugar and phosphate groups of DNA to thymine (T).

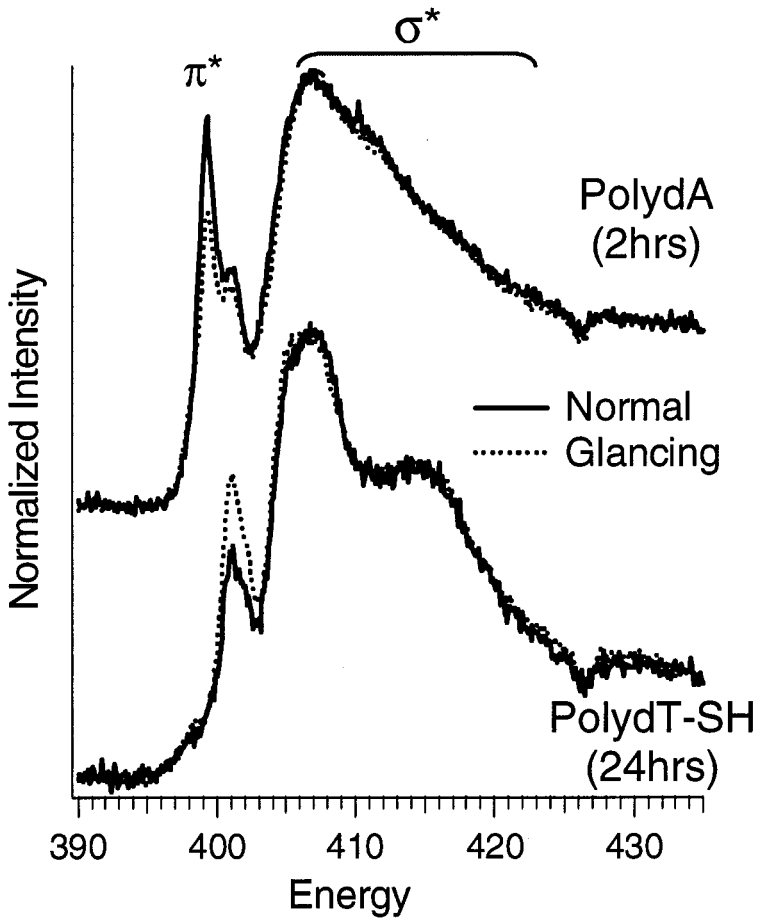

Figure 4.8 Nitrogen k-edge NEXAFS spectra at normal and glancing x-ray incidence for ssDNA oligomers adsorbed onto gold surfaces. (a) PolydA (24 hrs adsorption time) and (b) PolydT-SH (24 hrs adsorption time).

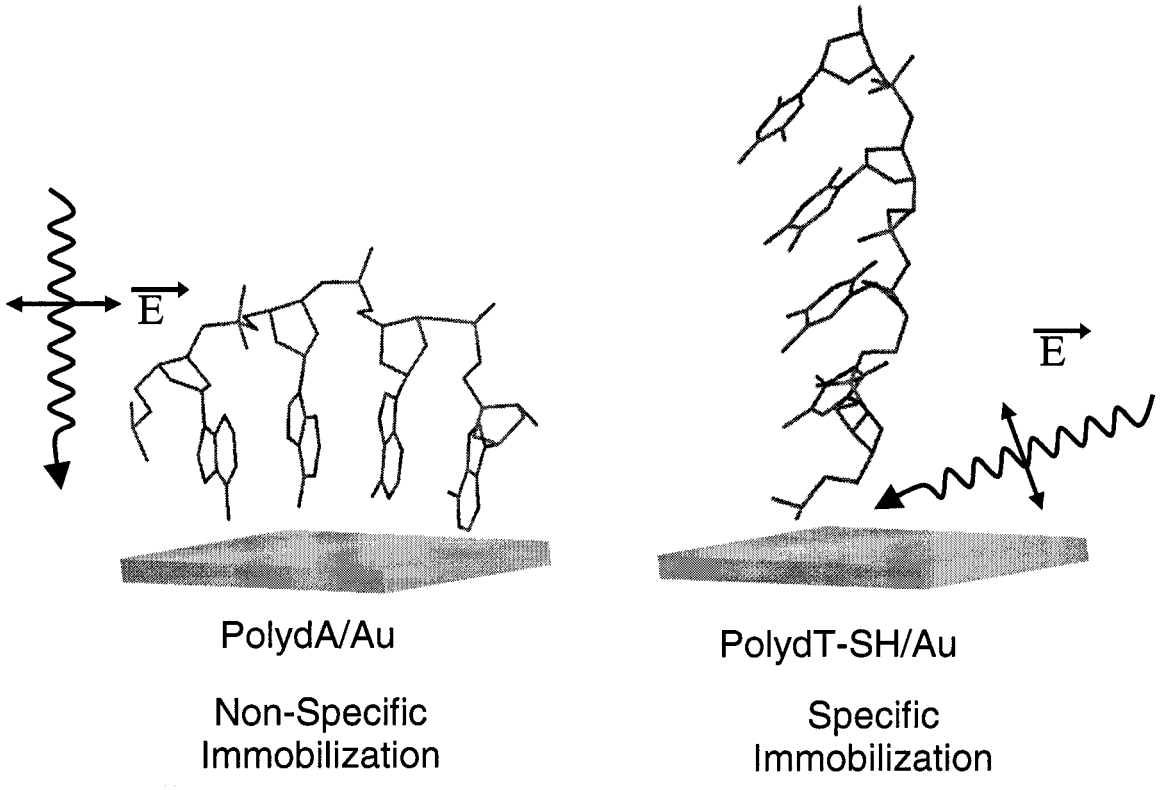

Figure 4.9 Idealized schematic indicating the orientation of the polydT-SH and polydA oligomers on gold surfaces. The orientations of the incident x-rays and electric vectors that produce maximum intensity in the π^* region for each ssDNA oligomer are also shown.

5 : NEXAFS Characterization of Surface-Bound Peptide Monolayers on Hydrophobic Surfaces

Controlling and characterizing the structure of surface-bound bioactive peptides is important for applications like diagnostics, tissue engineering, and biomedical implants. In this study, the ability to characterize the secondary structure of surface-bound peptides with near-edge x-ray absorption fine structure (NEXAFS) spectroscopy is demonstrated. Well-defined sequences of lysine (K) and leucine (L) containing peptides have been known to spontaneously adsorb onto hydrophobic substrates with their secondary structures intact. X-ray photoelectron spectroscopy (XPS) results confirmed the adsorption of the different peptides onto the hydrophobic substrates. The peptides showed characteristic polarization-dependence at their nitrogen and oxygen *k*-edge spectra based on their molecular structure. Complementary Infrared spectroscopy experiments also confirmed the different molecular structures of the peptides. The results reveal that the peptides adsorb with their secondary structures intact onto hydrophobic surfaces, and also demonstrate NEXAFS is a powerful tool for chemical and structural characterization of surface-bound peptides.

5.1 Introduction

Immobilization of bioactive peptides onto surfaces is an area of considerable interest in a range of research areas such as tissue engineering, diagnostics, affinity separations, cell-culture technologies, peptide microarrays and nanobiotechnology[5,164-170]. The surface region, the "Biomolecular interface," plays a crucial role in the above diverse applications[171]. The key element to retaining the biological specificity of the interface is to preserve the structure of immobilized peptides and proteins. As a result when characterizing biomolecules in the interfacial region it is important to address the following questions: identity, concentration, spatial distribution, conformation and orientation[6]. The ability to characterize the adsorbed structure of the interfacial region with near-edge x-ray absorption fine structure (NEXAFS) is shown using peptides which adsorb with different secondary structures.

Alpha-helices and beta-sheets are two secondary structural motifs in proteins. These two structures primarily differ in the way the backbone is folded. Beta-sheet is a more elongated structure that could be considered as a special helix with 2.0 residues per turn. In contrast, alpha-helix has a helical structure with 3.6 residues per turn. Short sequences of lysine and leucine containing peptides have been shown to spontaneously self-assemble at the air-water interface with well-defined secondary structures[172]. In particular, by changing the periodicity of the hydrophobic (leucine) and the hydrophilic (lysine) residues, they could be induced to fold into well-defined secondary structures (α-helix or β-sheet). Recently, the ability of the LK alpha-helical peptides to spontaneously adsorb onto hydrophobic surfaces retaining their α-helix secondary structure has been demonstrated with solid-state nuclear magnetic resonance (ssNMR)[95] and Sum Frequency Generation (SFG)[173]. The structure of the beta-sheet peptides has been characterized *in situ* at the air-water interface with polarization-modulation infrared reflection absorption spectroscopy (PMIRRAS) and found to retain their beta-sheet structure[174].

NEXAFS spectroscopy is a fairly new technique for characterization of biomolecules on surfaces. It is a core-level spectroscopic technique which can be used for chemical and structural characterization[32]. Since it uses polarized x-rays from a synchrotron source, it can be used for structural characterization by monitoring x-ray absorption as a function of the polar angle between the incoming x-rays and the sample surface. NEXAFS has been employed for structural characterization of self-assembled monolayers[175], DNA monolayers[111], peptide nucleic acid monolayers[163], protein adsorption on polymers[176]. Recently, the ability to chemically characterize amino acids and nucleic acids has been demonstrated[43-45]. Also, the ability to image protein-surface interactions at high spatial resolution using NEXAFS microscopy has been demonstrated[176].

Several analytical tools have been employed for chemical and structural characterization of biomolecules on surfaces[6]. Recently, detailed characterization of the structure of beta-sheet peptides on surfaces has been done with grazing incidence x-ray diffraction (GIXD)[177,178] and carbon nanotube modified atomic force microscopy (AFM)[179]. These

methods have demonstrated the ability to obtain high-resolution, detailed surface-structure information. However, these techniques lack chemical specificity. NEXAFS represents a method for characterizing biomolecules that can provide the chemical specificity. The main goal of the present work is to establish the ability to obtain secondary structural information with NEXAFS by using peptides with well-defined secondary structures. X-ray photoelectron spectroscopy (XPS) and infrared spectroscopy (IR) measurements were done to support the NEXAFS results.

5.2 Experimental Details

5.2.1 Radio Frequency Glow Discharge Deposition (RFGD)

Silicon wafers were obtained from Silicon Valley Microlectronics, Inc. They were cut into 1cmx1cm pieces. The cut silicon pieces were later cleaned by sonicating twice in methylene chloride, acetone and methanol, in that order. They were then blown dry with nitrogen and used as substrates for plasma deposition.

The hydrophobic fluoropolymer films (henceforth called HFP surfaces) were deposited from a hexafluoropropylene RFGD using a home-built, inductively-coupled RF reactor described in detail elsewhere[96]. Cleaned silicon pieces were placed in the glow region of the reactor. They were initially etched in an argon pressure of 150 mTorr for 5min at an input power of 40W. A fluorocarbon film was then deposited onto the windows using an input power of 80W for 1min followed by a 4min deposition with an input power of 20W. The fluorocarbon films were quenched for 5min under flowing hexafluoropropylene monomer with the RF power turned off. The coated silicon pieces were then later analyzed by x-ray photoelectron spectroscopy (XPS) to confirm the composition of the fluorocarbon films.

5.2.2 Preparation of Rubbed Polyethylene (PE) surface

Cleaned silicon pieces were cut into ~ 1x10 cm pieces. A block of polyethylene (PE) was cleaned by sonicating in methylene chloride, acetone and methanol sequentially and

then blown dry with nitrogen. The cleaned silicon pieces were placed on a hot plate heated to ~ 110°C. Once the silicon pieces reach the desired temperature, the PE blocks were drawn across the surface of the silicon pieces under a mass of ~1 kg and a speed of ~ 1 mm/s. This produced a surface of long parallel $(CH_2)_x$ chains with readily apparent grooves[51,180]. The rubbed PE surfaces prepared by this procedure were later cut into ~1cmx1cm pieces and used for the peptide adsorption experiments.

5.2.3 Peptide Synthesis

All the peptides were prepared on an Applied Biosystems automated synthesizer (ABI 433A) using MBHA resin. The 9-fluoroenylmethoxycarbonyl (Fmoc) protected amino acids and the resin were purchased from Anaspec, Inc. The peptides were cleaved from the resin using 95% trifluoroacetic acid with 2.5% triisopropylsilane and 2.5% water. The crude peptides were purified using a Waters reversed-phase high pressure liquid chromatography (HPLC) C-18 column using a water/acetonitrile solvent system containing 0.1% trifluoroacetic acid[95]. The purity and integrity of the peptides were analyzed with electrospray mass spectrometry.

5.2.4 Peptide Adsorption

Phosphate buffered saline (PBS, pH=7.4) was obtained from FischerBiotech. The samples were prepared by placing 1cm x 1cm pieces of the fluorocarbon coated silicon substrates in 20μg/ml of the peptide solution in PBS avoiding air-water interface. The sample with the peptide solution was held in 1.5ml polystyrene cups for 2hrs. The samples were then washed with DI water by dilution displacement and blown dry with nitrogen.

5.2.5 X-ray Photoelectron Spectroscopy

All XPS spectra were taken on a Surface Science Instruments X-probe spectrometer. This instrument has a monochromatized Al Kα x-ray source and a low energy electron flood gun for charge neutralization. X-ray spot size for these acquisitions was ~ 800μm.

Pressure in the analytical chamber during spectral acquisition was less than 5 x 10^{-9} Torr. The analyzer pass energy for the survey spectra (composition) was 150 eV and was 50eV for high resolution C1s spectra. The take-off angle (the angle between the sample normal and the input axis of the analyzer lens) was 55° (55 degree take-of angle ≈ 50 Å sampling depth). Further details about the XPS analysis procedures have been published elsewhere[31,97,98].

The Service Physics ESCAVB Graphics Viewer program was used to determine peak areas, to calculate the elemental compositions from peak areas and to peak fit the high resolution spectra. The binding energy scale of the high-resolution C1s spectra was calibrated by assigning the CF_2 peak in the C1s high-resolution spectrum a binding energy of 292.0 eV. The surface composition data represent the average over two different samples and 2 spots per sample. The data for the control samples represent the average over 8 different samples from several different depositions of the plasma polymer.

5.2.6 Infrared Spectroscopy

Infrared (IR) spectra were recorded with a Bruker Tensor 27 FT-IR spectrometer. The spectrum was recorded using a single reflection horizontal attenuated total reflectance (ATR) accessory (GATR™), which uses a Ge ATR crystal, supplied by Bruker. The angle of incidence of the incoming photon is 65°. The sample is pressed against the face of the crystal so the light is total internally reflected back into the crystal and detected. The spectra were recorded at a spectral resolution of 2 cm^{-1} and 512 scans were recorded and averaged for each spectrum. The sample chamber was purged with dry air for 15 min. between different samples. A background spectrum of the HFP surface was recorded and was subsequently subtracted from the spectrum of the peptide-adsorbed HFP surface to obtain the peptide spectrum.

5.2.7 Near-Edge x-ray Absorption Fine Structure (NEXAFS)

The NEXAFS experiments were done at the National Synchrotron Light Source (NSLS) U7-A beamline at Brookhaven National Laboratory. The beamline uses a ~85% polarized, high intensity beam and a monochromator with 600 l/mm grating, producing a full-width at half-maximum (FWHM) of ~0.15eV at the carbon *k*-edge. The monochromator energy scale was calibrated using the absorption peaks in the Io grid spectra for the carbon and oxygen edges. They were previously calibrated by setting the C(1s) $\rightarrow \pi^*$ transition in the graphite carbon *k*-edge NEXAFS spectrum to 285.35 eV[120]. The nitrogen edge was calibrated to the intense π^* amide feature of poly(glycine) at 401.5 eV[43,161]. The NEXAFS spectra were normalized with the signal from an *in situ* gold coated 90% transmission grid placed in the path of the x-rays. Partial electron yield (PEY) was monitored using a channeltron with a negatively applied bias voltage to monitor the Auger and photoelectron yield from the sample. The bias voltage was maintained at -150 V for the carbon *k*-edge spectrum, -280 V for the nitrogen *k*-edge spectrum and -390 V for the oxygen *k*-edge spectrum. The higher bias voltage for the nitrogen and the oxygen *k*-edges was used to reduce the auger yield from the carbon and the nitrogen atoms. This procedure allowed easier background subtraction and better normalization of the spectra obtained at different polar angles.

Figure 5.1a shows a schematic of the NEXAFS experimental setup for doing the polarization-dependent x-ray absorption experiments. Polarization-dependent experiments were done by monitoring the NEXAFS spectra at various polar angles (angle between the incoming x-ray and the sample surface). At normal x-ray incidence, the electric field vector (**E**) is in the plane of the surface while at glancing x-ray sincidence the **E** vector is 20° from the surface normal. The pre-edge was subtracted from the spectra using a linear background and the spectra were normalized to unit absorption jump height. The above procedure makes the edge-jump, which is the difference in the signal in the region about 40 eV above and below the first resonance, to be unity. A disordered system does not show any polarization-dependence because of random distribution of the molecular orientations. However, a polarization-dependence is indicative of directional alignment of the molecules in the overlayer[32].

5.3 Results and Discussion

5.3.1 XPS Characterization

Table 5.1 lists the surface composition of the HFP surface modified with the peptide molecules. The surface composition of the control HFP surface shows that the surface chemistry can be well-controlled. Upon addition of the different peptides, there is an increase in the nitrogen and the oxygen concentrations, followed by a significant decrease in the fluorine composition. The XPS data show that the different peptides adsorb onto the HFP surface, producing a nitrogen surface concentration of ~ 4 atomic percent. The XPS data for the rubbed PE surfaces also indicate the adsorption of the peptides, resulting in a nitrogen concentration of ~ 3 atomic percent. The above results demonstrate the ability to modify the HFP and PE surfaces with the peptides. The results are consistent with other recent reports for the adsorption of the peptides onto hydrophobic surfaces[173].

5.3.2 NEXAFS Characterization of HFP Surface

Previous experiments indicated that highly structured fluoropolymer surfaces could be obtained by plasma-deposition for samples placed downstream to the glow region[181,182]. The presence of surface structure in the fluorocarbon control samples could make the interpretation of the peptide carbon *k*-edge NEXAFS spectra more difficult. Hence, polarization-dependent NEXAFS experiments were done on the control HFP surface (Fig. 5.2). The main peaks in the HFP spectrum are from the fluorocarbon $\sigma^*_{C\text{-}F}$ and $\sigma^*_{C\text{-}C}$ transitions[51,181]. The peaks at 285 and 287.4 eV are from the hydrocarbon-like groups on the surface, since the plasma polymer does not retain the structure of the HFP monomer, as revealed from the XPS surface composition results (Table 5.1). The NEXAFS data for the HFP surface (Fig. 5.2) reveal the absence of polarization-dependence. Hence, these HFP fluorocarbon surfaces prepared by depositing in the glow region of the chamber are disordered.

5.3.3 NEXAFS Characterization of Adsorbed Peptides

The structure of the adsorbed peptide on the HFP surface was then examined with polarization-dependent NEXAFS. The structure of the different peptides and a schematic of their expected folded secondary structure are outlined in Figure 5.1b. The polarization-dependent nitrogen *k*-edge NEXAFS spectra of the LKα and LKβ 9mer peptides adsorbed onto the fluorocarbon surface are shown in Figure 5.3. The peak at 401.5 eV in the spectra is from the amide π^*_{CONH} peak in the backbone of the peptides[43,161]. The peaks seen in the spectra between 405 – 415 eV are due to the σ* resonance[43,161]. The small peak seen at 398.8 eV is due to the nitrogen contamination in the fluoropolymer surfaces (~0.2% by XPS). The spectra reveal the two different peptides exhibit a different polarization-dependence for the backbone π^*_{CONH} peak. Also, the polarization-dependence observed for the σ* peak of the beta-sheet peptide indicate the peptide adopts a flat orientation on the surface.

We hypothesized that the polarization-dependent NEXAFS spectra should be sensitive to different secondary structures of the peptide. This is motivated by previous theoretical calculations which revealed the polarization-dependent NEXAFS spectra to be sensitive to the helical structure of the fluorocarbon chains in rubbed poly (tetrafluoroethylene)[51]. The polarization-dependence is measured by varying the incoming x-ray angle of incidence, which varies the orientation of the electric vector of the incoming polarized x-ray beam with respect to the surface (shown in Fig. 5.1a). This results in a change of incident x-ray coupling to the different bonds in the molecule. The different secondary structures have different spatial orientations of the backbone atoms as shown in the schematic (Fig. 5.1b). The backbone atoms have a more periodic structure in the β-sheet compared to the α-helical peptide. Due to the three dimensional orientation of the backbone for the α-helix, the polarization-dependence should be markedly different compared to the β-sheet. To test this hypothesis, additional peptides were synthesized. The LK310 has a different primary sequence compared to the LKα and was shown to retain a α-helix structure upon adsorption onto the surface. A longer version of the β-sheet peptide was also synthesized.

Figure 5.4 shows the summary of the polarization-dependence seen at the π^*_{CONH} peak for all the different peptides at the nitrogen *k*-edge. The polarization-dependence was determined by first obtaining the difference spectra, which is the difference of the normalized spectra at glancing incidence to that at the normal incidence. The peak intensity for the π^* peak was then calculated by fitting a gaussian to the peak and determining the area under the peak. Each bar in the figure represents the average over two different samples of the adsorbed peptide on a fluorocarbon sample. As could be discerned from the Fig. 5.4, the different peptides have different polarization-dependences.

Figure 5.5 shows the polarization-dependent oxygen *k*-edge NEXAFS spectra for the peptides adsorbed onto the HFP surface. The main peak at 531.8 eV is from the peptide backbone π^*_{CO} peak[43,161]. The broader peaks at 540 eV and 545 eV are from the peptide σ^* peaks[43,161]. The LKβ 9mer peptide shows intense polarization-dependence at the π^* peak compared to the the LKα peptide. The oxygen π^* polarization-dependence for the different peptides adsorbed onto the HFP surface are summarized in Figure 5.6. The results show that the polarization-dependence from the π^* peak vary with the secondary structure of the adsorbed peptides, similar to the nitrogen *k*-edge data.

5.3.4 NEXAFS Characterization of Peptides on Rubbed PE Surface

Additionally, the effect of orienting the peptides in the plane of the substrate was determined by adsorbing the peptide onto a rubbed PE surface. The rubbed polymer surfaces show strong anisotropy in the plane of the substrate and has the polymer backbone oriented along the rubbing direction[180,183,184]. Rubbed PE has been extensively investigated because of its ability to orient liquid crystals. The XPS data in Table 5.1 shows that the peptides adsorb onto the rubbed PE surfaces (~3% nitrogen detected). The peptides are thought to adsorb onto the surface along the rubbing direction similar to liquid crystal alignment onto rubbed polymer surfaces. Figure 5.7 shows the nitrogen *k*-edge NEXAFS spectra of the peptides adsorbed onto the rubbed PE surface. The LKβ 9mer shows strong polarization-dependence in the π^*_{CONH} peak at 401.5 eV. Also, it

shows polarization-dependence in the σ* peak at ~415 eV indicative of the peptide adsorbed onto the surface with the backbone nearly parallel to the surface. However, the LKα peptide does not show intense polarization-dependence because of its α-helical structure. Hence, the results for the peptides adsorbed onto the rubbed PE surface shows trends similar to the peptides adsorbed onto the disordered HFP surface. The above results further support the conclusions for the peptide adsorbed onto the HFP surface – the observed polarization-dependence in the nitrogen and oxygen *k*-edge region are characteristic of the different secondary structures of the peptides.

5.3.5 Infrared Characterization

To verify the secondary structure of the adsorbed peptide on the HFP surface, complementary infrared experiments were done. The IR absorption data for the different adsorbed peptides in the amide I bands are shown in Figure 5.8. The amide I region principally corresponds to the C=O stretch which is weakly coupled with C-N stretch and N-H bending[185]. The position of the amide I is very sensitive to the secondary structure of proteins and peptides[185]. The control HFP surface does not show any peaks in the amide I region. The control surface shows intense peaks around 1200-1400 cm^{-1} from the C-F bonds present in the control polymer[181]. The LKα peptide adsorbed onto the HFP surface shows a strong amide I peak at 1656 cm^{-1} characteristic of the peptide in a α-helix structure. The LKβ 9mer adsorbed onto the HFP surface shows a strong amide I peak at 1630 cm^{-1} characteristic of the peptide in a β-sheet structure. Thus, the IR results confirm the peptides retain their secondary structure after adsorption onto the HFP surface.

5.4 Conclusions

The major conclusions from the present study are:

- Well-defined lysine and leucine containing peptides spontaneously adsorb onto hydrophobic surfaces.
- The polarization-dependent NEXAFS spectra in the nitrogen and oxygen *k*-edges are sensitive to the structure of the different adsorbed peptides.

- Complementary infrared measurements confirm the different molecular structures of the adsorbed peptides.

5.5 Credits

Financial support from NESAC/BIO (NIH Grant EB-002027) and NSF Grant DMR-0110505 are gratefully acknowledged. Dr. Zugen Fu and Dr. Daniel Graham are gratefully acknowledged for their help with the experiments and discussion. The NEXAFS studies were performed at the NSLS, Brookhaven National Laboratory, which is supported by the DOE, Division of Materials Science and Division of Chemical Sciences.

Table 5.1 Table 1 Elemental composition determined by XPS for the three different peptides adsorbed onto HFP and rubbed PE surfaces.

	C(1s)	N(1s)	O(1s)	F(1s)
HFP control	39.4±2.5	0.1±0.1	0.4±0.2	60.1±2.6
LKα on HFP	52.4±0.4	4.6±0.2	6.3±0.3	36.7±0.4
LK310 on HFP	52.8±1.1	4.3±0.4	4.8±0.6	38.1±1.9
LKβ 9mer on HFP	50.5±0.8	3.8±0.2	4.4±0.3	41.3±1.0
LKβ 15mer on HFP	50.2±0.4	3.8±0.3	5.5±0.4	40.6±0.7
Rubbed PE control	90.4±0.6	-	9.6±0.6	-
LKα on rubbed PE	91.8±1.6	3.1±0.4	5.1±1.2	
LKβ 9mer on rubbed PE	89.8±1.3	3.1±0.5	7.2±0.8	-

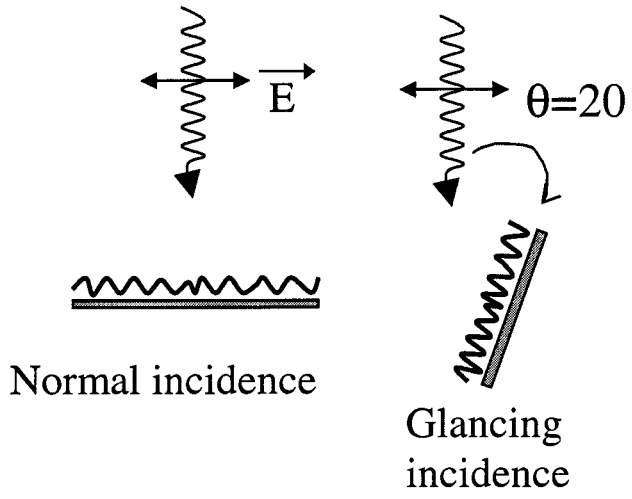

Figure 5.1 (a) Schematic showing the experimental sample geometry and the orientation of the electric vector for the incoming x-ray.

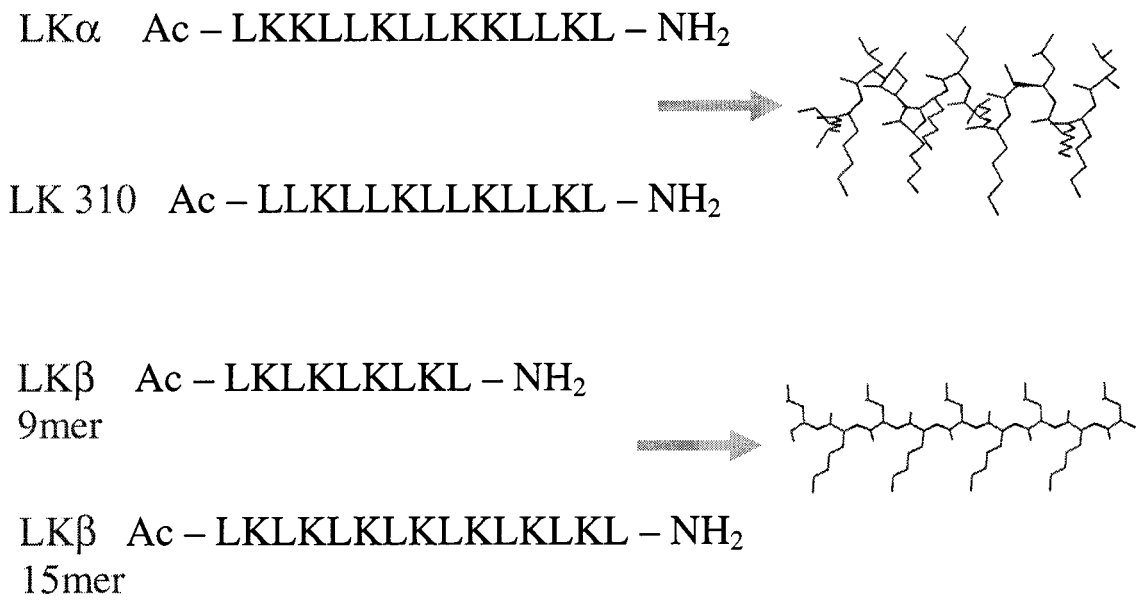

Figure 5.1 (b) Chemical structure of the different LK peptides, and schematic of their different folded secondary structures.

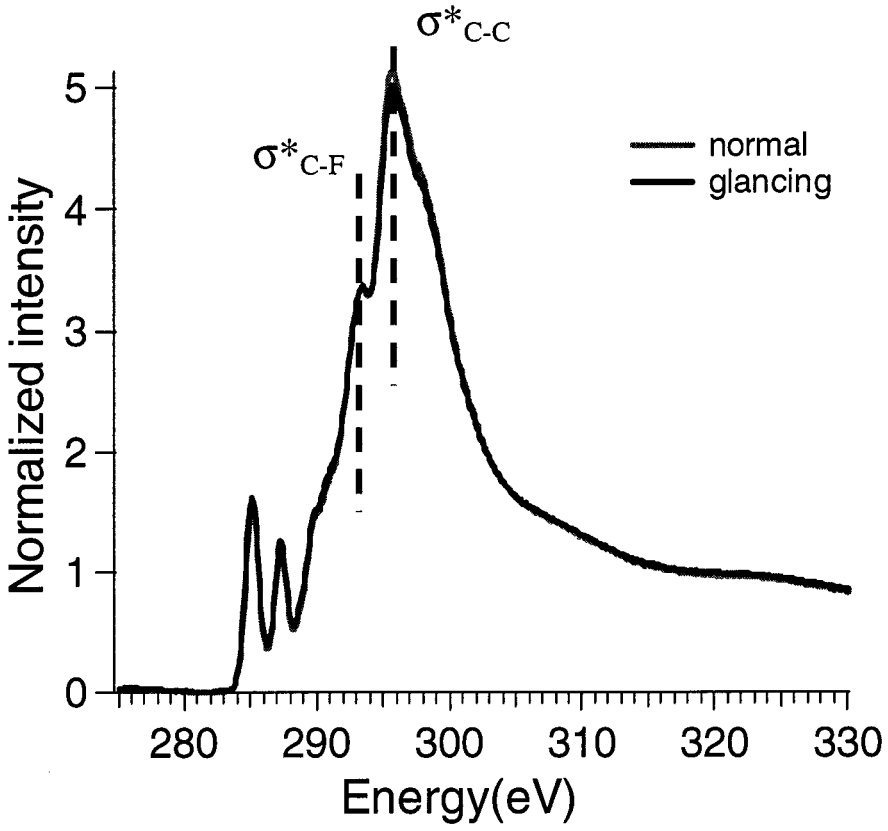

Figure 5.2 Polarization-dependent carbon k-edge NEXAFS spectra of the control HFP surface.

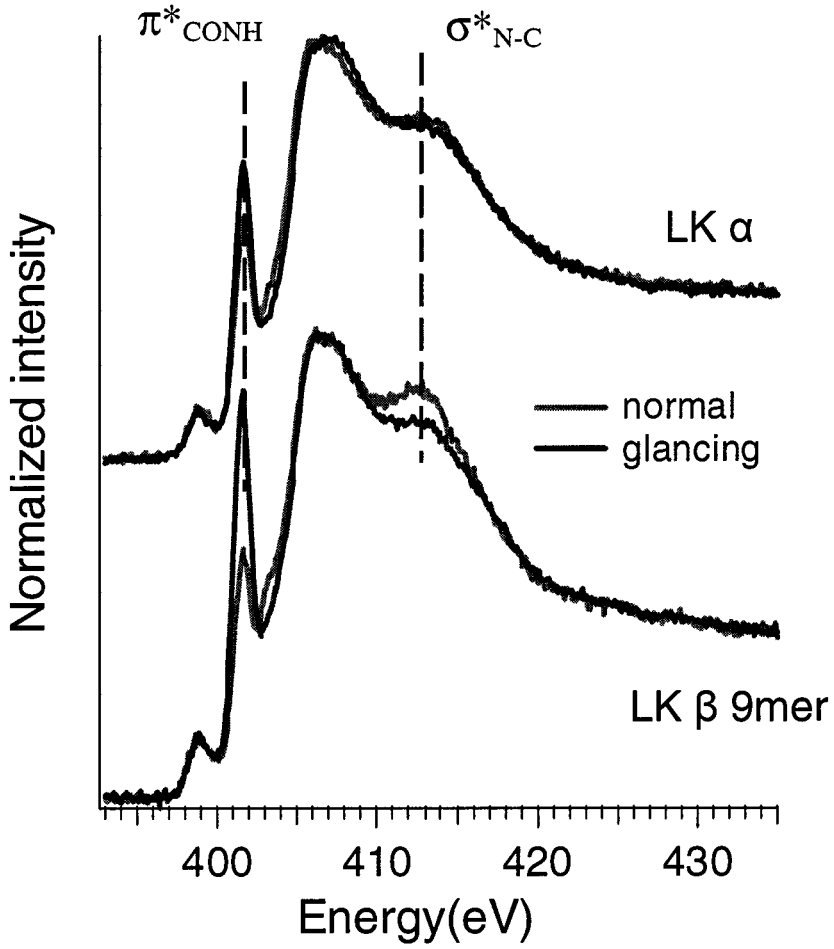

Figure 5.3 Polarization-dependent nitrogen k-edge NEXAFS data for the LKα and the LKβ 9mer peptides adsorbed onto the HFP surface.

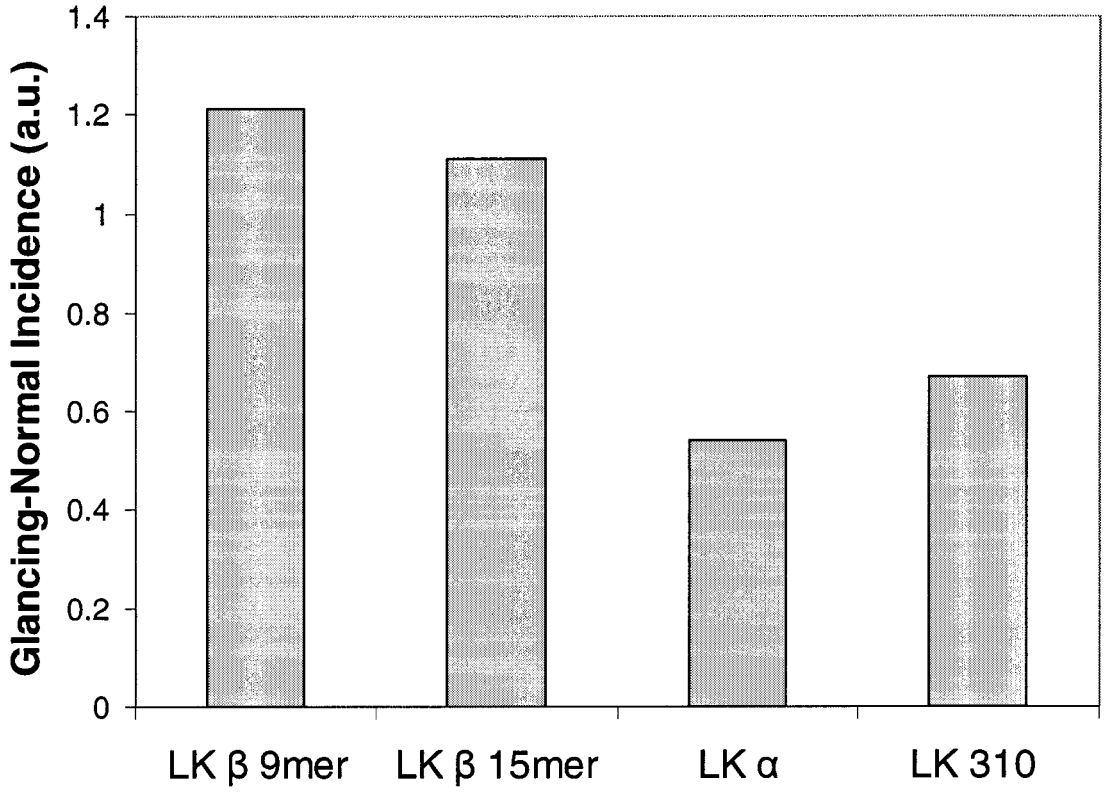

Figure 5.4 Summary of the polarization-dependent nitrogen k-edge NEXAFS data for the different peptides adsorbed ontoHFP surfaces. The different bars indicate the polarization-dependence of the π^*_{CONH} peak at 401.6 eV.

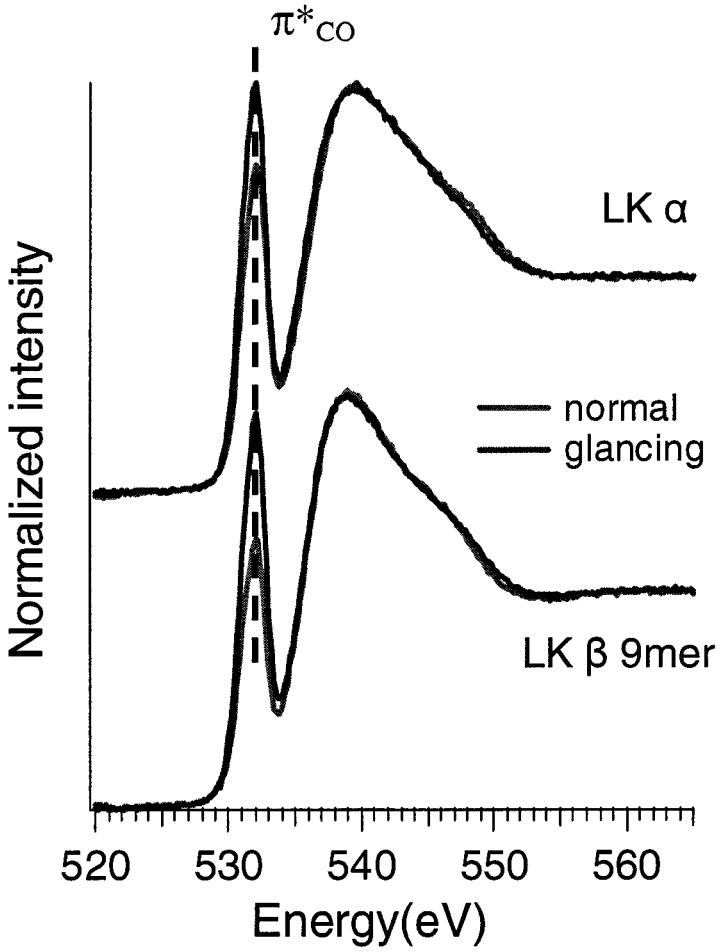

Figure 5.5 Polarization-dependent oxygen k-edge NEXAFS data for the LKα and the LKβ 9mer peptides adsorbed onto the HFP surface.

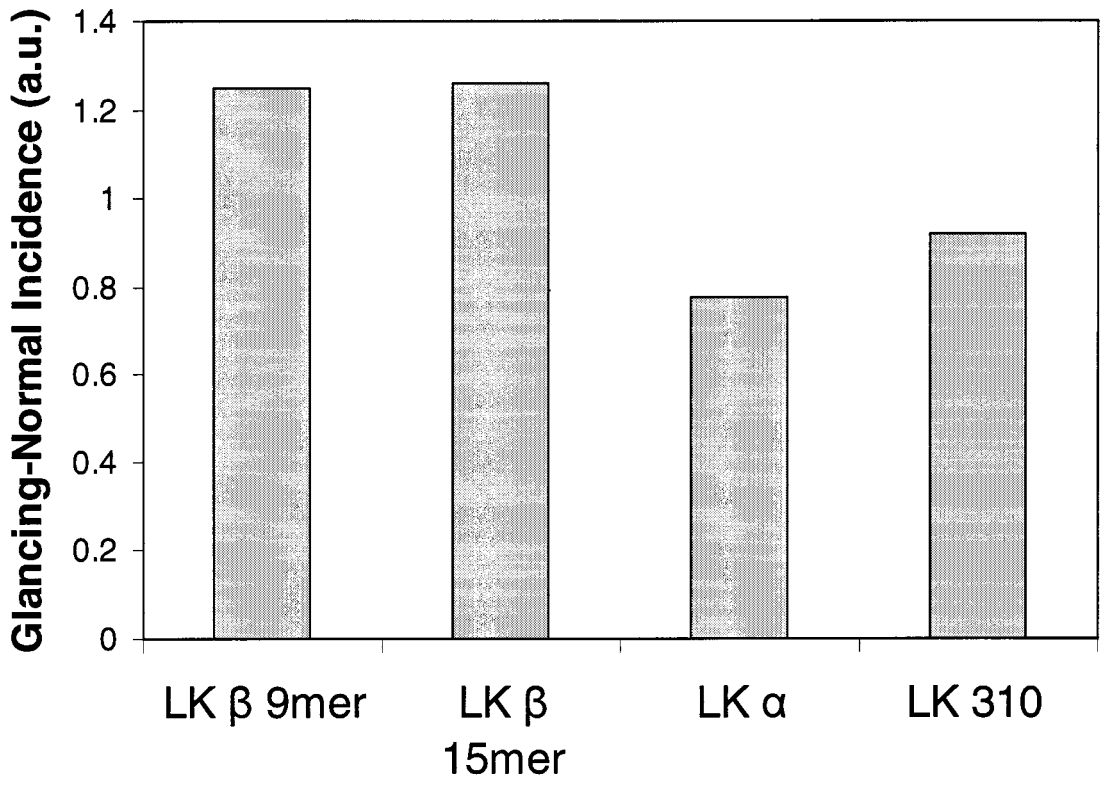

Figure 5.6 Summary of the polarization-dependent oxygen k-edge NEXAFS data for the different peptides adsorbed onto HFP surfaces. The different bars indicate the polarization-dependence of the π^*_{CONH} peak at 531.8 eV.

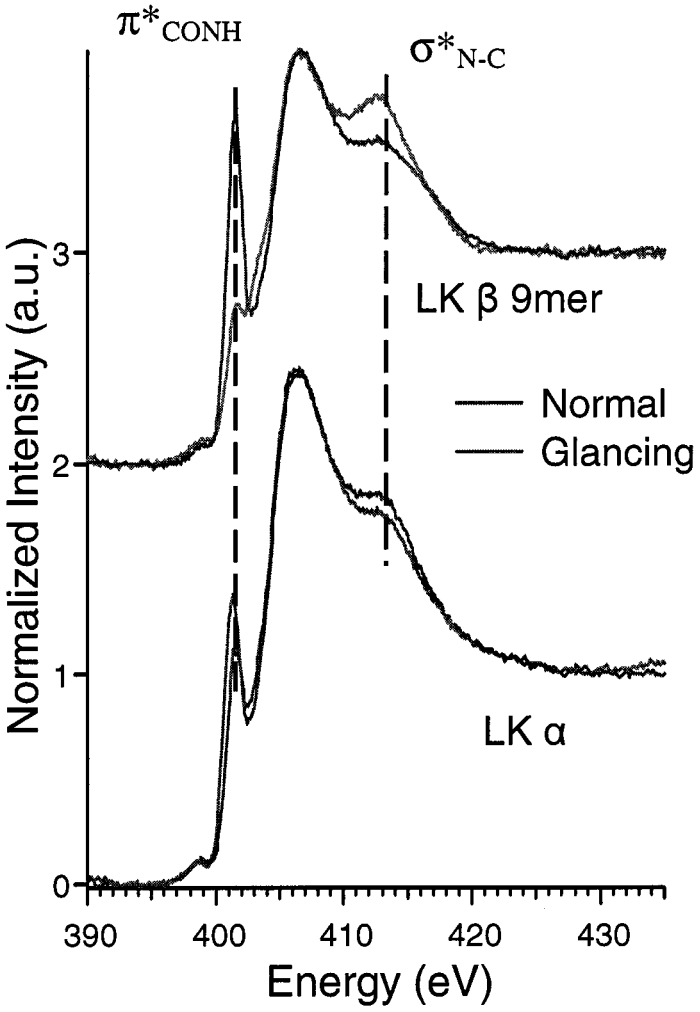

Figure 5.7 Polarization-dependent nitrogen k-edge NEXAFS data for the LKα and LKβ 9mer peptides adsorbed onto the rubbed PE surface.

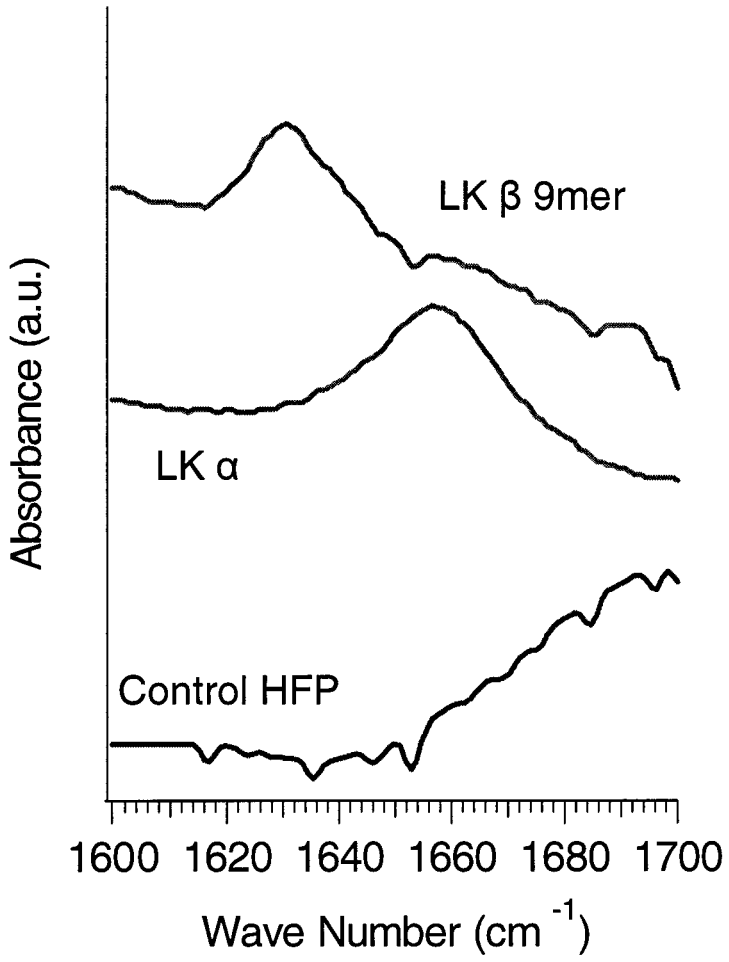

Figure 5.8 Infrared absorption data in the amide I region for the LKα and the LKβ 9mer peptides adsorbed onto HFP surfaces.

6 : In situ Sum Frequency Generation Characterization of Peptide Monolayers on Hydrophobic and Charged Surfaces

Immobilization of bioactive peptides is an active research area for diagnostics, cell culture and biomedical implants. Peptides with well-defined sequences of lysine (K) and leucine (L) have been shown to spontaneously adsorb onto hydrophobic substrates with α-helix secondary structure. In this study the adsorption of these peptides onto hydrophobic and charged surfaces has been characterized *in situ* with IR-Visible Sum Frequency Generation (SFG) spectroscopy. The SFG spectra in the CH and OH stretch regions show that the adsorption of the LK peptides onto hydrophobic and charged surfaces is mediated by interactions through their leucine and lysine residues respectively. These hydrophobic and electrostatic interactions are accompanied by ordering of the functional groups involved in the interaction. Ordering of water molecules at these interfaces is also observed. SFG spectra in the amide I region established that the peptides retain their alpha-helical structure upon adsorption onto the hydrophobic surface.

6.1 Introduction

Determination of the molecular structure of biomolecules immobilized at surfaces and interfaces is an important area of scientific study because of the role they play in a wide range of biological applications[6]. A variety of surface-specific tools have been developed as well as re-adapted from other research fields to examine the surface-structure of biological materials[5,6]. Although vacuum based techniques have excellent advantages and flexibility, they also have the inherent disadvantage of analyzing samples under vacuum instead of in an aqueous biological environment.

Sum-Frequency Generation (SFG) is a fairly new technique that has been recently applied to the investigation of biomolecules at solid surfaces[69,79-82,86,186,187]. SFG has the ability to probe a variety of interfaces. For example, solid-liquid, liquid-liquid and liquid-vapor interfaces can be accessed *in situ*[60,76,188]. SFG involves overlapping two laser beams in time and space onto a solid substrate. One of the incoming beams is a

fixed visible beam and the other a tunable Infrared (IR) beam. The beams mix through 2nd order non-linear optics to generate a third beam at the sum of the two input frequencies. The SFG beam is then detected after passing through a filter and a monochromator. The intensity of the SFG signal is proportional to the the second-order nonlinear susceptibility of the medium ($\chi^{(2)}$). The bulk of a material generally does not generate SFG signal ($\chi^{(2)}$ =0) because it is amorphous (polymers), isotropic (gases and liquids) or has inversion symmetry (centrosymmetric crystals and metals). However, at an interface where there is a break in inversion symmetry or where a media can re-structure to minimize its interfacial free energy, polar ordering can occur resulting in an SFG active interface. The second order non-linear susceptibility is given by, $\chi^{(2)}_{SFG} = \chi^{(2)}_{NR} + \chi^{(2)}_{R}$ where NR represents the non-resonant signal and R represents the resonant signal. By tuning the infrared beam over a frequency range of interest, an enhancement in the SFG signal occurs whenever the incoming IR is in resonance with a vibrational mode of functional groups at the interfacial layer. Hence a surface-vibrational spectrum of the interfacial layer[60,62] is generated providing molecular-level information about the interface. Therefore, SFG spectroscopy is highly surface-specific, chemically specific, and sensitive to the orientation of the functional group.

Various research groups have recently applied SFG to investigate protein adsorption on solid surfaces as well as proteins at the air-water interface[62,69,79,81,82,186,187,189]. Recently, Wang and co-workers reported the observation of amide I signals from adsorbed proteins, which allows for structural characterization of biomolecules at interfaces[86]. As the amide bands are sensitive to the secondary structure of biomolecules, they provide an avenue to investigate the conformation and molecular structure of biomolecules *in situ*. Although the earlier experiments performed in the CH and OH IR regions have provided useful information about the structure of adsorbed proteins[79,81,82,186], due to the complex nature of proteins it has not been possible to relate this information to detailed molecular structure of the proteins. Proteins and polymers typically adsorb onto surfaces in a random fashion. Due to their chemical and structural complexity, unambiguous interpretation of their SFG spectra could not be made. It is known that when proteins adsorb onto hydrophobic surfaces, they show strong alignment of hydrophobic functional

groups[81,82,186]. However, it is not clear whether the interaction between the proteins and surface induces the ordering of these functional groups or whether they were inherently ordered in the macromolecule and retained upon adsorption. Recently, Kim et.al.[83] highlighted the importance of water in hydrophobic interaction and also demonstrated the potential to use SFG to answer fundamental questions in these types of interactions.

In this work we have employed peptides which were designed to adsorb onto the surface with their secondary structures intact. This affords molecular-level control over their surface-structure. In addition, the peptides only contain lysine (K) and leucine (L) residues simplifying their chemical complexity. The sequences of the peptides studied here are:

LKα Ac – LKKLLKLLKKLLKL – NH_2

LK310 Ac – LLKLLKLLKLLKL – NH_2

Previous research has shown that by changing the periodicity of the leucine and lysine residues in the primary sequence of these peptides, they could be made to fold into different secondary structures[172]. In addition, solid-state NMR (SSNMR) studies have shown that these peptides adsorb onto hydrophobic surfaces and retain their secondary structure[95]. The LK310 peptide, which was designed to induce a 3_{10}-helix structure, showed a structure more characteristic of an α-helix based on the SSNMR data[95]. As shown above, the LK310 peptide has a different primary sequence from the LKα peptide.

The goals of the present work are to characterize *in situ* the molecular structure of the LKα and LK310 peptides adsorbed onto hydrophobic fluorocarbon and charged Quartz surfaces, determine the nature of the interaction of these peptides onto hydrophobic/charged surfaces and confirm the observation of amide I signals in SFG.

6.2 Experimental Details

6.2.1 Radio Frequency Glow Discharge Deposition (RFGD)

Circular, 9.53 mm thick CaF_2 windows were obtained from ISP Optics and circular, 6 mm thick quartz windows were obtained from Esco products. Quartz windows were used to acquire SFG spectra in the CH, NH and OH regions. Calcium fluoride windows were used to acquire SFG spectra in the amide region because the quartz windows absorb significant amounts of the incoming IR radiation in the amide region. The CaF_2 windows were cleaned by sonicating them in methanol for 10 minutes followed by blowing dry with nitrogen. The quartz windows were cleaned by sonicating them sequentially in methylene chloride, acetone and methanol for 5 minutes each followed by blowing dry with nitrogen. To create hydrophobic substrates, thin fluorocarbon films were deposited onto the substrates from a hexafluoropropylene RF glow discharge (RFGD), as described below.

The fluorocarbon films (henceforth called HFP surfaces) were deposited from a hexafluoropropylene RFGD using a home-built, inductively-coupled RF reactor described in detail elsewhere[96]. Cleaned SFG windows of CaF_2 and Quartz were placed in the glow region of the reactor. They were initially etched in an argon pressure of 150 mTorr for 5min at an input power of 40W. A fluorocarbon film was then deposited onto the windows using an input power of 80W for 1min followed by a 4min deposition with an input power of 20W. The fluorocarbon films were quenched for 5min under flowing hexafluoropropylene monomer with the RF power turned off. The RFGD-deposited films were thin enough to avoid any significant attenuation of the laser beams used in the SFG experiments. Cleaned silicon pieces (Silicon Valley Microelectronics, Inc.) placed near the windows were also coated. These coated silicon pieces were then later analyzed by x-ray photoelectron spectroscopy (XPS) to confirm the composition of the fluorocarbon films.

6.2.2 Peptide Synthesis

All the peptides were prepared on an Applied Biosystems automated synthesizer (ABI 433A) using MBHA resin. The 9-fluoroenylmethoxycarbonyl (Fmoc) protected amino acids and the resin were purchased from Anaspec, Inc. The peptides were cleaved from the resin using 95% trifluoroacetic acid with 2.5% triisopropylsilane and 2.5% water. The crude peptides were purified using a Waters reversed-phase high pressure liquid chromatography (HPLC) C-18 column using a water/acetonitrile solvent system containing 0.1% trifluoroacetic acid[95]. The purity and integrity of the peptides were analyzed with electrospray mass spectrometry.

6.2.3 Peptide Adsorption

Phosphate buffered saline (PBS, pH=7.4) was obtained from FischerBiotech. The samples for XPS analysis were prepared by placing 1cm x 1cm pieces of the fluorocarbon coated silicon pieces avoiding air-water interface in a 20μg/ml peptide PBS solution. The sample with the peptide solution was held in 1.5ml polystyrene cups for 2hrs. The samples were then washed with DI water (dilution displacement) and blown dry with nitrogen prior to XPS analysis. The buffers for the pH-dependent XPS experiments were prepared by adding 1N HCl to the PBS buffer solution to adjust their pH to the desired value (pH=2).

6.2.4 X-ray Photoelectron Spectroscopy

All XPS spectra were taken on a Surface Science Instruments X-probe spectrometer. This instrument has a monochromatized Al Kα X-ray source and a low energy electron flood gun for charge neutralization. X-ray spot size for these acquisitions was ~ 800μm. Pressure in the analytical chamber during spectral acquisition was less than 5×10^{-9} Torr. The analyzer pass energy for the survey spectra (composition) was 150 eV and was 50eV for high resolution C1s spectra. The take-off angle (the angle between the sample normal and the input axis of the analyzer lens) was 55° (55 degree take-of angle ≈ 50 Å sampling depth). Further details about the XPS analysis procedures have been published elsewhere[31,97,98].

The Service Physics ESCAVB Graphics Viewer program was used to determine peak areas, to calculate the elemental compositions from peak areas and to peak fit the high resolution spectra. The binding energy scale of the high-resolution C1s spectra was calibrated by assigning the CF_2 peak in the C1s high-resolution spectrum a binding energy of 292.0 eV.

6.2.5 Sum Frequency Generation

The fundamental beam of a Nd:YAG laser (EKSPLA, Lithuania) was used to pump an optical parametric generator/amplifier (OPG/OPA) manufactured by LaserVision (United States). The Nd:YAG laser operated at 10 Hz and provided a 20 pico-second pulse at 1064 nm with an energy of 35 mJ/pulse. A portion of the 1064 nm beam was frequency doubled to 532 nm using a KTP nonlinear crystal. This beam at 532 nm was then split with a portion being used for the visible beam of the SFG experiment while the second portion was sent through two counter-rotating KPT crystals to generate light in the near IR region (720-930 nm). The near IR light was then mixed with the remaining 1064 nm beam using a difference frequency generation (DFG) process through either a set of KTA crystals (2000-4000 cm^{-1}) or a single AgGaS crystal (1500-2000 cm^{-1}) The tunable IR radiation was then overlapped at the sample surface in time and space with the visible 532 nm beam. The SFG beam was collected by first using filters and a monochromator to remove any unconverted 532 nm light, and the SFG photons were detected using a photomultiplier tube. Multiple scans were collected and averaged to obtain spectra with good signal to noise ratios. A parallel signal of reflected IR radiation from a CaF_2 window was used to normalize the amide spectra. The amide region spectra were calibrated using the peak at 1606cm^{-1} and the spectra in the CH regions were calibrated using the peak at 2850cm^{-1} in the transmission spectra of polystyrene[100]. All the SFG spectra in this study were acquired with the polarization combination of s polarized SFG, s polarized visible and p polarized IR (ssp).

Figure 6.1 shows a simple schematic of the SFG experimental setup to access the solid-liquid interface *in situ*. The fluorocarbon coated or the uncoated quartz windows were immersed in PBS buffer solution. Then the peptide was pipetted into the solution to a concentration of 20μg/ml. The visible and the tunable IR radiation were then focused onto the side of the window in contact with the fluid and the outgoing SFG signal was collected and detected.

6.3 Results and Discussion

The composition of the RFGD deposited HFP surfaces were characterized by XPS. Only the presence of fluorine, carbon and a small amount of oxygen were detected by XPS (see Table 6.1). The high resolution C_{1s} spectrum (Figure 6.2) has peaks corresponding to C-CF_x (287eV), CF-CF_x (290eV), CF_2 (292eV) and CF_3 (294eV) species. The composition and C_{1s} spectrum are consistent with previously published results for HFP RFGD films deposited directly in the glow[190].

XPS analysis in Table 6.1 showed that after exposure of the HFP surfaces to LKα and LK310 peptide solutions at pH=7.4, nitrogen was detected and the percentage of oxygen increased. The carbon atomic % also increased while the fluorine decreased. These observations are consistent with adsorption of peptides onto the HFP surface. Relative atomic % of nitrogen (indicating peptide adsorption) was similar for LKα and LK310 on HFP surface regardless of pH, indicating similar surface concentration. Table 6.1 also compares the XPS surface compositions of the LKα peptide adsorbed onto the fluorocarbon and quartz surface at acidic (pH=2) versus neutral (pH =7.4) conditions. The composition results show the nitrogen signal, which originates from the peptide, drops by a factor of four on the quartz surface when the pH is decreased from 7.4 to 2.

Table 6.2 tabulates the elemental composition of the peptide modified surface recalculated without the fluorocarbon substrate contribution. The substrate contribution was removed using the C/F ratios of the control HFP surface and re-normalizing the carbon, oxygen and nitrogen signals to 100%. The theoretical compositions of the

different peptides are also listed for comparison. All the peptide modified samples had composition comparable to their stoichiometric values. However, all the samples had lower levels of nitrogen than the theoretically expected values. The XPS nitrogen to oxygen ratios of the samples were also slightly lower than their theoretical values.

Figure 6.3 shows a simple schematic illustrating the adsorption of the LKα peptide onto hydrophobic (HFP) and charged surfaces (quartz). The protonation/deprotonation of the surface silanol (Si-OH) groups in quartz has been well-characterized[68,70,191,192]. At pH 7.4 the silanol groups are deprotonated, resulting in a negative charge on the substrate. The theoretical pI of the LKα peptide was calculated to be 10.7[105]. Under neutral pH conditions, a limited number of the amines on the lysine residues will be protonated. Hence, the LKα peptide would be expected to adsorb onto the negatively charged quartz surface by electrostatic interaction through the positively charged amine groups on the lysine side chains. As the pH is lowered the surface silanol groups become increasingly protonated reducing the number of negative charges on the quartz surface. This results in reduced electrostatic interaction between the amine groups and the quartz surface leading to a decrease in the surface coverage of the peptide. The XPS data accordingly show changes in the surface coverage with the solution pH. However on the HFP surface, the LKα peptide interacts through the hydrophobic leucine residues shown in the schematic (Figure 6.3). Hence the amount of the adsorbed peptide is not influenced significantly by changes in the solution pH, consistent with XPS measured nitrogen concentrations.

Figure 6.4 shows the SFG spectra in the CH and OH regions for the adsorption of the LKα peptide onto the hydrophobic HFP and the charged quartz surfaces. Although the same peptide is adsorbed onto these two different substrates, the spectra are dramatically different. The two peaks observed in the CH region from the peptide adsorbed HFP surface (Figure 6.4a) are assigned to contributions from the CH_3 symmetric (2865 cm^{-1}) and the CH_3 fermi resonance (2935 cm^{-1}) of the symmetric stretch with the overtones of the methyl bending modes[79,82,193]. The broad peak seen in the OH region (around 3200cm^{-1}) is due to structuring of the water molecules resulting in a heavily hydrogen-

bonded network. The origin of this broad peak was also confirmed by experiments performed under deuterated water (data not shown). This hydrogen-bonded network of water molecules is similar to the structure of water in ice, where each individual water molecule is individually hydrogen bonded to four other water molecules[20].

The spectrum in Figure 6.4a indicates that on the HFP surface there is ordering of the methyl groups from the leucine side-chain due to the hydrophobic interaction with the substrate. Though previous researchers have observed strong ordering of methyl groups on hydrophobic surfaces[79,81,82,186], definite conclusions could not be made about molecular structure due to the random nature of polymer or protein adsorption. The hydrophobic nature of the interaction between the leucine methyl groups with the HFP surface is further supported by the loss of the 2865 and 2935 cm^{-1} resonance when the LKα peptide is adsorbed onto the charged quartz surface (Figure 6.4b). It is difficult to determine whether all the leucine residues, or only some, are interacting with the surface. It is also difficult to determine which terminal methyl group on the leucine side-chain is interacting with the surface or if both methyl groups interact. Additional experiments with isotopically labeled peptides are required to make these distinctions. However, based on the 3-D structure of the leucine residue, it can be speculated that both the methyl groups are involved in the interaction with the surface.

The SFG spectrum of the LKα peptide adsorbed onto the quartz surface under neutral pH conditions (pH=7.4) is shown in Figure 6.4b. The spectrum on the quartz surface exhibits a strong peak in the OH region with no discernible feature in the CH region (2800 cm^{-1} – 3000 cm^{-1}). A strong peak is observed at 3280 cm^{-1}. Recently, Jung et. al. observed a very similar peak and concluded that this peak is not from structured water molecules due to the nearly 80 cm^{-1} shift and the sharp nature of the peak. Instead, from isotopic labeling experiments, they concluded the peak is from the NH stretch; possibly from arginine or lysine residues[80]. We assign this peak at 3280 cm^{-1} to the NH stretch in the lysine side-chains as the lysine residues should interact electrostatically with the negatively charged substrate. The lack of features in the CH region even though the CH_3 groups are still present in the peptide, indicates the CH_3 groups are not ordered in a way

that presents a net dipole that satisfies the SFG selection rules. However, when the surface with the adsorbed peptide is removed from solution and exposed to air, the CH_3 groups becomes ordered by the hydrophobic air interface and strong peaks are observed in the CH region of the SFG spectrum (see discussion in following paragraphs). These observations reveal the importance of a strong hydrophilic or hydrophobic interaction to order the functional groups and make them SFG active. The shoulder at ~3200 cm^{-1} is attributed to the highly hydrogen-bonded water molecules when the LKα peptide is adsorbed on quartz surface.

The LK310 peptide has a different primary sequence of the amino acids than the LKα peptide. However, LK310 peptide has been shown by Solid sate NMR (SSNMR) to adsorb onto hydrophobic surfaces with a secondary structure similar to the LKα peptide[95]. Hence, experiments with the LK310 peptide were also done. Similar to the LKα peptide adsorbed onto HFP and quartz surfaces, the LK310 peptide shows (Figure 6.5) ordering of the methyl groups on HFP surface and ordering of the amine groups on quartz surface. The above data from the LK310 peptide confirms the nature of interaction on the hydrophobic HFP and the charged quartz surfaces.

To examine the secondary structure of the adsorbed peptides on the fluorocarbon substrates, the SFG spectrum was acquired in the amide I region (1500 – 1800 cm^{-1}). Figure 6.6 shows the amide I spectra of the different peptides (LKα and LK310) adsorbed onto HFP surface at pH=7.4. The amide I region corresponds to the C=O stretch which is weakly coupled with C-N stretch and N-H bending[185]. The position of the amide I is very sensitive to the secondary structure of proteins and peptides in solution[22]. The SFG spectrum in the amide I region for the control sample (a fluorocarbon blank) shows that there are no peaks in the amide region (Fig 6.5a). The LKα and the LK310 peptide show an intense amide I signal with similar peak positions near 1650 cm^{-1}(Fig 6.5b&d). This is typical of peptides and proteins with an alpha-helical secondary stucture[185]. The presence of the amide I peak for the LKα and LK310 peptides indicates that these peptides adsorb on the hydrophobic surface preserving their alpha-helical secondary structure. Solid state NMR (SSNMR) experiments have been

performed to determine the secondary structure of the adsorbed LKα and LK310 peptide on hydrophobic polystyrene surfaces[95]. The results from SSNMR experiments confirm the SFG results that the LKα and LK310 adopt similar adsorbed secondary structures.

As a control the amide I spectrum was acquired in deuterated water (D_2O) for the LKα peptide. Even in D_2O, there is still a strong peak at 1640 cm^{-1} confirming the presence of the amide I signals (Fig 6.5c). The peak is shifted by 10cm^{-1}. This peak shift results from the deuterium exchange of the amide hydrogen which causes a small chemical shift in the amide I peaks. Similar effects have been observed with proteins and have been used to obtain information about the structure of peptides/proteins based on their deuterium exchange ability[185].

The effect of air-drying on the structure of the adsorbed peptide is shown in Figure 6.7 for the LKα peptide. The LKα peptide was adsorbed onto quartz, then air-dried, and the resultant SFG spectrum obtained in the CH and OH regions (Figure 6.7a). There are many noticeable differences in the SFG spectrum compared with the corresponding spectrum in Figure 6.4b. The first observation is that the peak near 3200 cm^{-1} from highly hydrogen-bonded water molecules, is no longer present. Secondly, the spectrum at the air interface shows intense peaks in the CH region from structuring of the terminal methyl groups of the leucine residues due to exposure to the air [71]. Interestingly, the air-dried spectrum does not show the NH stretch peak from the terminal amine groups in lysine. This demonstrates the importance of water in the electrostatic interaction. The terminal groups interacting with the surface become disordered upon removal of the water, resulting in the loss of the NH SFG. The amide I spectrum of the LKα peptide adsorbed onto the fluorocarbon surface after air-drying is shown in Figure 6.7b. The spectrum in the amide I region still shows peaks indicative of an ordered peptide backbone in a α-helix conformation, indicating air drying does not affect the secondary structure of this peptide.

6.4 Conclusions

The major conclusions from this study are:

- The SFG data indicate that helical LK peptides form ordered structures on hydrophobic and charged surfaces.
- The peptide adsorption is mediated through leucine terminal methyl groups on hydrophobic surfaces and through lysine terminal amine groups on negatively charged surfaces.
- The amide I SFG signals indicate that the adsorbed LKα and LK310 peptides have a similar secondary structure, in agreement with SSNMR results.
- Air-dried LK 310 adsorbed samples onto hydrophobic substrates have the same ordered arrangements of the backbone carbonyls as the hydrated samples.

6.5 Credits

Financial support from NESAC/BIO (NIH Grant EB-002027) and NSF Grant DMR-0110505 is gratefully acknowledged.

Table 6.1 Elemental composition determined by XPS for the LKα and LK310 peptides adsorbed onto the fluorocarbon (FC) and quartz substrates (pH of buffers noted).

Atomic Percentages ± standard deviation

	C(1s)	N(1s)	O(1s)	F(1s)	Si(2p)
Peptide on HFP substrate					
FC substrate control	41.5±0.8	N/D*	0.9±0.3	57.6±1.0	-
LK α (pH=7.4)	52.4±0.4	4.6±0.2	6.3±0.3	36.7±0.4	-
LK α (pH=2)	49.3±0.1	3.7±0.3	5.1±0.3	41.9±0.5	-
LK310 (pH=7.4)	52.8±1.1	4.3±0.4	4.8±0.6	38.1±1.9	-
Peptide on Quartz substrate					
Quartz control	14.6±0.9	N/D*	56.6±1.2	-	28.8±1.1
LK α (pH=7.4)	25.4±3.2	3.2±0.4	44.8±2.8	-	26.6±2.2
LK α (pH=2)	19.7±1.9	0.8±0.1	51.4±1.7	-	28.2±0.6

*N/D = not detected

Table 6.2 Theoretical elemental composition of the peptides vs the XPS determined elemental composition of peptides on the fluorocarbon surface (fluorocarbon substrate contribution removed using C/F ratios from the control fluorocarbon substrate).

All peptides on FC substrate	C(1s)	N(1s)	O(1s)	N/O
LK α (pH=7.4)	71.6	12.7	15.7	0.7±0.1
LK α (theoretical)	70.5	17.2	12.3	1.4
LK310 (pH=7.4)	74.8	12.7	12.5	0.9±0.1
LK310 (theoretical)	71.4	16.1	12.5	1.3

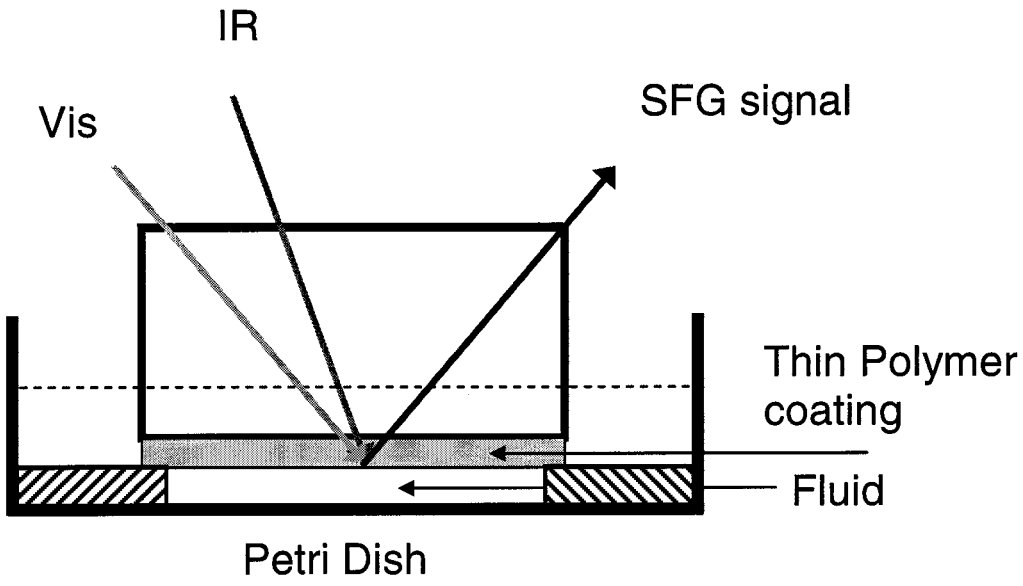

Figure 6.1 SFG experimental setup. The incoming laser beams are overlapped onto the side of the substrate immersed in the fluid. This allows the solid-liquid interface to be accessed *in situ*. The outgoing SFG beam is collected and detected. Quartz windows were used to access the CH/OH regions and CaF_2 windows were used to access the amide regions.

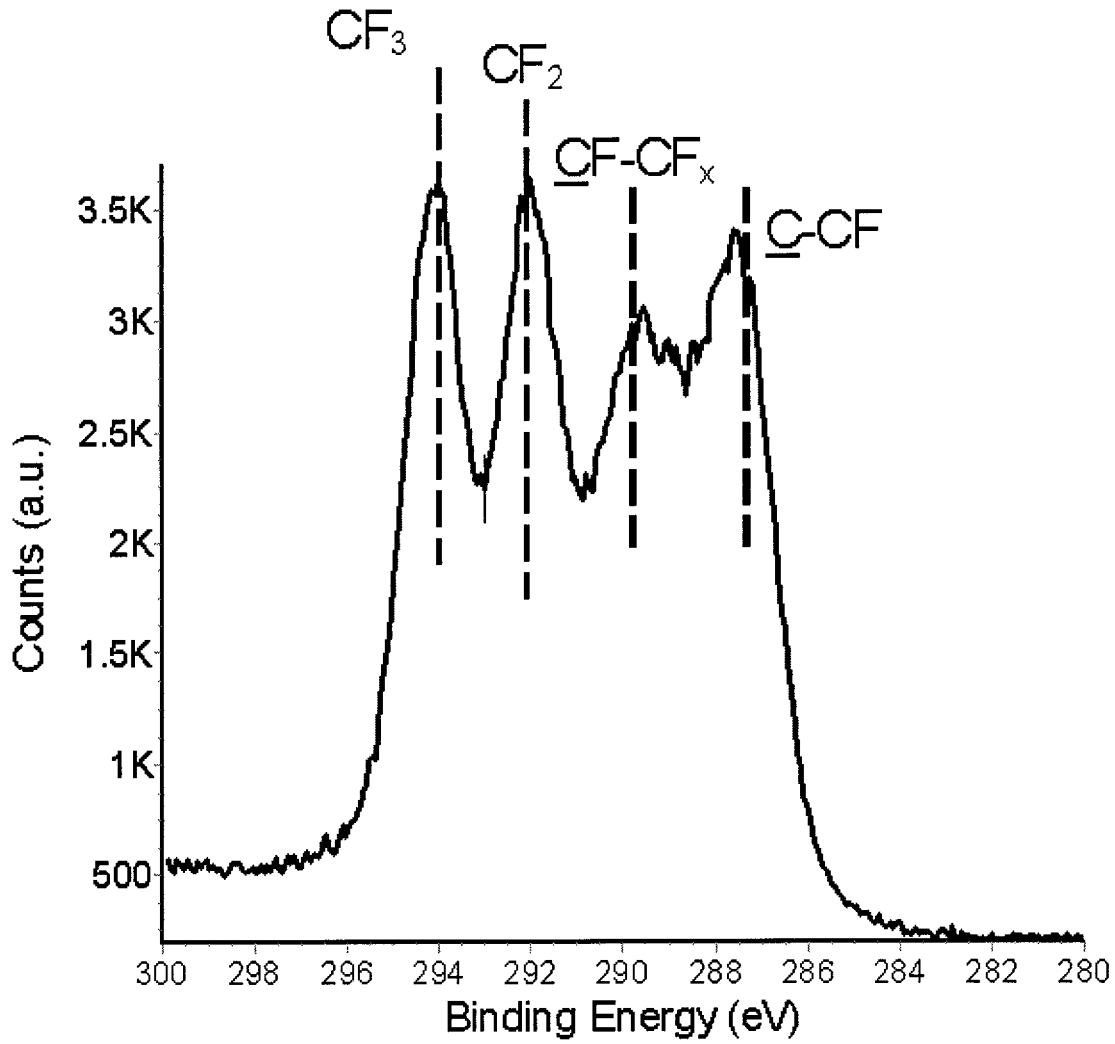

Figure 6.2 XPS high-resolution C_{1s} spectrum of the HFP coated silicon substrates. The spectrum indicates the presence of different C-F_x species, as expected from the structure of the monomer and RFGD deposition conditions.

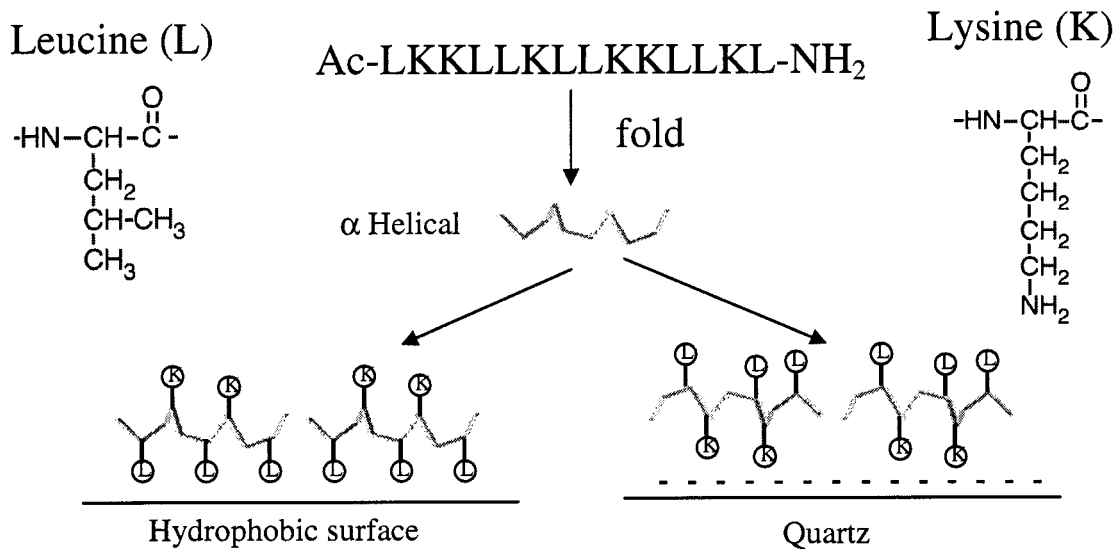

Figure 6.3 Proposed schematic of the adsorbed structure of the LKα peptide on hydrophobic and charged substrates. The primary sequence of the peptide determines its ability to fold into different secondary structures. On the hydrophobic substrate the peptide interacts through the leucine groups and through the charged lysine side-chains on the quartz substrate. The amine terminus of the peptides is acetylated and the carboxy terminus is amidated.

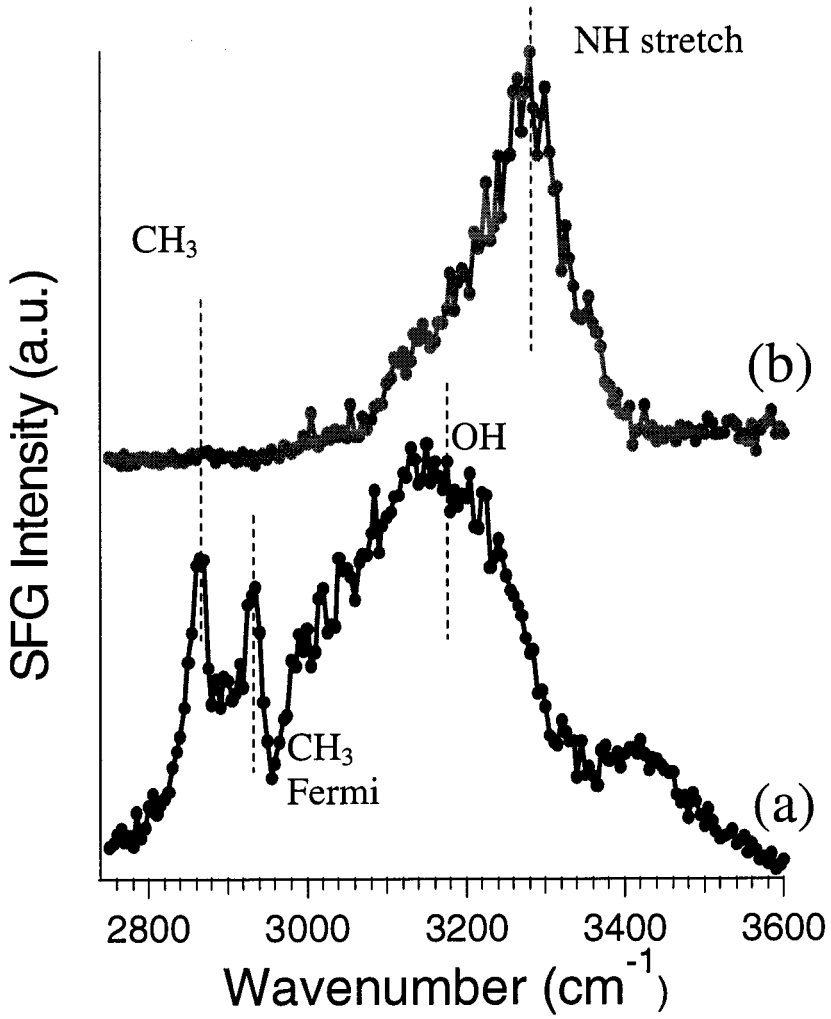

Figure 6.4 The CH/OH region SFG spectra of the LKα peptide adsorbed onto a (a) plasma-deposited fluorocarbon substrate (HFP surface) and an (b) uncoated quartz substrate. Note that the spectrum was acquired in situ in the presence of the peptide solution.

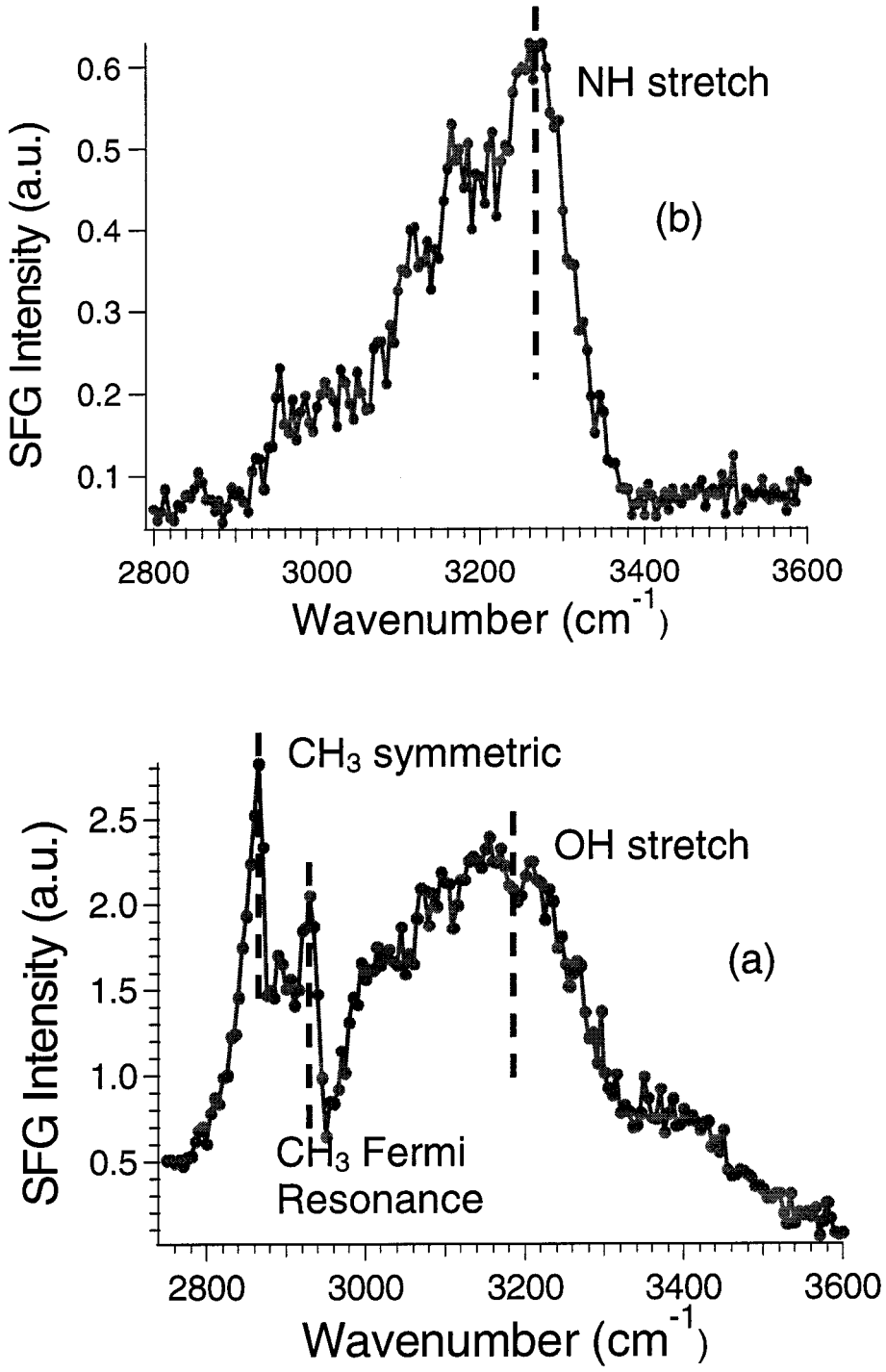

Figure 6.5 The CH/OH region SFG spectra of the LK310 peptide adsorbed onto a (a) plasma-deposited fluorocarbon substrate (HFP surface) and an (b) uncoated quartz substrate. Note that the spectrum was acquired in situ in the presence of the peptide solution.

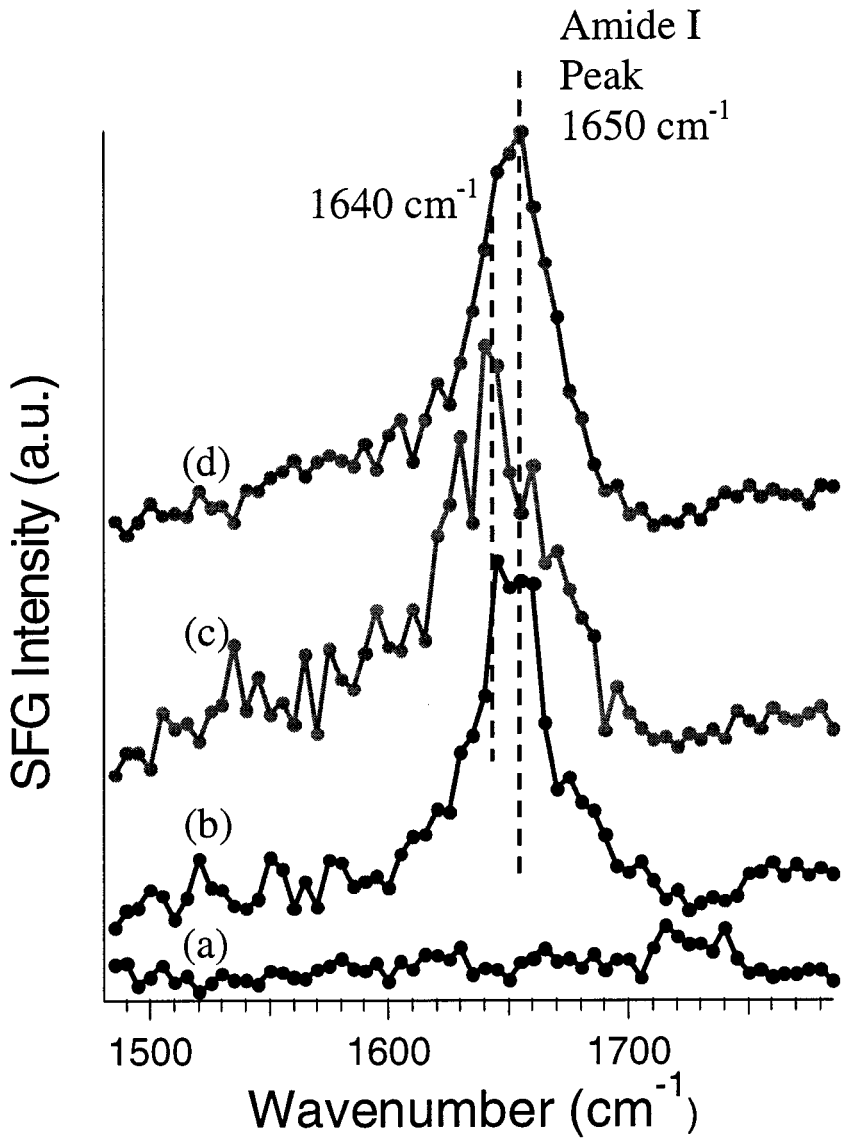

Figure 6.6 Amide I SFG spectra of: (a) fluorocarbon (FC) coated CaF_2 substrate (control sample), (b) LKα adsorbed onto the FC substrate, (c) LK α peptide adsorbed onto the FC substrate and placed under D_2O, and (d) LK310 peptide adsorbed onto the FC substrate.

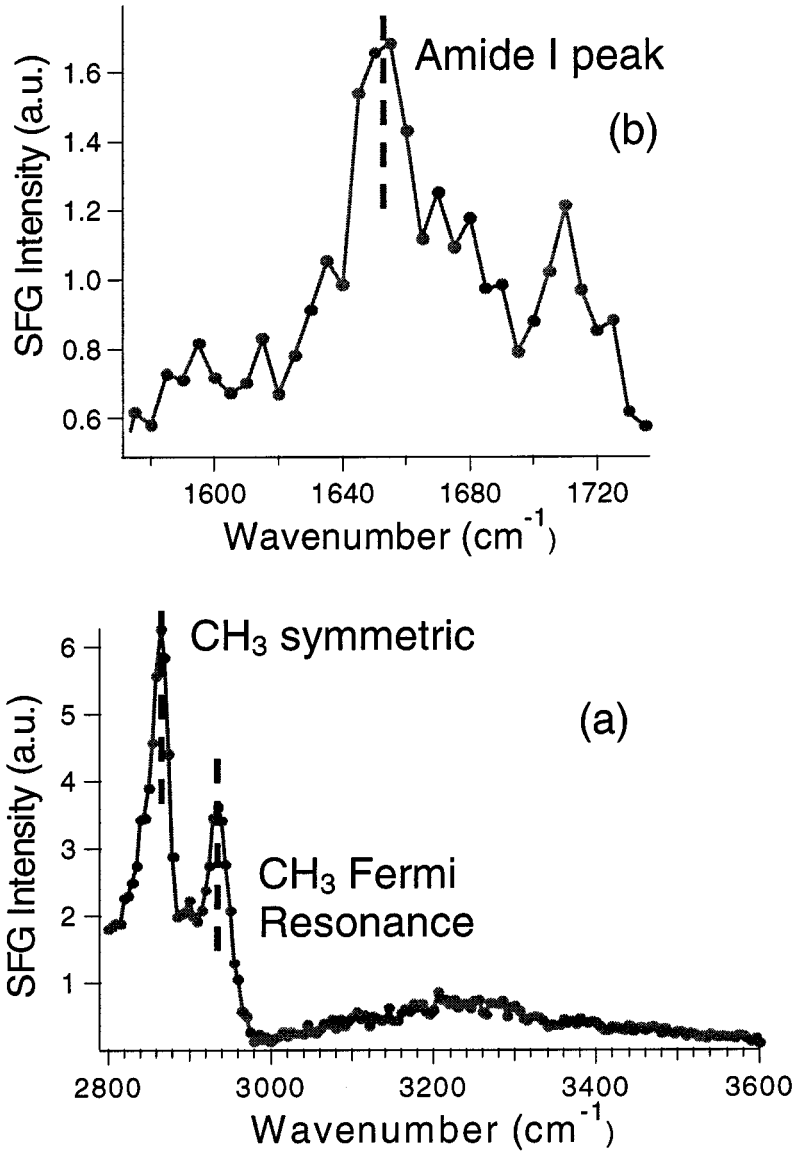

Figure 6.7 Effect of air-drying on the structure of adsorbed LKα peptide. (a) The SFG spectrum of the LKα peptide adsorbed onto quartz under buffer and then air-dried. Note that air-drying has significant effect on the ordering of the side-chain functional. (b) The amide I spectrum of the LK 310 peptide adsorbed onto the plasma-deposited fluorocarbon substrate under buffer and then air-dried. The spectrum still shows the presence of the amide I signal from the backbone carbonyls in an alpha-helical arrangement.

7 : Time-Dependent Sum Frequency Generation Characterization of Adsorbed Alpha-Helical Peptide Structure

Controlling and characterizing the structure of adsorbed biomolecules is important for several important applications such as diagnostics, tissue engineering and nanobiotechnological applications. The present study characterizes the immobilization of a lysine and leucine peptide onto the surface through two approaches – immersing the hydrophobic substrate through the air-water interface (AWI) and avoiding the AWI. The peptide adsorbed avoiding the AWI shows time-dependent changes in the amide I intensities. X-ray Photoelectron Spectroscopy (XPS) analysis showed no significant time dependence of the nitrogen surface concentration. Similarly, the CH region of the SFG spectrum shows no time-dependence. The above results indicate that the amide I SFG spectrum follows the time-dependent ordering of the peptide molecules on the hydrophobic surface. Further experiments were done by heating the system radiatively, which resulted in faster rates and increased ordering; supporting the above conclusions. Bringing the substrate through the AWI results in a Langmuir-Blodgett type deposition on the surface.

7.1 Introduction

Chemical and structural characterization of biomolecules at interfaces plays an important role in several diverse applications like diagnostics, microarrays, tissue engineering, nanobiotechnological applications, etc[164,165,169,170]. Though there are several analytical tools that can probe the "Biomolecular Interface," Sum Frequency Generation (SFG) has some features which make it an important tool for studying the biointerfacial region[60,62,76]. For example, the ability of SFG to probe the interface *in situ* enables time-dependent information to be obtained about the structure of the interface.

SFG involves overlapping tunable IR and fixed visible laser beams onto the sample surface and collecting the outgoing photon at the sum of the incoming frequencies (SFG photon). The SFG photon has several unique characteristics: surface-specific, chemically specific, sensitive to functional group orientation and allows *in situ* studies[60,62,76]. For a

chemical species at the interface to be SFG active, it has to be both Raman and IR active and be ordered. The substrate used in this study is a hydrophobic plasma-deposited fluoropolymer on a calcium fluoride crystal. The plasma-deposited polymer does not absorb light in the IR and the visible region. This enables the solid-liquid interface between the polymer and the contacting liquid to be probed *in situ*; so the interaction of the peptide with the hydrophobic surface can be monitored in real time.

The ability of peptides containing lysine and leucine to fold into well-defined secondary structures at the air-water interface has been demonstrated[172]. Solid state NMR (ssNMR)[95] and SFG[194] also show these peptides adsorb onto hydrophobic surfaces and retain their helical secondary structure. The LKα peptide folds into an alpha-helical secondary structure with well-separated hydrophobic/hydrophilic residues in its three-dimensional structure, so it adsorbs onto hydrophobic surfaces by interaction through the hydrophobic leucine residues. The adsorption of this peptide onto hydrophobic surfaces has been previously characterized with ssNMR, SFG, X-ray photoelectron spectroscopy (XPS), near-edge X-ray absorption fine structure spectroscopy (NEXAFS) and ATR-IR experiments[95,174,194,195]. These experiments confirm the ability of the peptides to adsorb onto the surface retaining their secondary structure.

In the present work, SFG is used to characterize the immobilization of the alpha-helical peptide (LKα) onto the hydrophobic surfaces through two different approaches: via the air-water interface (AWI) and avoiding the AWI. The two schemes cause significant differences in the time dependent ordering of adsorbed peptide. The results demonstrate the ability to probe the time-dependent ordering of the peptide molecules with SFG.

7.2 Experimental Details

7.2.1 Radio Frequency Glow Discharge Deposition (RFGD)

Circular, 9.53 mm thick CaF_2 windows were obtained from ISP Optics and circular, 6 mm thick quartz windows were obtained from Esco products. Quartz windows were used to acquire SFG spectra in the CH, NH and OH regions. Calcium fluoride windows were

used to acquire SFG spectra in the amide region because the quartz windows absorb significant amounts of the incoming IR radiation in the amide region. The CaF_2 windows were cleaned by sonicating them in methanol for 10 minutes followed by blowing dry with nitrogen. The quartz windows were cleaned by sonicating them sequentially in methylene chloride, acetone and methanol for 5 minutes each followed by blowing dry with nitrogen. To create hydrophobic substrates, thin fluorocarbon films were deposited onto the substrates from a hexafluoropropylene RF glow discharge (RFGD), as described below.

The fluorocarbon films (henceforth called HFP surfaces) were deposited from a hexafluoropropylene RFGD using a home-built, inductively-coupled RF reactor described in detail elsewhere[96]. Cleaned SFG windows of CaF_2 and Quartz were placed in the glow region of the reactor. They were initially etched in an argon pressure of 150 mTorr for 5min at an input power of 40W. A fluorocarbon film was then deposited onto the windows using an input power of 80W for 1min followed by a 4min deposition with an input power of 20W. The fluorocarbon films were quenched for 5min under flowing hexafluoropropylene monomer with the RF power turned off. The RFGD-deposited films were thin enough to avoid any significant attenuation of the laser beams used in the SFG experiments. Cleaned silicon pieces (Silicon Valley Microelectronics, Inc.) placed near the windows was also coated. These coated silicon pieces were then later analyzed by x-ray photoelectron spectroscopy (XPS) to confirm the composition of the fluorocarbon films.

7.2.2 Peptide Synthesis

All the peptides were prepared on an Applied Biosystems automated synthesizer (ABI 433A) using MBHA resin. The 9-fluoroenylmethoxycarbonyl (Fmoc) protected amino acids and the resin were purchased from Anaspec, Inc. The peptides were cleaved from the resin using 95% trifluoroacetic acid with 2.5% triisopropylsilane and 2.5% water. The crude peptides were purified using a Waters reversed-phase high pressure liquid chromatography (HPLC) C-18 column using a water/acetonitrile solvent system

containing 0.1% trifluoroacetic acid. The purity and integrity of the peptides were analyzed with electrospray mass spectrometry[95].

7.2.3 Peptide Adsorption

Phosphate buffered saline (PBS, pH=7.4) was obtained from FischerBiotech. The samples for XPS analysis were prepared by placing 1cm x 1cm pieces of the fluorocarbon coated silicon pieces avoiding the AWI in a 20μg/ml peptide PBS solution. Alternatively, the peptide was also immobilized through the AWI by immersing the samples in 20μg/ml solution of the peptide through the AWI. The sample with the peptide solution was held in 1.5ml polystyrene cups for 2hrs. The samples were then washed with DI water (dilution displacement) and blown dry with nitrogen prior to XPS analysis.

7.2.4 X-ray Photoelectron Spectroscopy

All XPS data were taken on a Surface Science Instruments X-probe spectrometer. This instrument has a monochromatized Al Kα X-ray source and a low energy electron flood gun for charge neutralization. X-ray spot size for these acquisitions was ~ 800μm. Pressure in the analytical chamber during spectral acquisition was less than 5×10^{-9} Torr. The analyzer pass energy for the survey spectra (composition) was 150 eV and was 50eV for high resolution C1s spectra. The take-off angle (the angle between the sample normal and the input axis of the analyzer lens) was 55° (55 degree take-of angle ≈ 50 Å sampling depth). Further details about the XPS analysis procedures have been published elsewhere[31,97,98].

The Service Physics ESCAVB Graphics Viewer program was used to determine peak areas, to calculate the elemental compositions from peak areas and to peak fit the high resolution spectra. The binding energy scale of the high-resolution C1s spectra was calibrated by assigning the CF_2 peak in the C1s high-resolution spectrum a binding energy of 292.0 eV.

7.2.5 Sum Frequency Generation

The fundamental beam of a Nd:YAG laser (EKSPLA, Lithuania) was used to pump an optical parametric generator/amplifier (OPG/OPA) manufactured by LaserVision (United States). The Nd:YAG laser operated at 10 Hz and provided a 20 pico-second pulse at 1064 nm with an energy of 35 mJ/pulse. A portion of the 1064 nm beam was frequency doubled to 532 nm using a KTP nonlinear crystal. This beam at 532 nm was then split with a portion being used for the visible beam of the SFG experiment while the second portion was sent through two counter-rotating KPT crystals to generate light in the near IR region (720-930 nm). The near IR light was then mixed with the remaining 1064 nm beam using a difference frequency generation (DFG) process through either a set of KTA crystals (2000-4000 cm^{-1}) or a single AgGaS crystal (1500-2000 cm^{-1}) The tunable IR radiation was then overlapped at the sample surface in time and space with the visible 532 nm beam. The SFG beam was collected by first using filters and a monochromator to remove any unconverted 532 nm light, and then the SFG photons were detected using a photomultiplier tube. Multiple scans were collected and averaged to obtain spectra with good signal to noise ratios. A parallel signal of reflected IR radiation from a CaF_2 window was used to normalize the amide spectra. The amide region spectra were calibrated using the peak at 1606cm^{-1} and the spectra in the CH regions were calibrated using the peak at 2850cm^{-1} in the transmission spectra of polystyrene[100]. All the SFG spectra in this study were acquired with the polarization combination of s polarized SFG, s polarized visible and p polarized IR (ssp).

Figure 7.1 shows a simple schematic of the experimental setup to access the solid-liquid interface *in situ*. The fluorocarbon coated window was immersed in PBS buffer solution. Then the peptide was pipetted into the solution to a concentration of 20μg/ml. For immobilizing the peptide through the AWI, the coated window was immersed through the AWI of a 20μg/ml peptide solution. The visible and the tunable IR radiation were then focused onto the side of the window in contact with the fluid and the outgoing SFG signal was collected and detected.

The time-dependent spectra were acquired immediately after injection of the peptide. Each spectrum is an average over 5 scans and each scan takes 2 min to acquire. Careful measurements of the time evolution of the signal were monitored by following the main peak of interest in the spectrum as a function of time. The intensities reflect the average over three points near the main peak. For example, in the amide I region, the peak of interest is at 1650 cm-1. The intensity was monitored by collecting the average of the following three points: 1645, 1650 and 1655 cm-1, as a function of time. In the amide I region as well as the CH region, a reference background peak intensity was also monitored as a function of time. A custom Labview program was written to automate the collection of the time-dependent peak intensities and the corresponding time points.

7.3 Results and Discussion

7.3.1 LKα adsorbed through the AWI

Figure 7.2 shows the spectrum of the LKα peptide at the air-water interface of a 20ug/ml peptide solution. The spectra are obtained by reflecting the two incoming laser beams from the air-water interface, thereby probing the air-water interface. The CH/OH spectrum of the peptide at the air-water interface is shown in Figure 7.2b. The major peaks observed in the CH region are from the CH_3 symmetric (2865 cm^{-1}) and the CH_3 fermi resonance (2935 cm^{-1}) of the symmetric stretch with the overtones of the methyl bending modes peak from the leucine residues[194]. The terminal methyl groups from the leucine residues are ordered at the air-water interface due to exposure to the hydrophobic air interface.

The peptide backbone in α-helix arrangement typically has the amide I peak around 1650-1660 cm^{-1}. The amide I region principally corresponds to the C=O stretch which is weakly coupled with C-N stretch and N-H bending and is sensitive to the secondary structure of the peptide[185]. The peak seen in the spectrum at 1656 cm^{-1} is characteristic of the peptide adopting an alpha-helical secondary structure on the hydrophobic surface (Fig. 7.2a). The data in the amide I region and the CH/OH data shows that the peptide

indeed aggregates at the AWI, maintaining the ordered alpha-helical secondary structure of the LKα peptide.

The immobilization of the peptide onto the HFP surface was then done by immersing the surface through the AWI containing the peptide solution. The time-dependent amide I spectrum is shown in Figure 7.3. The spectrum does not show any detectable time-dependence. Hence, the pre-ordered LKα at the AWI, as shown in Figure 7.2, is deposited onto the surface as a Langmuir-Blodgett type monolayer when the substrate is taken through the AWI. This justifies the absence of time-dependence in the amide I region when adsorbed through the AWI.

7.3.2 LKα adsorbed avoiding the AWI

The secondary structure of the peptide adsorbing onto the HFP surface avoiding the AWI was characterized in the amide I region (Figure 7.4). The SFG spectra were acquired after the peptide is introduced into the liquid cell at a concentration of 20 μg/ml, avoiding the AWI. The peak seen in the spectrum at 1656 cm^{-1} is characteristic of the peptide adopting an alpha-helical secondary structure on the hydrophobic surface. Figure 7.4 shows increasing adsorption time results in an increase in the magnitude of the amide I peak. The intensity of the amide I peak saturates after about an hour of adsorption.

The adsorption of the peptide was next examined *in situ* in the CH region of the spectrum, to follow the ordering of the terminal methyl groups on the surface. Figure 7.5 shows the time-dependent data for the LKα peptide adsorbing onto the HFP surface in the CH region of the SFG spectrum following injection of the peptide solution. It is seen from the data that the CH region of the SFG spectrum does not show any detectable time-dependent changes in the intensity of the peaks, unlike the amide I region of the spectrum. Hence, the LKα peptide interacts with the HFP surface through the leucine methyl groups but does not show any changes in their orientation or order.

Figure 7.6 shows further time-dependent experiments in the amide I and CH regions on the adsorption of the LKα peptide. The intensity changes in the main peaks as well as the background signals were measured simultaneously. Upon injection of the LKα peptide there is a slow increase in the amide I signal which saturates around 1hr (Fig. 7.6a). In contrast, upon injection of the LKα peptide, the CH region of the spectrum shows an instantaneous jump in the signal which remains time-invariant (Fig. 7.6b). This is similar to the trends seen in Figure 7.5, where the terminal methyl groups order immediately (in the time scale of the experiment) upon injection of the peptide.

The surface composition of the adsorbed peptide on the HFP surface was analyzed ex situ using XPS to determine whether the time-dependent amide I signal is due to additional LKα adsorbing on the surface. Table 7.1 lists the time-dependent surface composition of the peptide adsorbed onto the HFP surface. The surface composition (~4% nitrogen) determined by the XPS measurements remains constant over the 2 hr adsorption of the LKα peptide.

The SFG peak intensity has been shown to be sensitive to the ordering of the functional groups at the interface[60,62,76]. For example, a random collection of the molecules at the interface causes the SFG intensity to vanish. Recently, Roke et. al. demonstrated the ability to probe the ordering of the lipid molecules at the air-water interface *in situ*[196]. The ordering of the molecules resulted in significant changes in the SFG spectrum. In a similar manner, the XPS results for the LKα adsorbed avoiding the AWI, along with the time-dependent SFG data in the CH and the amide I region of the spectrum, show that the amide I region follows the ordering of the peptides on the surface. To summarize, the above data reveal initial fast adsorption of the peptide (XPS composition) through the terminal methyl groups (CH region SFG data), and with increased time, inter-molecular ordering of the adsorbed peptide on the surface occurs (amide I SFG data), which saturates around 1 hr. Figure 7.6a shows the side-view of the folded peptide with separation of the hydrophobic (leucine) and the hydrophilic (lysine) residues in its structure, enabling interaction with the surface. Figure 7.6b shows a proposed schematic of the time-dependent changes in the surface structure of the LKα on the surface.

7.3.3 Effect of heat on the ordering of the adsorbed peptide

To further examine the time-dependent ordering of the peptide on the surface the system was heated. This was achieved by using an infrared heating lamp to transfer energy to the system radiatively. The temperature of the system was also followed upon by using a thermocouple, and reached a steady state temperature of ~ 40 C after ~10min of heating. Figure 7.8a shows the intensity changes in the amide I region upon switching on the heat lamp. Heating the system resulted in a significant increase in the rate of peptide ordering on the surface, as evidenced from the increased slopes and peak intensities. The background peak showed little change upon heating. The increase in the signal in the main peak (1655 cm^{-1}) in the amide I region upon heating could also be due to the adsorption of more molecules onto the surface. To test this, additional experiments were done in the CH region of the spectrum.

Figure 7.8b shows the time-dependent changes in the intensity of the main peaks of interest in the CH region of the SFG spectrum that occurred upon heating the system. A decrease in the signal for both the two major peaks in the spectrum with increasing time was observed. The decrease in the signal (~20%) could be due to (1) peptide molecules desorbing from the surface, or (2) loss of alignment of the laser beams on the sample surface. The latter was checked by moving to a different spot. This resulted in recovery of ~50% of the lost signal (data not shown). Hence, the observed signal loss in Fig. 7.8b probably indicates the removal of the peptide molecules from the surface and will be investigated further in the future. In summary, the data in the CH region does not show any evidence for increased adsorption of the peptide on the surface with the addition of heat but indicate some possible loss of peptide molecules from the surface.

7.4 Conclusions

The main conclusions from the time-dependent characterization of the adsorbed alpha-helical peptide structure are:

- Adsorption through the AWI results in Langmuir-Blodgett deposition of the peptide molecules onto the surface.
- Instantaneous adsorption of the peptide and ordering of the methyl groups occurs when adsorbed avoiding the AWI. Adsorption avoiding AWI also results in time-dependent inter-molecular ordering of the molecules on the surface.
- Addition of thermal heat results in increased rates and ordering of the peptide molecules on the surface.

7.5 Credits

Financial support from NESAC/BIO (NIH Grant EB-002027) and NSF Grant DMR-0110505 is gratefully acknowledged.

Table 7.1 Elemental composition determined by XPS for the LKα peptide adsorbed onto the fluorocarbon (HFP) surface.

Atomic Percentages ± standard deviation

	C(1s)	N(1s)	O(1s)	F(1s)
HFP control surface	39.4±2.5	0.1±0.1	0.4±0.2	60.1±2.6
5 min.	49.7±1.0	4.3±0.3	6.1±0.3	39.9±1.3
10 min.	50.4±0.3	4.3±0.2	5.6±0.1	39.6±0.3
30 min.	51.7±0.2	4.5±0.2	5.7±0.1	38.1±0.1
1hr	50.5±0.5	4.3±0.1	6.1±0.4	39.0±0.6
2hr	52.1±1.8	4.2±0.4	5.7±0.2	38.0±1.6
LKα adsorbed through AWI (2hr)	50.7±1.2	4.0±0.3	5.3±0.5	40.1±1.7

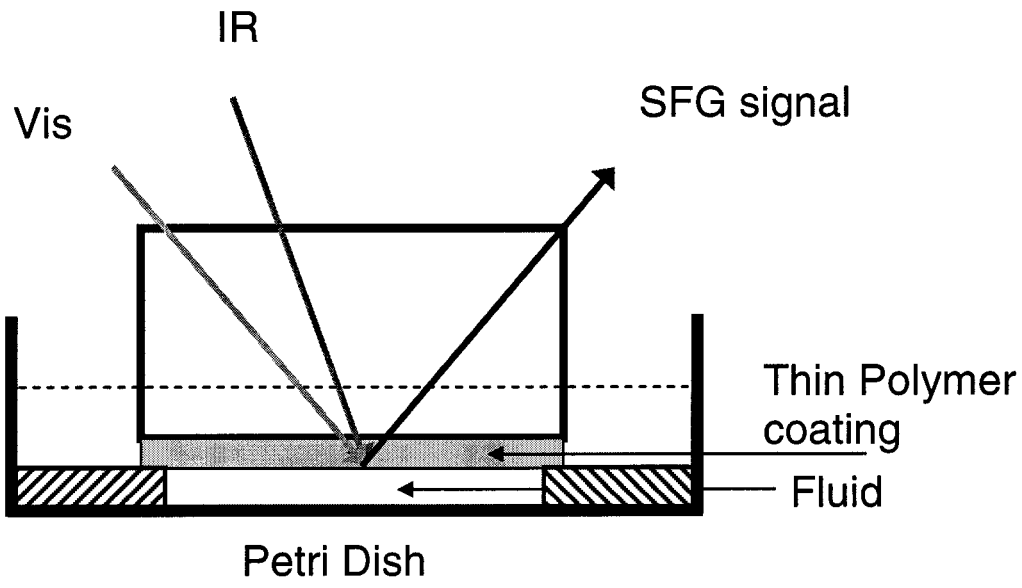

Figure 7.1 SFG experimental setup. The incoming laser beams are overlapped onto the side of the substrate immersed in the fluid. This allows *in situ* access of the solid-liquid interface. The outgoing SFG beam is collected and detected. Quartz windows were used to access the CH/OH regions and CaF_2 windows were used to access the amide regions.

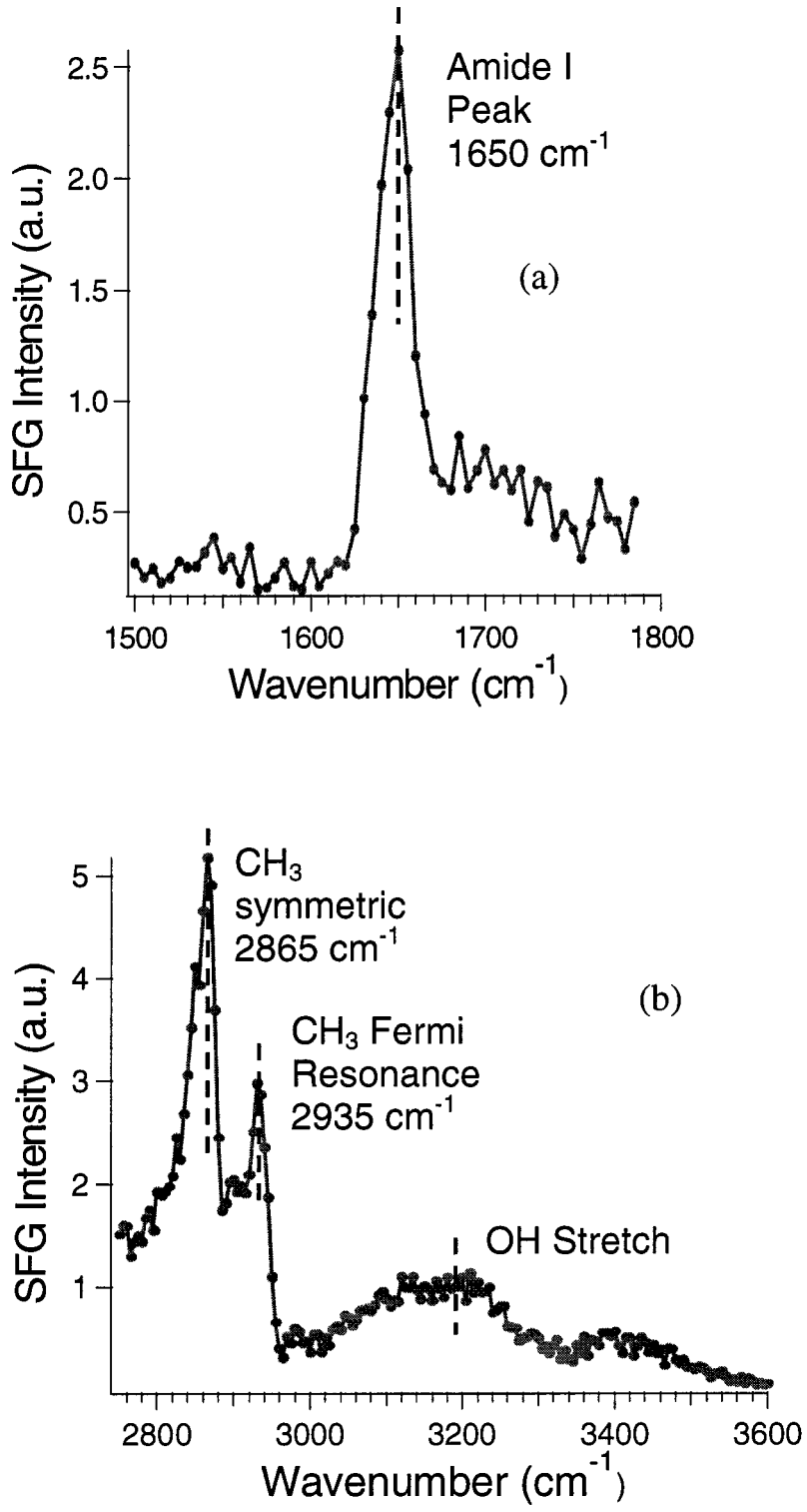

Figure 7.2 (a) Amide I SFG spectra of the LKα peptide at the air-water interface and (b) CH/OH SFG spectra of the LKα peptide at the air-water interface.

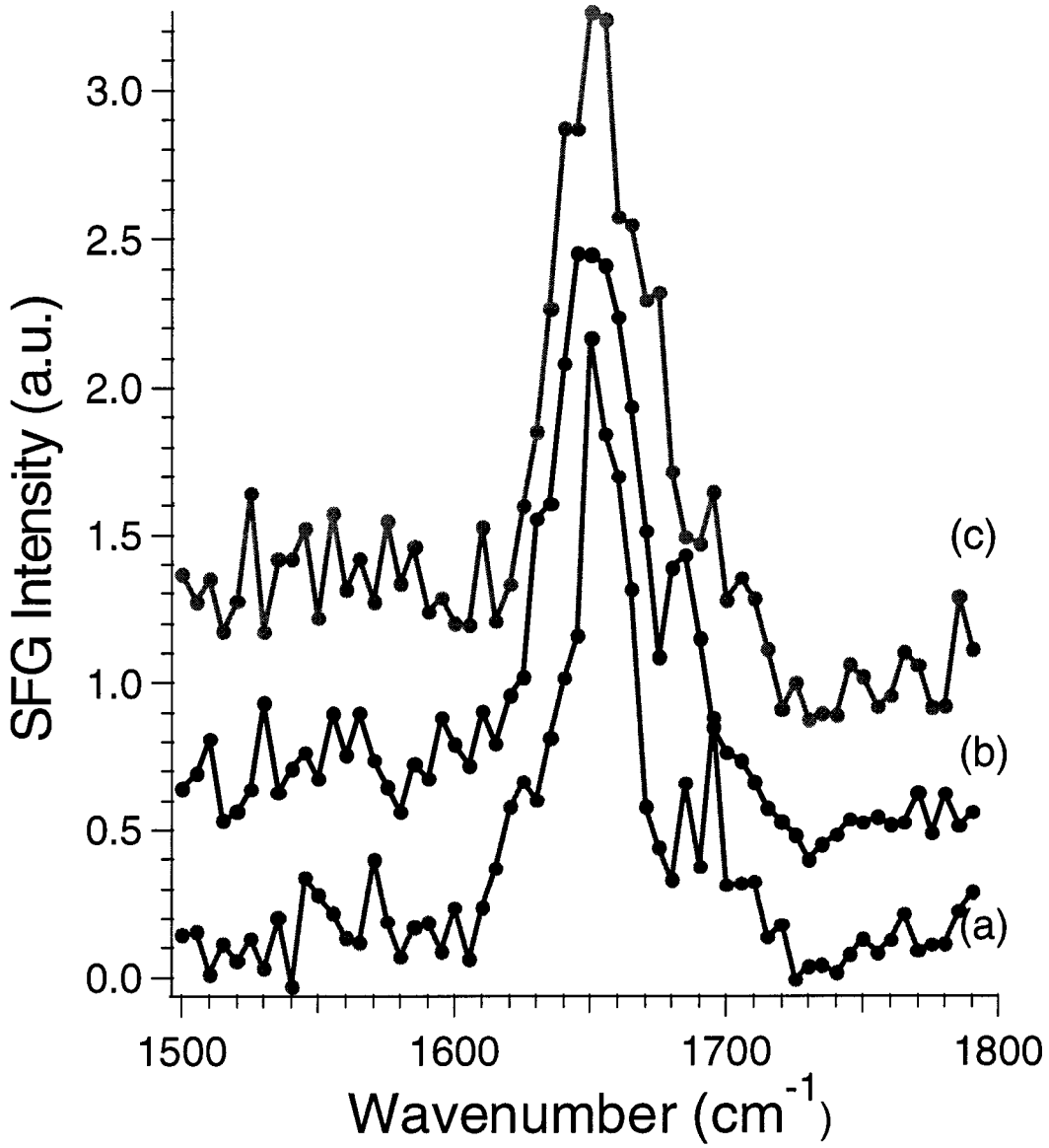

Figure 7.3 Time-dependent SFG spectra of the LKα peptide deposited onto the HFP surface through the AWI in the amide I region (a) 10 min (b) 25 min and (c) 60 min.

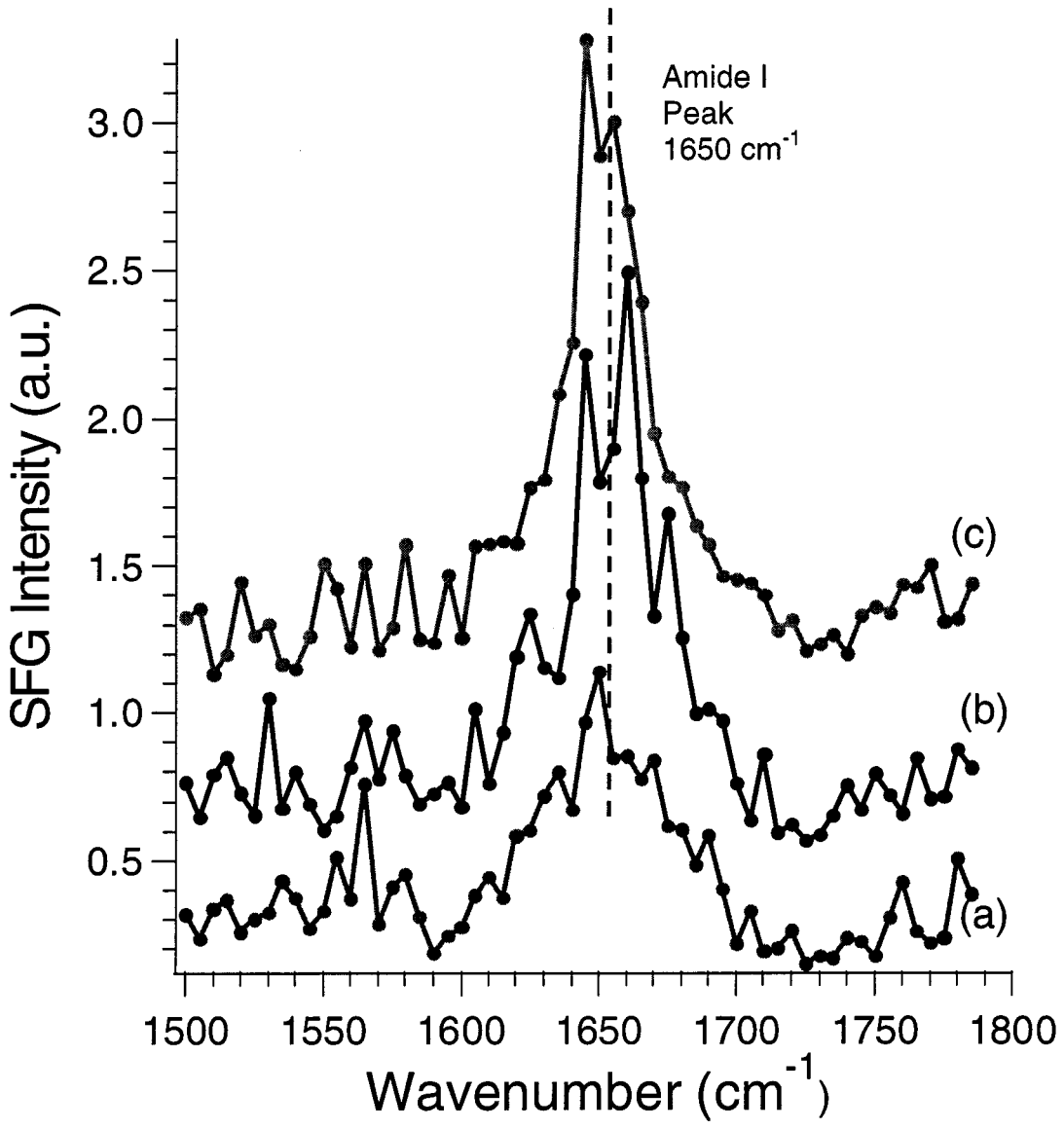

Figure 7.4 Time-dependent amide I SFG spectra for the LKα peptide adsorbed onto the HFP surface avoiding the AWI (a) 10 min (b) 25 min and (c) 60 min.

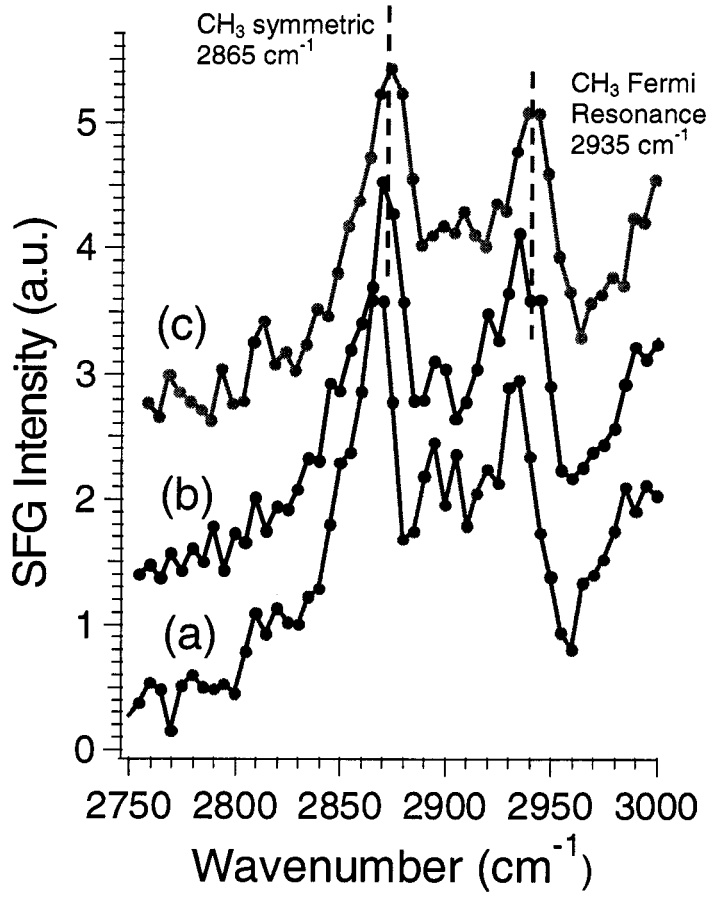

Figure 7.5 Time-dependent SFG spectra in the CH region of the LKα peptide adsorbed onto the HFP surface avoiding the AWI (a) 10 min (b) 25 min and (c) 60 min.

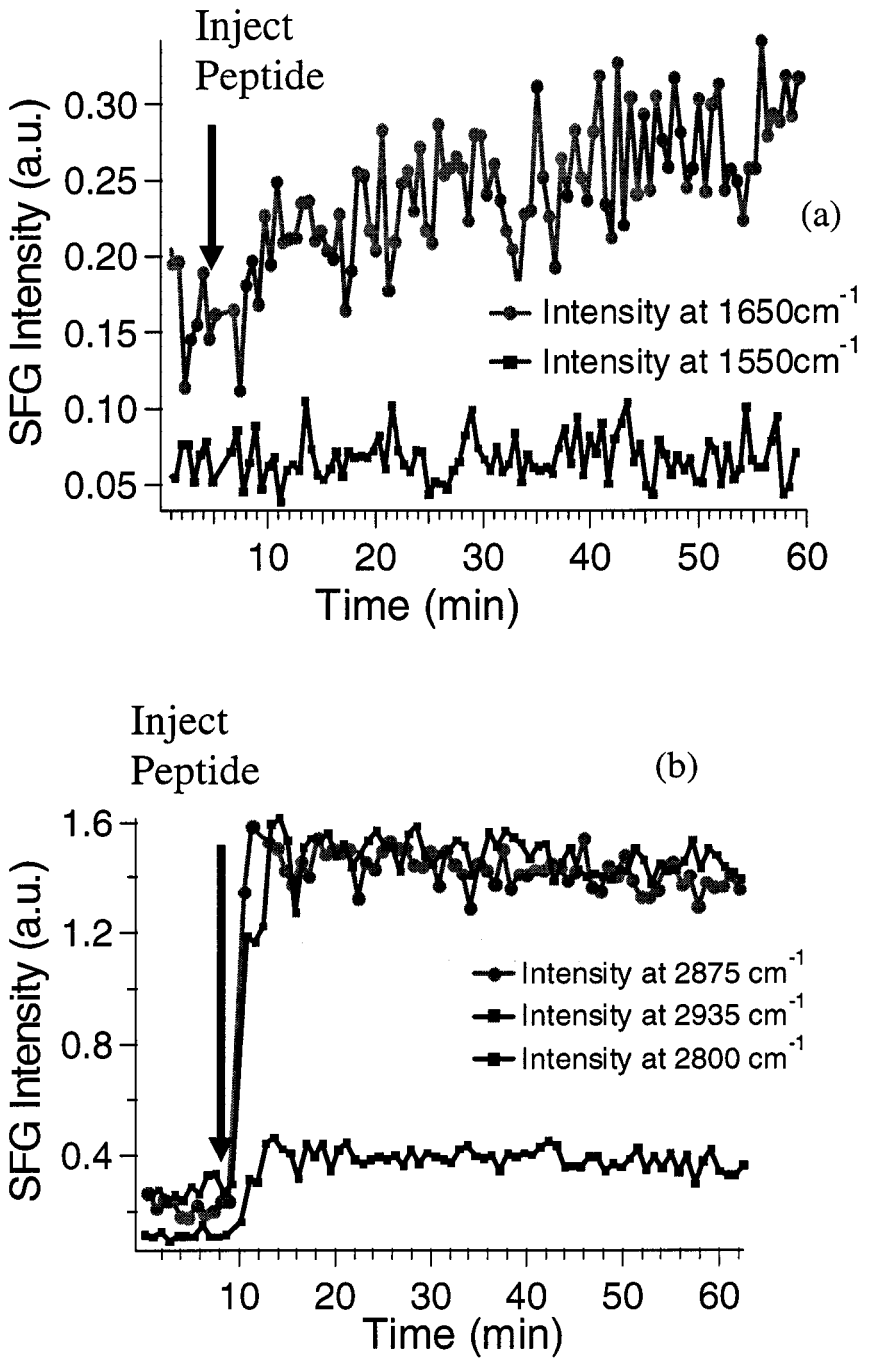

Figure 7.6 Time-dependent data of the LKa adsorbed onto the HFP surface in the (a) amide I region and (b) CH region. The separate graphs represent the intensity at different wavenumbers measured as a function of time for the same spot on the sample. The arrows mark the instant when the peptide was introduced into the solution.

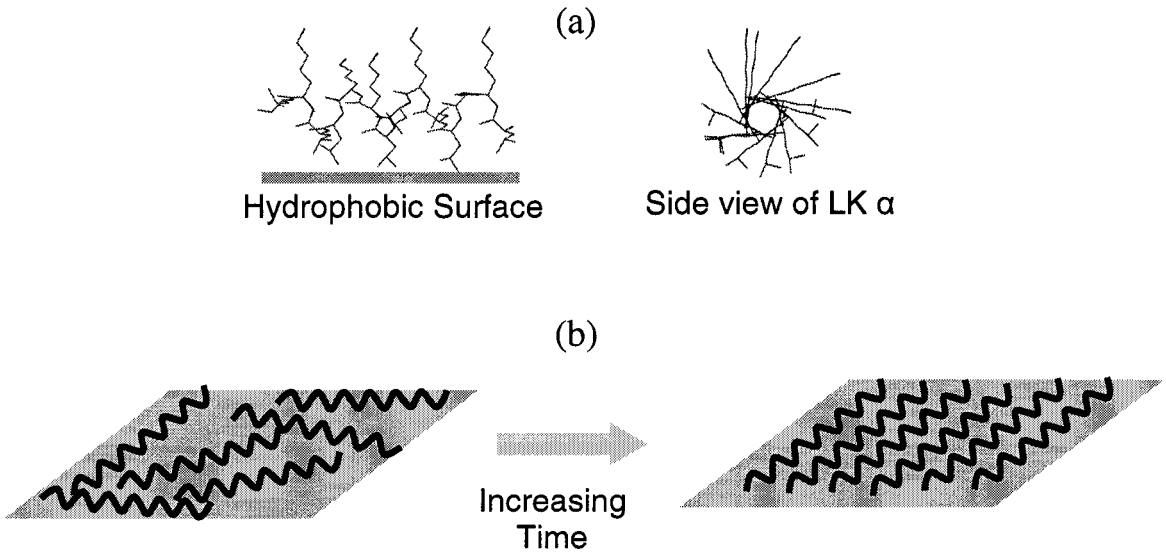

Figure 7.7 (a) Proposed structure of the LKα on the HFP surface and (b) Proposed schematic showing the time-dependent re-organization of the adsorbed LKα on the HFP surface.

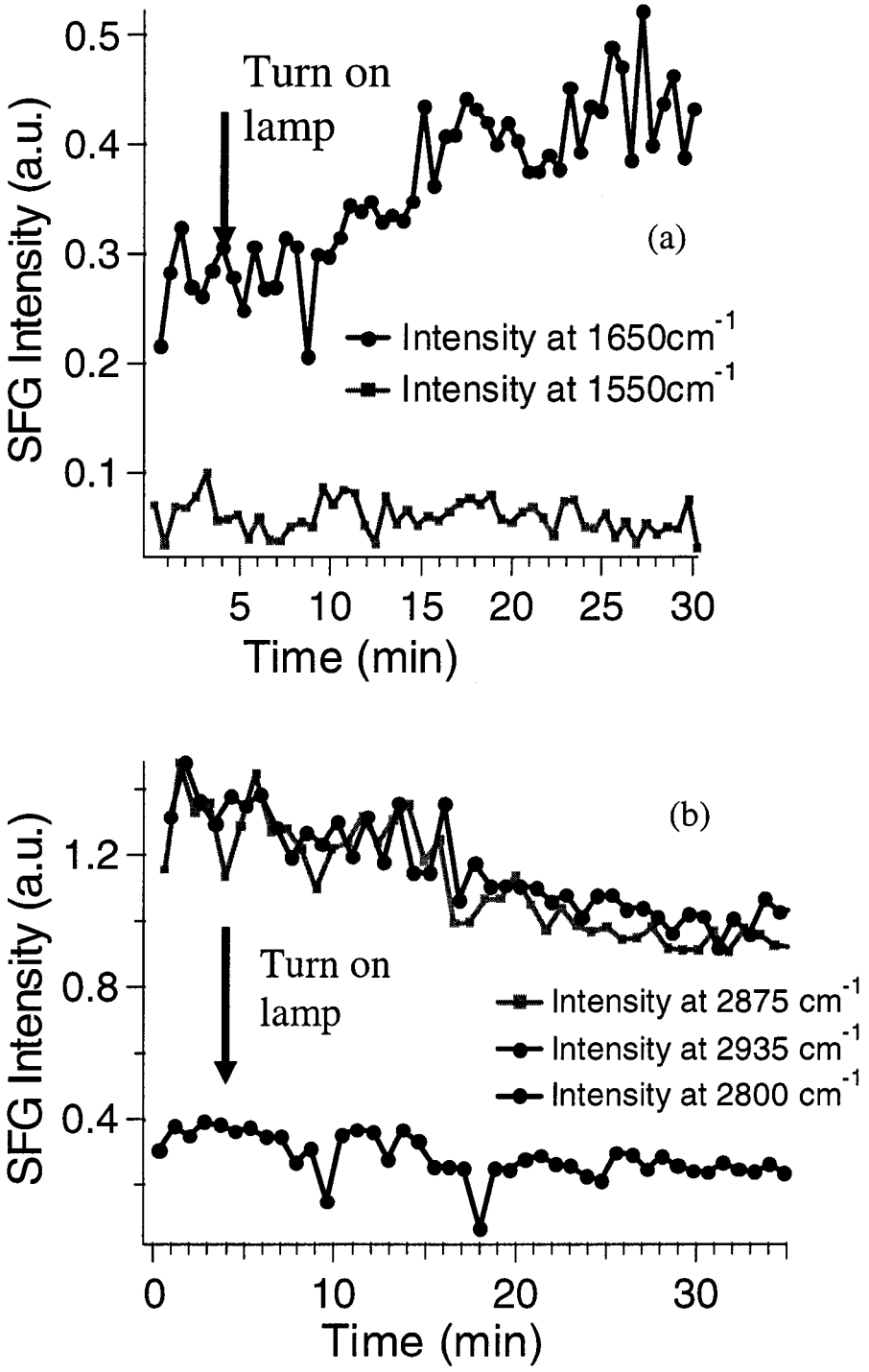

Figure 7.8 Time-dependent data of the LKα adsorbed onto the HFP surface in the (a) amide I region and (b) CH region. The separate graphs represent the intensity at different wavenumbers measured as a function of time for the same spot on the sample. The arrows mark the instant when the IR heat lamp was turned on.

8 : Probing locally the interaction of an Alpha-helical Peptide with Fluorocarbon Surfaces: Deuterium Labeling Experiments

A well-defined sequence of a lysine and leucine peptide has been shown to spontaneously adsorb onto a hydrophobic surface retaining its alpha-helical secondary structure. However, not much is known regarding the specific leucine amino acid residues involved in the interaction between the peptide and the surface. Herein, we propose using stable, deuterium labeled leucine residues to locally probe the peptide-surface interaction using Sum Frequency Generation (SFG) spectroscopy. The results demonstrate that obtaining *in situ* information in the C-D stretch region (2100 – 2300 cm^{-1}) for the labeled peptides is difficult. However, peptide-surface interactions at single amino acid resolution could be readily probed in the CH region of the spectrum. The results demonstrate the ability of SFG to probe specific peptide residues using stable deuterium labeled amino acids.

8.1 Introduction

Understanding biomolecule-surface interactions is an very important problem in areas such as biomaterials, diagnostics, etc[5,6]. Usually the random adsorption of a biomolecule onto a solid substrate results in a random distribution of adsorbed orientations and significant changes in the structure of the biomolecule[6]. We are interested in a series of peptides, which adsorb onto hydrophobic surface retaining their secondary structure[95,194,195]. This affords molecular-level control over their structure on hydrophobic surfaces. Hydrophobic polymers are ubiquitous and find applications in many areas. Hence, this approach provides a method for peptide modification of "real" surfaces.

Previous research identified the highly ordered structure of leucine-lysine (LK) peptides adsorbed onto hydrophobic substrates[95,194,195]. The peptide was observed to interact with the hydrophobic surface through the terminal methyl groups in the leucine residue[194]. However, it is not clear which individual side-chain residues are involved in this interaction with the surface. This study uses deuterium-labeling of individual leucine

residues to demonstrate the feasibility to *in situ* probe local interactions of the peptides with the surface.

Recently, Wang et. al. demonstrated the ability to observe C-D stretch signals in SFG for adsorbed protein molecules[88]. The full potential of SFG can be realized by specific labeling of the amino acid residues with stable deuterium labels, which enables probing locally in the biomolecule of interest on the surface. Isotopic labeling is routinely done in other techniques like infrared spectroscopy and mass spectrometry, to probe the local structure and also for quantification studies[185].

The main goal of this study is to evaluate the ability to probe the interaction of the molecule with the surface at a single amino acid resolution using stable deuterium labeled leucine residues. To approach this problem, LK310 was chosen as a model peptide and peptides with different amounts of deuterium labels were synthesized.

8.2 Experimental Details

8.2.1 Radio Frequency Glow Discharge Deposition (RFGD)

Circular, 9.53 mm thick CaF_2 windows were obtained from ISP Optics and circular, 6 mm thick quartz windows were obtained from Esco products. Quartz windows were used to acquire SFG spectra in the CH, NH and OH regions. Calcium fluoride windows were used to acquire SFG spectra in the CD region. The CaF_2 windows were cleaned by sonicating them in methanol for 10 minutes followed by blowing dry with nitrogen. The quartz windows were cleaned by sonicating them sequentially in methylene chloride, acetone and methanol for 5 minutes each followed by blowing dry with nitrogen. To create hydrophobic substrates, thin fluorocarbon films were deposited onto the substrates from a hexafluoropropylene RF glow discharge (RFGD), as described below.

The fluorocarbon films (henceforth called HFP surfaces) were deposited from a hexafluoropropylene RFGD using a home-built, inductively-coupled RF reactor described in detail elsewhere[96]. Cleaned SFG windows of CaF_2 and Quartz were placed

in the glow region of the reactor. They were initially etched in an argon pressure of 150 mTorr for 5min at an input power of 40W. A fluorocarbon film was then deposited onto the windows using an input power of 80W for 1min followed by a 4min deposition with an input power of 20W. The fluorocarbon films were quenched for 5min under flowing hexafluoropropylene monomer with the RF power turned off. The RFGD-deposited films were thin enough to avoid any significant attenuation of the laser beams used in the SFG experiments. Cleaned silicon pieces (Silicon Valley Microelectronics, Inc.) placed near the windows was also coated. These coated silicon pieces were then later analyzed by x-ray photoelectron spectroscopy (XPS) to confirm the composition of the fluorocarbon films.

8.2.2 Peptide Synthesis

Deuterium labeled leucine was purchased from Cambridge Isotopes. FMOC-O-Su was obtained from EMD Biosciences. The leucines were Fmoc labeled by the following procedure. First 2.25mmol of the unprotected leucine was dissolved in 20ml of warm 5% Na_2CO_3 solution. Then 2.25mmol of the FMOC-O-Su was dissolved in 5ml of dioxane. The above solution was later mixed with the solution of the unprotected leucine Na_2CO_3 solution and stirred for 24hrs at room temperature. After 24hrs the solution was diluted with 20ml of water and extracted three times with ethyl ether. The aqueous layer was adjusted to pH=2 using concentrated HCl. The solution turned turbid. This solution was then extracted with ethyl acetate solution. The ethyl acetate solution was then taken and the ethyl acetate removed with a rotovap. The final traces of the ethyl acetate were removed by vacuum drying. A small amount of the solid was dissolved in methanol and analyzed by electrospray ionization mass spectrometry (ESI-MS). The ESI mass spectrum for the Fmoc labeled protected leucine is shown in the appendix I. This spectrum confirms the synthesis of the Fmoc labeled protected leucine.

All the peptides were prepared on an Applied Biosystems automated synthesizer (ABI 433A) using MBHA resin. The 9-fluoroenylmethoxycarbonyl (Fmoc) protected amino acids and the resin were purchased from Anaspec, Inc. The peptides were cleaved from

the resin using 95% trifluoroacetic acid with 2.5% triisopropylsilane and 2.5% water. The crude peptides were purified using a Waters reversed-phase high pressure liquid chromatography (HPLC) C-18 column using a water/acetonitrile solvent system containing 0.1% trifluoroacetic acid[95]. The purity and integrity of the peptides were analyzed with electrospray mass spectrometry (data shown in the appendix). The structures of the different synthesized peptides are:

LK310 ctrl Ac – LLKLLKLLKLLKL – NH_2

LK310Lab1 Ac – LLKLLK**L**LKLLKL – NH_2

LK310Lab2 Ac – LLKL**L**K**L**LKLLKL – NH_2

LK310Lab8 Ac – **LL**K**LL**KL**L**K**LL**K**L** – NH_2

Where, **L** represents the deuterium labeled leucine residue. The structure of the deuterium labeled leucine is shown in Figure 8.1.

8.2.3 Peptide Adsorption

Phosphate buffered saline (PBS, pH=7.4) was obtained from FischerBiotech. The fluorocarbon-coated window was immersed in PBS buffer solution. Then the peptide was pipetted into the solution to a concentration of 20μg/ml avoiding the air-water interface. The visible and the tunable IR radiation were then focused onto the side of the window in contact with the fluid and the outgoing SFG signal was collected and detected.

8.2.4 Sum Frequency Generation

The fundamental beam of a Nd:YAG laser (EKSPLA, Lithuania) was used to pump an optical parametric generator/amplifier (OPG/OPA) manufactured by LaserVision (United States). The Nd:YAG laser operated at 10 Hz and provided a 20 pico-second pulse at 1064 nm with an energy of 35 mJ/pulse. A portion of the 1064 nm beam was frequency doubled to 532 nm using a KTP nonlinear crystal. This beam at 532 nm was then split with a portion being used for the visible beam of the SFG experiment while the second

portion was sent through two counter-rotating KPT crystals to generate light in the near IR region (720-930 nm). The near IR light was then mixed with the remaining 1064 nm beam using a difference frequency generation (DFG) process through either a set of KTA crystals (2000-4000 cm^{-1}) or a single AgGaS crystal (1500-2000 cm^{-1}) The tunable IR radiation was then overlapped at the sample surface in time and space with the visible 532 nm beam. The SFG beam was collected by first using filters and a monochromator to remove any unconverted 532 nm light, then the SFG photons were detected using a photomultiplier tube. Multiple scans were collected and averaged to obtain spectra with good signal to noise ratios. The CH region spectra were calibrated using the peak at 2850cm^{-1} in the transmission spectra of polystyrene[100]. The SFG spectra in this study were acquired with the polarization combination of s polarized SFG, s polarized visible and p polarized IR (ssp) and also with the polarization combination of p polarized SFG, p polarized visible and p polarized IR (ppp).

8.3 Results and Discussion

Previously we have demonstrated the ability of SFG to probe the interaction of the LK310 peptide with the HFP surface [194]. Briefly, the interaction of the peptide with the HFP surface was accompanied by strong ordering of the terminal methyl groups from the peptide. In contrast, when adsorbed onto a negatively charged surface, the electrostatic interaction with the positively charged side-chain lysine groups resulted in ordering on the amine groups instead of the methyl groups. However on the HFP surface it is not clear which of the individual leucine residues are involved in the interaction with the surface. To address this problem, we are using stable deuterium labeled leucine residues to locally probe the interaction of the peptide with the surface. This enables experiments to be done in both the CH (2800 – 3000 cm^{-1}) and C-D regions (2100-2300 cm^{-1}) of the SFG spectrum.

Figure 8.2 shows the SFG spectrum of the LK310ctrl peptide adsorbed onto the HFP surface. The peptide was adsorbed onto the surface, washed with buffer, air-dried and then the SFG spectrum was acquired with the ppp polarization combination. The

spectrum shows an intense peak at 2965 cm^{-1} which is assigned to the CH_3 (asymmetric) stretches from the terminal methyl groups in the leucine residue[79,82,193]. Surprisingly, the spectrum is marked by absence of signal from the other methyl peaks. Previously, we have shown the appearance of intense signal from the CH_3 (symmetric) and the CH_3 Fermi resonance peak for air-dried adsorbed peptide samples in the ssp polarization combination[194]. The appearance of the CH_3 (asymmetric) stretch peak in the ppp mode can be explained based on the recent work by Lu et. al[197]. Their studies indicate the ssp combination is sensitive to the methyl symmetric stretch and the Fermi resonance mode, while the ppp combination is sensitive to the methyl asymmetric stretch modes. In fact, they recommended acquiring SFG spectra in both the ssp and the ppp modes to assign the symmetric stretch and asymmetric methyl stretching peaks. These experiments will help interpret the features seen in the C-D region of the SFG spectrum.

8.3.1 Characterization of the adsorbed peptides in the C-D region

Initially, the adsorbed peptides were probed in the C-D region of the SFG spectrum, to detect the uniquely labeled leucine residues. With the current experimental setup the C-D signals could not be detected *in situ* (i.e., at the solid-liquid interface) with the ssp or ppp polarization combinations (data not shown). The samples with the adsorbed peptides were later washed and air-dried. Figure 8.3 shows the ppp spectra in the C-D region for the different deuterium labeled peptides acquired after air-drying. The data reveal that the singly-labeled peptides could not be differentiated from the control samples. However, when the peptide carries two labels, they could be detected in the C-D region. The peak seen in the spectrum is from the CD_3 asymmetric stretch from the labeled methyl groups in the adsorbed peptide. As shown previously, the SFG spectrum acquired with the ppp polarization combination probes the asymmetric stretch modes. The spectrum for the multiply labeled peptide shows a very intense signal because of the abundance of the labeled methyl groups (Figure 8.3d). Air-dried samples when probed with the ssp polarization did not show any signal (data not shown). The reason for the absence of any signal in the ssp polarization is not clear. However, it has to be mentioned that Paszti et. al.[198] reported data for air-dried protein films with only the ppp

polarization combination. To summarize, the results from the C-D region suggest it will be difficult to locally probe individual residues *in situ*. Since our main goal was to characterize *in situ* the interaction of the peptide with the surface, we decided to test the other combination – label all the leucines except the residue to be probed.

8.3.2 Characterization of the adsorbed peptides in the C-H region

Figure 8.4 shows the data in the CH region of the spectrum for the two-labeled peptide adsorbed onto the HFP surface. The ssp spectrum shows intense peaks from the CH_3 symmetric (2865 cm^{-1}) and the CH_3 fermi resonance (2935 cm^{-1}), similar to the data for the LK310 peptide reported earlier (Figure 8.4b)[194]. The sample was later washed and then re-immersed into the D_2O solution. The spectrum still shows peaks in the CH region characteristic of the methyl groups from the leucine residue (Figure 8.4c).

The adsorption of the LK310lab8 peptide onto the HFP surface was examined in next (Figure 8.5). The control spectrum of the HFP surface immersed in the buffer solution (Fig. 8.5a) and the deuterated water (Fig. 8.6a) did not show any features in the CH region of the spectrum, as expected. Upon injection of the peptide into the solution a characteristic signal in the CH region is seen. The peaks are from the different methyl stretches as was observed for the LK310lab2 peptide (Figure 8.4). To further confirm the observation of the methyl stretches, the sample was washed and then immersed in a deuterated solution. Any exchangeable protons should be deuterated by this procedure. The signal from the methyl stretches are still observed in the spectrum (Fig. 8.6b). This indicates the signal observed in the CH region (Fig. 8.5b) is from the unlabeled methyl groups and not from any hydrogen-exchanged CD_3 groups.

8.4 Conclusions

The main goal of the present work is to determine the ability to *in situ* probe the local structure of adsorbed peptides using deuterium labeled leucine residues. The results show that *in situ* no signal is detected for the different labeled leucine residues in the C-D region of the SFG spectrum. However, for air-dried samples containing at least two

labels, they could be readily detected in the C-D region with ppp polarization. The interaction of a single residue with the surface could be detected in the C-H region of the spectrum by deuterium labeling the remaining leucine residues. This represents a promising approach to probe the *in situ* local structure of the adsorbed molecules using deuterium labels.

8.5 Credits

Financial support from NESAC/BIO (NIH Grant EB-002027) and NSF Grant DMR-0110505 is gratefully acknowledged.

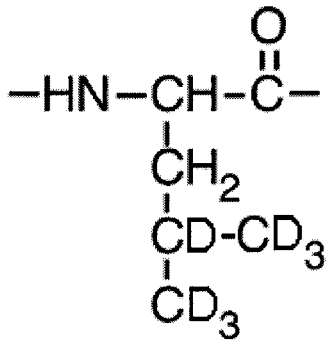

Figure 8.1 Chemical structure of the deuterium labeled leucine residue.

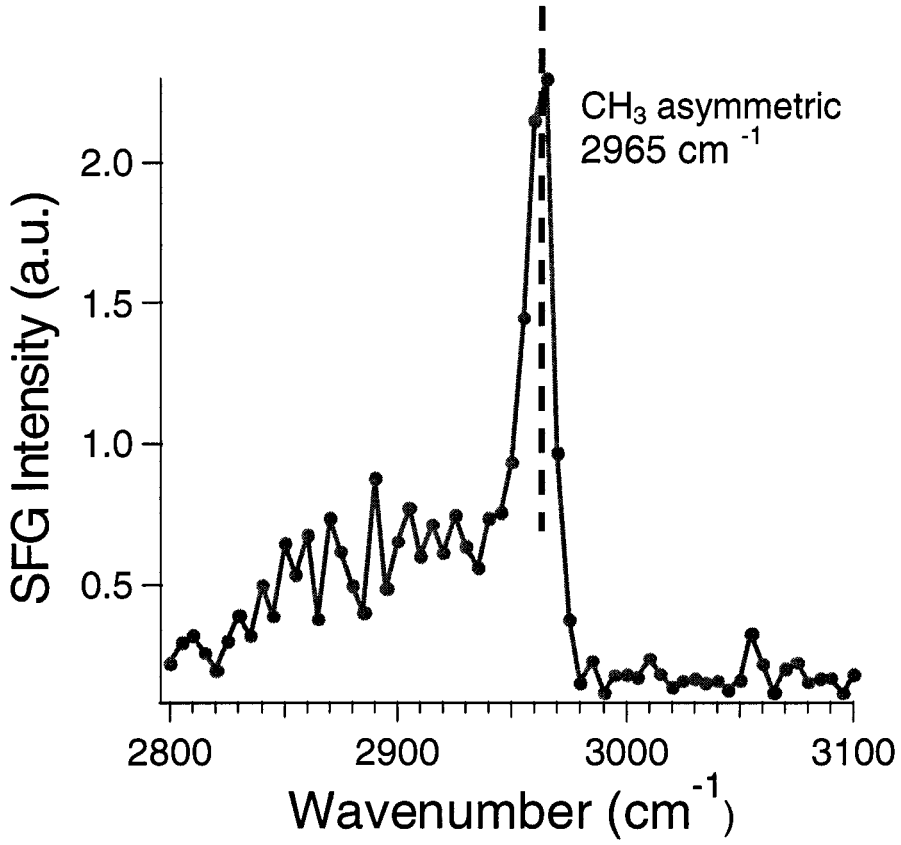

Figure 8.2 The CH region SFG spectra of LK310ctrl adsorbed onto the HFP surface. Note that the spectrum was acquired for the air-dried sample and with ppp polarization.

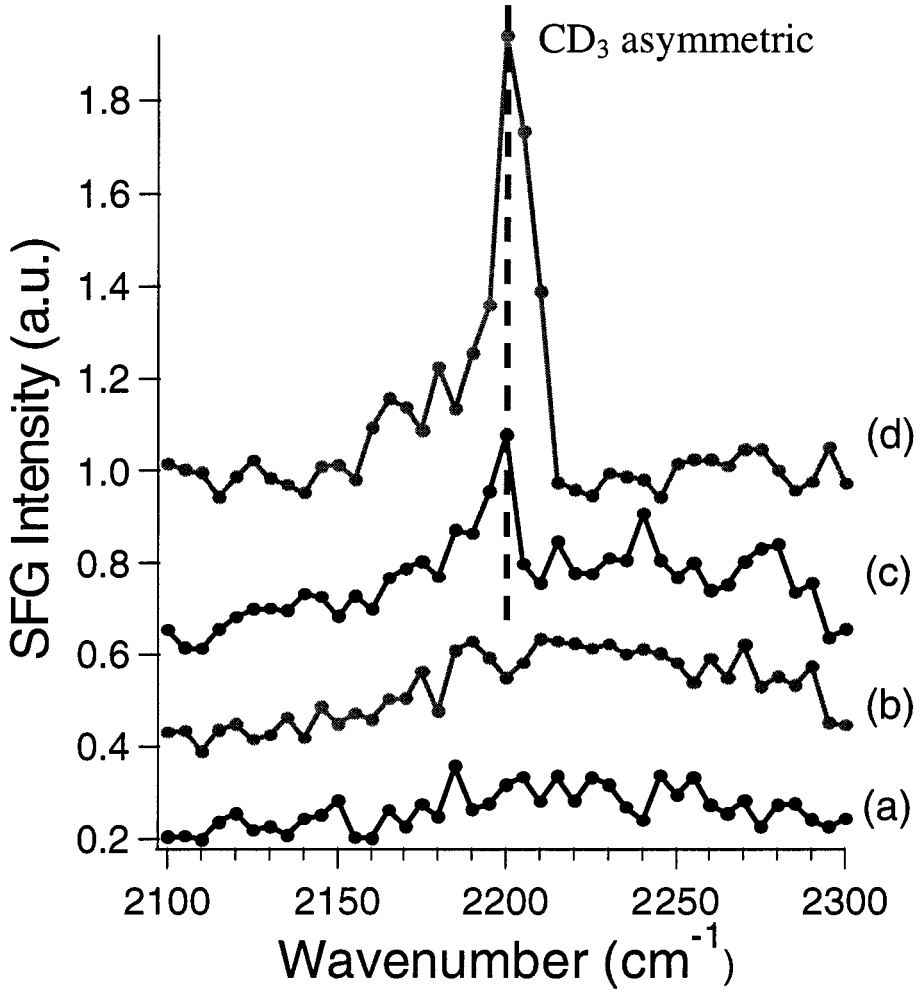

Figure 8.3 The CD region SFG spectra for the different LK310 peptides adsorbed onto the HFP surface, (a) LK310ctrl, (b) LK310Lab1, (c) LK310Lab2, and (d) LK310Lab8. Note that the data were acquired after adsorbing the peptide onto the HFP surface and then air-drying. All the spectra were acquired with ppp polarization.

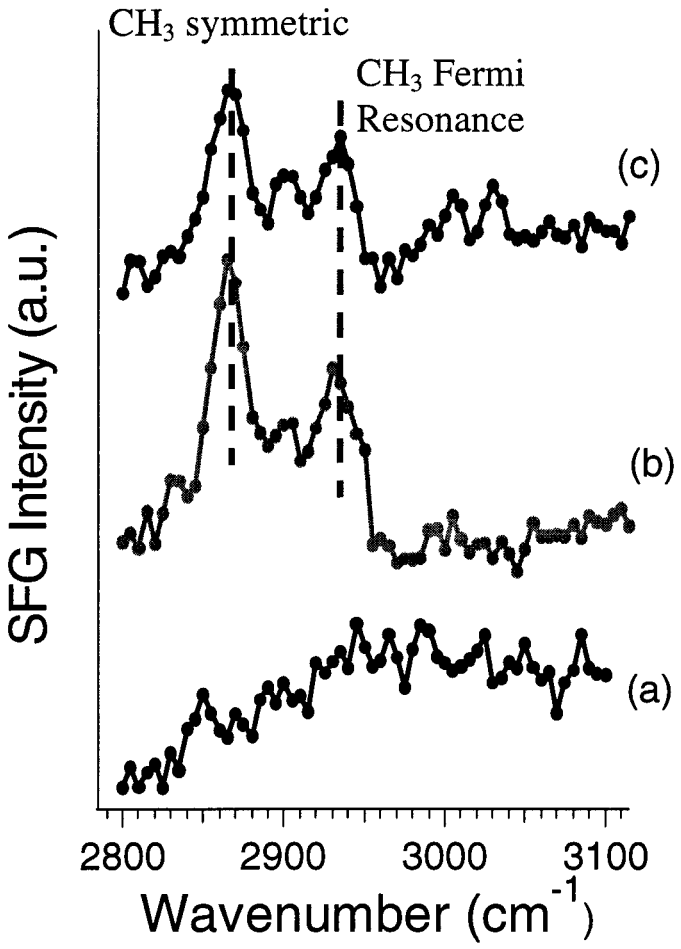

Figure 8.4 The CH region SFG spectrum of the LK310Lab2 peptide adsorbed onto the HFP surface. (a) Control sample without any peptide, (b) LK310Lab2 peptide adsorbed onto HFP in situ, and (c) the sample washed and then re-immersed in D_2O. Note that the spectra were acquired with ssp polarization.

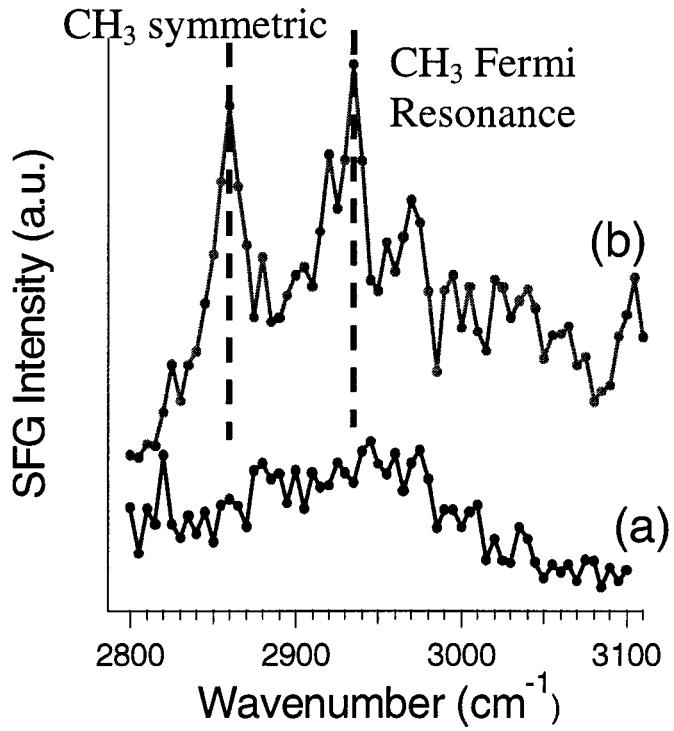

Figure 8.5 CH region SFG spectra of LK310Lab8 adsorbed onto the HFP surface. (a) The control HFP surface immersed in buffer and (b) LK310Lab8 peptide adsorbed onto the HFP surface. Note that the spectra were acquired with ssp polarization.

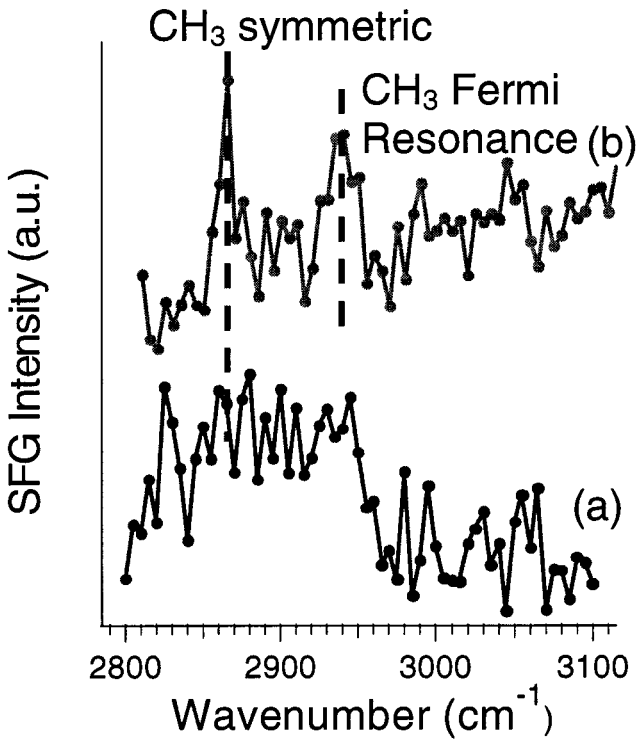

Figure 8.6 CH region SFG spectra of LK310Lab8 adsorbed onto the HFP surface and immersed in D_2O. (a) control HFP surface immersed in D_2O and (b) LK310Lab8 adsorbed onto the HFP surface, washed with buffer and re-immersed in D_2O. Note that the spectra were acquired with ssp polarization.

9 : Summary and Conclusions

Immobilization of bioactive peptides onto surfaces is an area of considerable interest in research areas such as tissue engineering, diagnostics, affinity separations, cell-culture technologies, peptide microarrays and nanobiotechnology[5,6,164]. Specific examples include the identification of peptides that selectively bind to a target element[164,170], peptides that promote cell adhesion[165], and high-throughput microarray methods for identifying peptide ligands for protein binding[166-169]. The surface region, the "biomolecular interface" between a material and the biological environment, plays a crucial role in biomaterials applications[5,6]. As a result, characterization of the biomolecules bound to the surface, especially with respect to their identity, concentration, spatial distribution, conformation and orientation, is very important[6]. Previous studies have demonstrated the ability to probe the identity, concentration, spatial distribution and conformation of adsorbed biomolecules[6,28,29,98,99,116,127]. The key element to retaining the biological specificity of the interface is to preserve their structure. The ability to characterize the adsorbed structure is demonstrated using peptides which adsorb with well-defined secondary structures. Alpha helices and beta sheets are the primary secondary structural motifs in proteins. These two structures primarily differ in the way the backbone is folded.

The primary techniques employed in this project are near-edge X-ray absorption fine structure spectroscopy (NEXAFS) and sum frequency generation (SFG) spectroscopy. NEXAFS uses polarized X-rays from the synchrotron for chemical and structural characterization. SFG is a non-linear optical technique which employs a fixed visible beam and a tunable infrared (IR) beam. The outgoing photon at the sum of the frequencies is collected which gives the technique the surface sensitivity. In addition, it is able to probe the interface *in situ* and obtain time-dependent measurements.

To develop methods for determining the structure of adsorbed biomolecules we employ synthetic peptides that are chemically and structurally well-defined when adsorbed onto surfaces. These peptides contain lysine (K) and leucine (L) amino acids. By changing the sequence of the two amino acids, the secondary structure of the adsorbed peptide can be

controlled. Complementary solid-state nuclear magnetic resonance and infrared spectroscopy measurements of the adsorbed peptides were also done.

Research Progress I:

The first part of the project involved using NEXAFS to probe the structure of the LK peptides adsorbed onto hydrophobic surface. Initially the project involved a comprehensive characterization of amino acid homopolymers at the carbon, nitrogen and oxygen absorption edges. The peaks in the NEXAFS spectra of poly(amino acids) from these three edges were assigned to characteristic bonds based on earlier quantum mechanical calculations for monomeric amino acids. Our research provided a comprehensive characterization of poly(amino acids) peak assignments in NEXAFS spectra, including the amide π^* feature in the nitrogen *k*-edge. The results from this study of amino acid homopolymers provide spectral assignment database required to identify the spectral features in the NEXAFS spectra of adsorbed peptides.

X-ray Photoelectron Spectroscopy (XPS) was used to determine the amount of each peptide that was adsorbed onto the hydrophobic surface. We hypothesized that the polarization-dependence of the NEXAFS spectra from the adsorbed α-helix and β-sheet LK peptides should be different. To test the hypothesis, we synthesized LK peptides with α-helix and β-sheet structures. The polarization-dependence of the backbone amide π^* peak was similar for all the α-helical peptides and was distinct from the polarization-dependence of the β-sheet peptides. This showed the sensitivity of the NEXAFS spectra to different peptide secondary structures. Similar differences in polarization dependence were observed in the π^*_{CO} peak from the backbone carbonyls in the oxygen *k*-edge spectra. Complementary IR measurements also confirm the different structures adopted by the adsorbed peptides.

Research Progress II:

The second part of the project involved *in situ* characterization of the adsorbed peptide structures with Sum Frequency generation (SFG) spectroscopy.

To probe the structure of the peptides interacting with a hydrophobic surface, a fluorocarbon plasma polymer was deposited onto a CaF_2 substrate. These samples are transparent in the IR and the visible region used, so the solid-liquid interface could be probed *in situ* with SFG. Also, the plasma polymer could be deposited onto other substrates for complementary measurements with other analysis techniques. The results for the α-helical peptide adsorbed onto hydrophobic and charged surfaces (negatively charged quartz was used to electrostatically immobilize the peptide to the surface) demonstrated that the peptide adsorbs onto the hydrophobic surface through the terminal methyl groups from the leucine residues and onto the charged surface through the terminal amine groups from the lysine residues. The peptide on the hydrophobic surface was found to be in an ordered, α-helical structure, based on the amide I SFG spectrum.

The α-helical peptide adsorbed onto the hydrophobic surface avoiding the air-water interface showed time-dependent changes in the amide I region. This was monitored by following the intensity changes from the amide I peak (1655 cm^{-1}). Interestingly, the ordering of the methyl groups, based on lack of intensity charges in the C-H spectrum is instantaneous (on the time scale of the experiment). Also, the surface concentration of the adsorbed peptide measured by XPS does not change with time. These results demonstrate there is an initial rapid adsorption of the peptide into a disordered state, followed by a slower conversion to an ordered structure. The above conclusion was further tested by monitoring the intensity of the amide I peak after irradiating the sample with an IR heat lamp. Increasing the sample temperature resulted in an increased rate of ordering of the peptide.

The ability to probe the interaction of the α-helical peptide with the surface was further characterized by using deuterium labeled leucine residues. Deuterium labeling of the methyl groups is stable and causes a significant spectrum shift (~750 cm^{-1}). All the leucine residues except one were labeled so interactions of the unlabeled leucine with the surface could be probed by measuring the C-H spectrum. Results were successful and demonstrated the ability to probe the interaction at a single amino acid resolution in the

CH region. This represents an unprecedented ability to probe locally the structure of interfacial biomolecules.

Significance of Present Research:

The present research identified peptides which spontaneously adsorb onto hydrophobic surfaces retaining their secondary structure. The ability to obtain *in situ*, detailed molecular information (structure, ordering, and surface interactions) about peptide molecules on surfaces was demonstrated for the first time. The unique contribution of the present work is the combination of synthetic chemical approaches with advanced surface analytical tools to address complex biological surface science problems. The results from the present research establish SFG and NEXAFS as powerful techniques for chemical and structural characterization of surfaces and biomolecules immobilized onto those surfaces.

Future Recommendations:

The results from the present study establish the ability of SFG and NEXAFS to obtain detailed molecular information for the peptide adsorbed on the surface. The following are some concrete recommendations to both extend the applicability of SFG and also answer important questions in biointerfacial science. These are designed to both extend the nature and scope of the present work as well as complement the experiments from the present work.

- The experimental results from the NEXAFS characterization of the adsorbed peptides demonstrate the sensitivity of polarization-dependent NEXAFS to adsorbed secondary structure. During the last few years, there has been a tremendous increase in the understanding of the near-edge structure and the ability to simulate the features from ab initio density functional computer codes[43-45]. This has led to the development of detailed understanding of the near-edge features and the ability to ascribe useful meaning to hitherto unknown features[199]. One promising and very successful code is the Stockholm-Berlin code from Prof. Lars Pettersson's group (Stockholm University). Hence, it will be useful and pertinent to follow-up the experimental results with calculations capturing the

sensitivity of polarization-dependent experiments to different backbone secondary structures.

- One of the unique aspects of SFG is the ability to probe the structure of the interfacial water molecules. Even though there are significant efforts from leading groups to glean useful information about water structure from the SFG experiments, there is still room for significant contributions. Our experience with the water region, as well as numerous reports from other groups, demonstrate that there is still a need for more understanding of the peaks from the different states of water at the interface[71,77,200,201]. The peptide adsorbed onto the hydrophobic surface is a good model system embodying the complexity of the origin of the water signal. A recent grant application submitted by my advisor (Prof. Castner), proposes using an integrated approach to understanding this problem, could offer some clues. This approach involves correlating the SFG signal with measurements from solid-state NMR and molecular dynamics simulations to better assign the origin of the different signals in the water region.
- The results for the beta-sheet peptide adsorbed onto the hydrophobic surface show the interaction of the peptide with the surface is mediated through the terminal methyl groups from the leucine residues. However, the amide I region is difficult to interpret and appears to show no signal in the ssp polarization combination. Recently, Chen et.al. showed that some of the amide I modes from the beta-sheets are chiral active (they appear in different polarization combinations) [202,203]. This represents an additional method to obtained structural information of the interfacial biomolecules. Since different structural regions of the biomolecule should appear under different polarization combinations. However, these experiments are only possible in the total internal reflection geometry.
- The results for the beta-sheet peptides, along with results from previous research (the present thesis and from Prof. Chen's group[202,203]) suggest the ability to probe different structural elements of proteins with different polarization combinations. A low molecular weight protein, whose structure is known, would be a good model to establish the ability to probe different structural components of the protein. Due to the unique ability of the different structural elements of the

protein to appear under different polarization combinations, this would represent an elegant approach to obtain straight-forward, high-resolution structural information at the interface.

- All the experiments outlined in this thesis are done using circular windows and collecting the reflected SFG from the interface. Another modality is to use the total internal geometry. This would lead the way to do experiments with different polarization combinations and also obtain more intense signal[204-206]. However, the right angled prisms are very expensive and also more difficult to handle for doing careful experiments.
- Chapter 8 demonstrated the ability to probe peptide-surface interactions at a single amino acid resolution using stable deuterium labeled leucine residues. This is a promising start towards locally probing the interaction of biomolecule with surfaces. A polarization-mapping experiment could be done for the peptide with the single amino acid label in the total internal geometry. In principle, this experiment should be able to determine the complete orientation of the amino acid residue being probed. Repeating the above experiment with another amino acid residue located in a different position in the primary sequence, should determine the complete orientation of the molecule on the hydrophobic surface.
- Several attempts have been reported to probe the gold-liquid interface with SFG. The main challenges are: to probe the interface *in situ* reproducibly and de-convoluting the vibrational peaks at the interface from the underlying metal response (the metal substrate has a strong non-linear response contributing to the SFG output). These problems can be circumvented by using a thin metal overlayer (~5nm)[205]. However, the challenges with this approach are to collect data reproducibly and handling the thin overlayer. Even though a titanium adhesion layer could be employed, de-lamination issues with the overlayer represent a challenge. Also, beam damage should be a concern for the thin metal overlayers. The advantages of probing the gold-liquid interface *in situ* are: the surface chemistry and structure could be spatially and functionally controlled using self-assembled monolayers (SAMs). SAMs also provide good control over the thickness of the organic overlayer. Although the plasma polymer enables

good control over the surface chemistry, controlling film thickness can be a challenge. This prevents the ability to compare the signal intensities collected from different experiments and to do quantitative studies.

- The results from the SFG experiments for the adsorbed peptides demonstrated the ability to obtain useful molecular structure information. However, it will be helpful to follow-up with high-resolution AFM experiments to probe the spatial organization of the adsorbed peptides to complement the NEXAFS and the SFG experiments. Recently, the ability to obtain high-resolution structural characterization of interfacial peptides has been demonstrated with carbon nanotube-modified AFM tips[179]. However, the challenge is to obtain an atomically flat hydrophobic surface and to do careful measurements. One possibility is to use atomically flat Au(111) surfaces modified with self-assembled monolayers.

Bibliography

(1) Horbett, T. A. *Colloids and Surfaces B: Biointerfaces* **1994**, *2*, 225-240.

(2) Baier, R. E.; Dutton, R. C. *Journal of Biomedical Materials Research* **1969**, *3*, 191-206.

(3) Lopez, G. P.; Ratner, B. D.; Tidwell, C. D.; Haycox, C. L.; R.J., R.; Horbett, T. A. *Journal of Biomedical Materials Research* **1992**, *26*, 415-439.

(4) Heller, M. J. *Annual Review of Biomedical Engineering* **2002**, *4*, 129-153.

(5) Kasemo, B. *Surface Science* **2002**, *500*, 656-677.

(6) Castner, D. G.; Ratner, B. D. *Surface Science* **2002**, *500*, 28-60.

(7) Mrksich, M.; Chen, C. S.; Xia, Y. N.; Dike, L. E.; Ingber, D. E.; Whitesides, G. M. *Proceedings of the National Academy of Sciences of the United States of America* **1996**, *93*, 10775-10778.

(8) Sigal, G. B.; Bamdad, C.; Barberis, A.; Strominger, J.; Whitesides, G. M. *Analytical Chemistry* **1996**, *68*, 490-497.

(9) Xia, Y. N.; Whitesides, G. M. *Angewandte Chemie-International Edition* **1998**, *37*, 551-575.

(10) Qin, D.; Xia, Y. N.; Xu, B.; Yang, H.; Zhu, C.; Whitesides, G. M. *Advanced Materials* **1999**, *11*, 1433-1437.

(11) Shi, H. Q.; Tsai, W. B.; Garrison, M. D.; Ferrari, S.; Ratner, B. D. *Nature* **1999**, *398*, 593-597.

(12) Sampson, N. S.; Mrksich, M.; Bertozzi, C. R. *Proceedings of the National Academy of Sciences of the United States of America* **2001**, *98*, 12870-12871.

(13) Demers, L. M.; Ginger, D. S.; Park, S. J.; Li, Z.; Chung, S. W.; Mirkin, C. A. *Science* **2002**, *296*, 1836-1838.

(14) Houseman, B. T.; Mrksich, M. *Chemistry & Biology* **2002**, *9*, 443-454.

(15) Lee, K. B.; Park, S. J.; Mirkin, C. A.; Smith, J. C.; Mrksich, M. *Science* **2002**, *295*, 1702-1705.

(16) Murphy, W. L.; Mercurius, K. O.; Koide, S.; Mrksich, M. *Langmuir* **2004**, *20*, 1026-1030.

(17) Yeo, W. S.; Yousaf, M. N.; Mrksich, M. *Journal of the American Chemical Society* **2003**, *125*, 14994-14995.

(18) Lahann, J.; Mitragotri, S.; Tran, T. N.; Kaido, H.; Sundaram, J.; Choi, I. S.; Hoffer, S.; Somorjai, G. A.; Langer, R. S. *Science* **2003**, *299*, 371-374.

(19) Adriaens, A.; Van Vaeck, L.; Adams, F. *Mass Spectrometry Reviews* **1999**, *18*, 48-81.

(20) Pacholski, M. L.; Winograd, N. *Chemical Reviews* **1999**, *99*, 2977-+.

(21) Van Vaeck, L.; Adriaens, A.; Gijbels, R. *Mass Spectrometry Reviews* **1999**, *18*, 1-47.

(22) Belu, A. M.; Graham, D. J.; Castner, D. G. *Biomaterials* **2003**, *24*, 3635-3653.

(23) Mantus, D. S.; Ratner, B. D.; Carlson, B. A.; Moulder, J. F. *Analytical Chemistry* **1993**, *65*, 1431-1438.

(24) Wood, M.; Zhou, Y.; Brummel, C. L.; Winograd, N. *Analytical Chemistry* **1994**, *66*, 2425-2432.

(25) Adraens, A.; vanVaeck, L.; Adams, F. *Mass Spectrometry Reviews* **1999**, *18*, 48-81.

(26) Leonard, D.; Mathieu, H. J. *Fresenius Journal of Analytical Chemistry* **1999**, *365*, 3-11.

(27) vanVaeck, L.; Adraens, A.; Gijbels, R. *Mass Spectrometry Reviews* **1999**, *18*, 1-47.

(28) Wagner, M. S.; Castner, D. G. *Langmuir* **2001**, *17*, 4649-4660.

(29) Xia, N.; May, C. J.; McArthur, S. L.; Castner, D. G. *Langmuir* **2002**, *18*, 4090-4097.

(30) Ratner, B. D.; Castner, D. G. *Colloids and Surfaces B: Biointerfaces* **1994**, *2*, 333-346.

(31) Ratner, B. D.; Castner, D. G. In *Surface Analysis - The Principle Techniques*; Vickerman, J. C., Ed.; Johh Wiley & Sons: Chichester, 1997; pp 43-98.

(32) Stohr, J. *NEXAFS Spectroscopy*; Springer-Verlag: Heidelberg, 1992.

(33) Dhez, O.; Ade, H.; Urquhart, S. G. *J. Electron Spectrosc. Relat. Phenom.* **2003**, *128*, 85-96.

(34) Boese, J.; Osanna, A.; Jacobsen, C.; Kirz, J. *J. Electron Spectrosc. Relat. Phenom.* **1997**, *85*, 9-15.

(35) Kikuma, J.; Tonner, B. P. *J. Electron Spectrosc. Relat. Phenom.* **1996**, *82*, 53-60.

(36) Kirtley, S. M.; Mullins, O. C.; Chen, J.; Vanelp, J.; George, S. J.; Chen, C. T.; Ohalloran, T.; Cramer, S. P. *Biochimica Et Biophysica Acta* **1992**, *1132*, 249-254.

(37) Tanaka, M.; Nakagawa, K.; Koketsu, T.; Agui, A.; Yokoya, A. *J. Synchrot. Radiat.* **2001**, *8*, 1009-1011.

(38) Hahner, G.; Woll, C.; Buck, M.; Grunze, M. *Langmuir* **1993**, *9*, 1955-1958.

(39) Kinzler, M.; Schertel, A.; Hahner, G.; Woll, C.; Grunze, M.; Albrecht, H.; Holzhuter, G.; Gerber, T. *Journal of Chemical Physics* **1994**, *100*, 7722-7735.

(40) Bierbaum, K.; Kinzler, M.; Woll, C.; Grunze, M. *Langmuir* **1995**, *11*, 512-518.

(41) Efimenko, K.; Novick, B.; Carbonell, R. G.; DeSimone, J. M.; Genzer, J. *Langmuir* **2002**, *18*, 6170-6179.

(42) Zubavichus, Y.; Zharnikov, M.; Schaporenko, A.; Grunze, M. *J. Electron Spectrosc. Relat. Phenom.* **2004**, *134*, 25-33.

(43) Gordon, M. L.; Cooper, G.; Morin, C.; Araki, T.; Turci, C. C.; Kaznatcheev, K.; Hitchcock, A. P. *J. Phys. Chem. A* **2003**, *107*, 6144-6159.

(44) Fujii, K.; Akamatsu, K.; Muramatsu, Y.; Yokoya, A. *Nuclear Instruments and Methods in Physics Research B* **2003**, *199*, 249-254.

(45) Kaznacheyev, K.; Osanna, A.; Jacobsen, C.; Plashkevych, O.; Vahtras, O.; Agren, H. *J. Phys. Chem. A* **2002**, *106*, 3153-3168.

(46) Hasselstrom, J.; Karis, O.; Weinelt, M.; Wassdahl, N.; Nilsson, A.; Nyberg, M.; Pettersson, L. G. M.; Samant, M. G.; Stohr, J. *Surf. Sci.* **1998**, *407*, 221-236.

(47) Carravetta, V.; Plashkevych, O.; Agren, H. *J. Chem. Phys.* **1998**, *109*, 1456-1464.

(48) Burnett, D. J.; Gabelnick, A. M.; Marsch, A. L.; Fischer, D. A.; Gland, J. L. *Surface Science* **2004**, *553*, 1-12.

(49) Srivastava, P.; Baberschke, K. *Topics in Catalysis* **2000**, *10*, 199-207.

(50) Chen, J. G. *Surface Science Reports* **1997**, *30*, 5-152.

(51) Gamble, L. J.; Ravel, B.; Fischer, D. A.; Castner, D. G. *Langmuir* **2002**, *18*, 2183-2189.

(52) Ade, H.; Winesett, D. A.; Smith, A. P.; Qu, S.; Ge, S.; Sokolov, J.; Rafailovich, M. *Europhysics Letters* **1999**, *45*, 526-532.

(53) Zhu, S.; Liu, Y.; Rafailovich, M. H.; Sokolov, J.; Gersappe, D.; Winesett, D. A.; Ade, H. *Nature* **1999**, *400*, 49-51.

(54) Morin, C.; Ikeura-Sekiguchi, H.; Tyliszczak, T.; Cornelius, R.; Brash, J. L.; Hitchcock, A. P.; Scholl, A.; Nolting, F.; Appel, G.; Winesett, D. A.; Kaznacheyev, K.; Ade, H. *Journal of Electron Spectroscopy and Related Phenomena* **2001**, *121*, 203-224.

(55) Sloop, C. C.; Ade, H.; Fornes, R. E.; Gilbert, R. D.; Smith, A. P. *Journal of Polymer Science Part B-Polymer Physics* **2001**, *39*, 531-535.

(56) Smith, A. P.; Urquhart, S. G.; Winesett, D. A.; Mitchell, G.; Ade, H. *Applied Spectroscopy* **2001**, *55*, 1676-1681.

(57) Ade, H.; Zhang, X.; Cameron, S.; Costello, C.; Kirz, J.; Williams, S. *Science* **1992**, *258*, 972-975.

(58) Hitchcock, A. P.; Morin, C.; Tyliszczak, T.; Koprinarov, I. N.; Ikeura-Sekiguchi, H.; Lawrence, J. R.; Leppard, G. G. *Surface Review and Letters* **2002**, *9*, 193-201.

(59) Hitchcock, A. P.; Morin, C.; Heng, Y. M.; Cornelius, R. M.; Brash, J. L. *Journal of Biomaterials Science-Polymer Edition* **2002**, *13*, 919-937.

(60) Bain, C. D. *Journal of the Chemical Society-Faraday Transactions* **1995**, *91*, 1281-1296.

(61) Shen, Y. R. *Nature* **1989**, *337*, 519-525.

(62) Chen, Z.; Shen, Y. R.; Somorjai, G. A. *Annual Review of Physical Chemistry* **2002**, *53*, 437-465.

(63) Guyotsionnest, P.; Superfine, R.; Hunt, J. H.; Shen, Y. R. *Chemical Physics Letters* **1988**, *144*, 1-5.

(64) Yeganeh, M. S.; Dougal, S. M.; Polizzotti, R. S.; Rabinowitz, P. *Physical Review Letters* **1995**, *74*, 1811-1814.

(65) Ye, S.; Nihonyanagi, S.; Uosaki, K. *Physical Chemistry Chemical Physics* **2001**, *3*, 3463-3469.

(66) Himmelhaus, M.; Eisert, F.; Buck, M.; Grunze, M. *Journal of Physical Chemistry B* **2000**, *104*, 576-584.

(67) Wang, J.; Chen, C. Y.; Buck, S. M.; Chen, Z. *Journal of Physical Chemistry B* **2001**, *105*, 12118-12125.

(68) Kim, J.; Kim, G.; Cremer, P. S. *Langmuir* **2001**, *17*, 7255-7260.

(69) Kim, J.; Cremer, P. S. *Chemphyschem* **2001**, *2*, 543.

(70) Du, Q.; Freysz, E.; Shen, Y. R. *Physical Review Letters* **1994**, *72*, 238-241.

(71) Du, Q.; Freysz, E.; Shen, Y. R. *Science* **1994**, *264*, 826-828.

(72) Gurau, M. C.; Kim, G.; Lim, S. M.; Albertorio, F.; Fleisher, H. C.; Cremer, P. S. *Chemphyschem* **2003**, *4*, 1231-1233.

(73) Scatena, L. F.; Richmond, G. L. *Journal of Physical Chemistry B* **2004**, *108*, 12518-12528.

(74) Scatena, L. F.; Richmond, G. L. *Chemical Physics Letters* **2004**, *383*, 491-495.

(75) Scatena, L. F.; Richmond, G. L. *Journal of Physical Chemistry B* **2001**, *105*, 11240-11250.

(76) Richmond, G. L. *Annual Review of Physical Chemistry* **2001**, *52*, 357-389.

(77) Scatena, L. F.; Brown, M. G.; Richmond, G. L. *Science* **2001**, *292*, 908-912.

(78) Ward, R. N.; Davies, P. B.; Bain, C. D. *Journal of Physical Chemistry* **1993**, *97*, 7141-7143.

(79) Kim, J.; Somorjai, G. A. *Journal of the American Chemical Society* **2003**, *125*, 3150-3158.

(80) Jung, S. Y.; Lim, S. M.; Albertorio, F.; Kim, G.; Gurau, M. C.; Yang, R. D.; Holden, M. A.; Cremer, P. S. *Journal of the American Chemical Society* **2003**, *125*, 12782-12786.

(81) Kim, G.; Gurau, M.; Kim, J.; Cremer, P. S. *Langmuir* **2002**, *18*, 2807-2811.

(82) Wang, J.; Buck, S. M.; Chen, Z. *Journal of Physical Chemistry B* **2002**, *106*, 11666-11672.

(83) Kim, J.; Opdahl, A.; Chou, K. C.; Somorjai, G. A. *Langmuir* **2003**, *19*.

(84) Wang, J.; Woodcock, S. E.; Buck, S. M.; Chen, C. S.; Chen, Z. *Journal of the American Chemical Society* **2001**, *123*, 9470-9471.

(85) Hong, S. C.; Zhang, C.; Shen, Y. R. *Applied Physics Letters* **2003**, *82*, 3068-3070.

(86) Wang, J.; Even, M. A.; Chen, X. Y.; Schmaier, A. H.; Waite, J. H.; Chen, Z. *Journal of the American Chemical Society* **2003**, *125*, 9914-9915.

(87) Raschke, M. B.; Hayashi, M.; Lin, S. H.; Shen, Y. R. *Chemical Physics Letters* **2002**, *359*, 367-372.

(88) Wang, J.; Clarke, M. L.; Zhang, Y. B.; Chen, X. Y.; Chen, Z. *Langmuir* **2003**, *19*, 7862-7866.

(89) Drobny, G. P.; Long, J. R.; Karlsson, T.; Shaw, W.; Popham, J.; Oyler, N.; Bower, P.; Stringer, J.; Gregory, D.; Mehta, M.; Stayton, P. S. *Annual Review of Physical Chemistry* **2003**, *54*, 531-571.

(90) Bower, P. V., Ph.D. Thesis: Department of Chemistry, University of Washington, Seattle, 2001.

(91) Bower, P. V.; Oyler, N.; Mehta, M. A.; Long, J. R.; Stayton, P. S.; Drobny, G. P. *Journal of the American Chemical Society* **1999**, *121*, 8373-8375.

(92) Long, J. R.; Shaw, W. J.; Stayton, P. S.; Drobny, G. P. *Biochemistry* **2001**, *40*, 15451-15455.

(93) Shaw, W. J.; Long, J. R.; Campbell, A. A.; Stayton, P. S.; Drobny, G. P. *Journal of the American Chemical Society* **2000**, *122*, 7118-7119.

(94) Shaw, W. J.; Long, J. R.; Dindot, J. L.; Campbell, A. A.; Stayton, P. S.; Drobny, G. P. *Journal of the American Chemical Society* **2000**, *122*, 1709-1716.

(95) Long, J. R.; Oyler, N.; Drobny, G. P.; Stayton, P. S. *Journal of the American Chemical Society* **2002**, *124*, 6297-6303.

(96) Shen, M. C.; Pan, Y. V.; Wagner, M. S.; Hauch, K. D.; Castner, D. G.; Ratner, B. D.; Horbett, T. A. *Journal of Biomaterials Science-Polymer Edition* **2001**, *12*, 961-978.

(97) Lu, H. B.; Campbell, C. T.; Graham, D. J.; Ratner, B. D. *Anal. Chem.* **2000**, *72*, 2886-2894.

(98) Wagner, M. S.; McArthur, S. L.; Shen, M. C.; Horbett, T. A.; Castner, D. G. *Journal of Biomaterials Science-Polymer Edition* **2002**, *13*, 407-428.

(99) Tidwell, C. D.; Castner, D. G.; Golledge, S. L.; Ratner, B. D.; Meyer, K.; Hagenhoff, B.; Benninghoven, A. *Surf. Interface Anal.* **2001**, *31*, 724-733.

(100) Bower, D. I.; Maddams, W. F. *The vibrational spectroscopy of polymers*; Cambridge University Press, 1989.

(101) Kasemo, B. *Surf. Sci.* **2002**, *500*, 656-677.

(102) Markley, J. L.; Meadows, D. H.; Jardetzky, O. *Journal of Biological Chemistry* **1967**, *27*, 25-40.

(103) Poland, D.; Scheraga, H. A. *J. Chem. Phys.* **1966**, *45*, 1456-1463.

(104) Shotts, W. J.; Sievers, A. J. *Biopolymers* **1974**, *13*, 2593-2614.

(105) Silverman, D. N.; Scheraga, H. A. *Biochemistry* **1971**, *10*, 1340-1347.

(106) Fasman, G. D. *Poly-a-Amino Acids: Protein Models for Conformational Studies*; Marcel Dekker, INC.: New York, 1967; Vol. 1.

(107) Shard, A. G.; Whittle, J. D.; Beck, A. J.; Brookes, P. N.; Bullett, N. A.; Talib, R. A.; Mistry, A.; Barton, D.; McArthur, S. L. *J. Phys. Chem. B* **2004**, *108*, 12472-12480.

(108) Wu, W. L.; Sambasivan, S.; Wang, C. Y.; Wallace, W. E.; Genzer, J.; Fischer, D. A. *European Physical Journal E* **2003**, *12*, 127-132.

(109) Genzer, J.; Sivaniah, E.; Kramer, E. J.; Wang, J. G.; Korner, H.; Char, K.; Ober, C. K.; DeKoven, B. M.; Bubeck, R. A.; Fischer, D. A.; Sambasivan, S. *Langmuir* **2000**, *16*, 1993-1997.

(110) Urquhart, S. G.; Smith, A. P.; Ade, H. W.; Hitchcock, A. P.; Rightor, E. G.; Lidy, W. *J. Phys. Chem. B* **1999**, *103*, 4603-4610.

(111) Crain, J. N.; Kirakosian, A.; Lin, J. L.; Gu, Y. D.; Shah, R. R.; Abbott, N. L.; Himpsel, F. J. *J. Appl. Phys.* **2001**, *90*, 3291-3295.

(112) Mantus, D. S.; Ratner, B. D.; Carlson, B. A.; Moulder, J. F. *Anal. Chem.* **1993**, *65*, 1431-1438.

(113) Wagner, M. S.; Castner, D. G. *Langmuir* **2001**, *17*, 4649-4660.

(114) Xia, N.; May, C. J.; McArthur, S. L.; Castner, D. G. *Langmuir* **2002**, *18*, 4090-4097.

(115) Wagner, M. S.; Horbett, T. A.; Castner, D. G. *Langmuir* **2003**, *19*, 1708-1715.

(116) Wang, H.; Castner, D. G.; Ratner, B. D.; Jiang, S. *Langmuir* **2004**, *20*, 1877-1887.

(117) Bartiau, S., Undergraduate Thesis: Faculte des Sciences Agronomiques, Unite de Chimie des interfaces, Universite Catholique de Louvain, Louvain-la-Neuve, 1995.

(118) Samuel, N. T.; Wagner, M. S.; Dornfeld, K. D.; Castner, D. G. *Surface Science Spectra* **2001**, *8*, 163-184.

(119) Long, J. R.; Oyler, N.; Drobny, G. P.; Stayton, P. S. *Journal of the American Chemical Society* **2002**, *124*, 6297-6303.

(120) Morar, J. F.; Himpsel, F. J.; Hollinger, G.; Jordon, J. L.; Hughes, G.; McFeely, F. R. *Phys. Rev. B* **1986**, *33*, 1346-1349.

(121) Ratner, B. D.; Castner, D. G. In *Surface Analysis - The Principal Techniques*; Vickerman, J. C., Ed.; John Wiley and Sons Ltd.: Chichester, 1997; pp 43-98.

(122) Bomben, K. D.; Dev, S. B. *Anal. Chem.* **1988**, *60*, 1393-1397.

(123) Urquhart, S. G.; Hitchcock, A. P.; Priester, R. D.; Rightor, E. G. *Journal of Polymer Science: Part B: Polymer Physics* **1995**, *33*, 1603-1620.

(124) Zwahlen, M.; Brovelli, D.; Caseri, W.; Hahner, G. *Journal of Colloid and Interface Science* **2002**, *256*, 262-267.

(125) Apen, E.; Hitchcock, A. P.; Gland, J. L. *Journal of Physical Chemistry* **1993**, *97*, 6859-6866.

(126) Urquhart, S. G.; Ade, H. *J. Phys. Chem. B* **2002**, *106*, 8531-8538.

(127) Xia, N.; Castner, D. G. *Journal of Biomedical Materials Research Part A* **2003**, *67A*, 179-190.

(128) Chanda, S. K.; Caldwell, J. S. *Drug Discovery Today* **2003**, *8*, 168-174.

(129) Pollack, J. R.; Sorlie, T.; Perou, C. M.; Rees, C. A.; Jeffrey, S. S.; Lonning, P. E.; Tibshirani, R.; Botstein, D.; Borresen-Dale, A. L.; Brown, P. O. *Proceedings of the National Academy of Sciences of the United States of America* **2002**, *99*, 12963-12968.

(130) He, P.; Tang, Z. Y.; Liu, B. B.; Ye, S. L.; Liu, Y. K. *Journal of Cancer Research and Clinical Oncology* **1999**, *125*, 77-82.

(131) Wang, D. G.; Fan, J. B.; Siao, C. J.; Berno, A.; Young, P.; Sapolsky, R.; Ghandour, G.; Perkins, N.; Winchester, E.; Spencer, J.; Kruglyak, L.; Stein, L.; Hsie, L.; Topaloglou, T.; Hubbell, E.; Robinson, E.; Mittmann, M.; Morris, M. S.; Shen, N. P.; Kilburn, D.; Rioux, J.; Nusbaum, C.; Rozen, S.; Hudson, T. J.; Lipshutz, R.; Chee, M.; Lander, E. S. *Science* **1998**, *280*, 1077-1082.

(132) Cheung, V. G.; Gregg, J. P.; Gogolin-Ewens, K. J.; Bandong, J.; Stanley, C. A.; Baker, L.; Higgins, M. J.; Nowak, N. J.; Shows, T. B.; Ewens, W. J.; Spielman, R. S. *Nature Genetics* **1998**, *18*, 225-230.

(133) Wodicka, L.; Dong, H. L.; Mittmann, M.; Ho, M. H.; Lockhart, D. J. *Nature Biotechnology* **1997**, *15*, 1359-1367.

(134) Heller, R. A.; Schena, M.; Chai, A.; Shalon, D.; Bedilion, T.; Gilmore, J.; Woolley, D. E.; Davis, R. W. *Proceedings of the National Academy of Sciences of the United States of America* **1997**, *94*, 2150-2155.

(135) DeRisi, J.; Penland, L.; Brown, P. O.; Bittner, M. L.; Meltzer, P. S.; Ray, M.; Chen, Y. D.; Su, Y. A.; Trent, J. M. *Nature Genetics* **1996**, *14*, 457-460.

(136) Niemeyer, C. M. *Current Opinion in Chemical Biology* **2000**, *4*, 609-618.

(137) Elghanian, R.; Storhoff, J. J.; Mucic, R. C.; Letsinger, R. L.; Mirkin, C. A. *Science* **1997**, *277*, 1078-1081.

(138) Chrisey, L. A.; Lee, G. U.; Oferrall, C. E. *Nucleic Acids Research* **1996**, *24*, 3031-3039.

(139) Herne, T. M.; Tarlov, M. J. *Journal of the American Chemical Society* **1997**, *119*, 8916-8920.

(140) Dolan, P. L.; Wu, Y.; Ista, L. K.; Metzenberg, R. L.; Nelson, M. A.; Lopez, G. P. *Nucleic Acids Research* **2001**, *29*.

(141) Charles, P. T.; Vora, G. J.; Andreadis, J. D.; Fortney, A. J.; Meador, C. E.; Dulcey, C. S.; Stenger, D. A. *Langmuir* **2003**, *19*, 1586-1591.

(142) Kumar, P.; Choithani, J.; Gupta, K. C. *Nucleic Acids Research* **2004**, *32*.

(143) Strother, T.; Cai, W.; Zhao, X. S.; Hamers, R. J.; Smith, L. M. *Journal of the American Chemical Society* **2000**, *122*, 1205-1209.

(144) Rogers, Y. H.; Jiang-Baucom, P.; Huang, Z. J.; Bogdanov, V.; Anderson, S.; Boyce-Jacino, M. T. *Analytical Biochemistry* **1999**, *266*, 23-30.

(145) Proudnikov, D.; Timofeev, E.; Mirzabekov, A. *Analytical Biochemistry* **1998**, *259*, 34-41.

(146) Rasmussen, S. R.; Larsen, M. R.; Rasmussen, S. E. *Analytical Biochemistry* **1991**, *198*, 138-142.

(147) Schena, M.; Shalon, D.; Davis, R. W.; Brown, P. O. *Science* **1995**, *270*, 467-470.

(148) Wolf, L. K.; Gao, Y.; Georgiadis, R. M. *Langmuir* **2004**, *20*, 3357-3361.

(149) Kimura-Suda, H.; Petrovykh, D. Y.; Tarlov, M. J.; Whitman, L. J. *Journal of the American Chemical Society* **2003**, *125*, 9014-9015.

(150) Wackerbarth, H.; Grubb, M.; Zhang, J. D.; Hansen, A. G.; Ulstrup, J. *Langmuir* **2004**, *20*, 1647-1655.

(151) Parak, W. J.; Pellegrino, T.; Micheel, C. M.; Gerion, D.; Williams, S. C.; Alivisatos, A. P. *Nano Letters* **2003**, *3*, 33-36.

(152) Kelley, S. O.; Barton, J. K.; Jackson, N. M.; McPherson, L. D.; Potter, A. B.; Spain, E. M.; Allen, M. J.; Hill, M. G. *Langmuir* **1998**, *14*, 6781-6784.

(153) Liu, M. Z.; Amro, N. A.; Chow, C. S.; Liu, G. Y. *Nano Letters* **2002**, *2*, 863-867.

(154) Crozier, P. S.; Stevens, M. J. *Journal of Chemical Physics* **2003**, *118*, 3855-3860.

(155) Petrovykh, D. Y.; Kimura-Suda, H.; Whitman, L. J.; Tarlov, M. J. *Journal of the American Chemical Society* **2003**, *125*, 5219-5226.

(156) Levicky, R.; Herne, T. M.; Tarlov, M. J.; Satija, S. K. *Journal of the American Chemical Society* **1998**, *120*, 9787-9792.

(157) Mourougou-Candoni, N.; Naud, C.; Thibaudau, F. *Langmuir* **2003**, *19*, 682-686.

(158) Moewes, A.; MacNaughton, J.; Wilks, R.; Lee, J. S.; Wettig, S. D.; Kraatz, H. B.; Kurmaev, E. Z. *Journal of Electron Spectroscopy and Related Phenomena* **2004**, *137-40*, 817-822.

(159) Fujii, K.; Akamatsu, K.; Yokoya, A. *Journal of Physical Chemistry B* **2004**, *108*, 8031-8035.

(160) May, C. J.; Canavan, H. E.; Castner, D. G. *Analytical Chemistry* **2004**, *76*, 1114-1122.

(161) Samuel, N. T.; Fischer, D. A.; Castner, D. G. *to be submitted* **2005**.

(162) Furukawa, M.; Fujisawa, H.; Katano, S.; Ogasawara, H.; Kim, Y.; Komeda, T.; Nilsson, A.; Kawai, M. *Surface Science* **2003**, *532*, 261-266.

(163) Briones, C.; Mateo-Marti, E.; Gomez-Navarro, C.; Parro, V.; Roman, E.; Martin-Gago, J. A. *Physical Review Letters* **2004**, *93*.

(164) Sarikaya, M.; Tamerler, C.; Jen, A. K. Y.; Schulten, K.; Baneyx, F. *Nature Materials* **2003**, *2*, 577-585.

(165) Shin, H.; Jo, S.; Mikos, A. G. *Biomaterials* **2003**, *24*, 4353-4364.

(166) Houseman, B. T.; Gawalt, E. S.; Mrksich, M. *Langmuir* **2003**, *19*, 1522-1531.

(167) Houseman, B. T.; Huh, J. H.; Kron, S. J.; Mrksich, M. *Nature Biotechnology* **2002**, *20*, 270-274.

(168) Schulze, W. X.; Mann, M. *Journal of Biological Chemistry* **2004**, *279*, 10756-10764.

(169) Duburcq, X.; Olivier, C.; Malingue, F.; Desmet, R.; Bouzidi, A.; Zhou, F. L.; Auriault, C.; Gras-Masse, H.; Melnyk, O. *Bioconjugate Chemistry* **2004**, *15*, 307-316.

(170) Whaley, S. R.; English, D. S.; Hu, E. L.; Barbara, P. F.; Belcher, A. M. *Nature* **2000**, *405*, 665-668.

(171) Chilkoti, A.; Hubbell, J. A. *MRS Bulletin* **2005**, *30*, 175-176.

(172) Degrado, W. F.; Lear, J. D. *Journal of the American Chemical Society* **1985**, *107*, 7684-7689.

(173) Samuel, N. T.; McCrea, K.; Gamble, L. J.; Ward, R. S.; Stayton, P. S.; Somorjai, G. A.; Castner, D. G. *to be submitted* **2005**.

(174) Castano, S.; Desbat, B.; Dufourcq, J. *Biochimica Et Biophysica Acta-Biomembranes* **2000**, *1463*, 65-80.

(175) Hahner, G.; Woll, C.; Buck, M.; Grunze, M. *Langmuir* **1993**, *9*, 1955-1958.

(176) Morin, C.; Hitchcock, A. R.; Cornelius, R. M.; Brash, J. L.; Urquhart, S. G.; Scholl, A.; Doran, A. *Journal of Electron Spectroscopy and Related Phenomena* **2004**, *137-40*, 785-794.

(177) Sneer, R.; Weygand, M. J.; Kjaer, K.; Tirrell, D. A.; Rapaport, H. *Chemphyschem* **2004**, *5*, 747-750.

(178) Rapaport, H.; Kjaer, K.; Jensen, T. R.; Leiserowitz, L.; Tirrell, D. A. *Journal of the American Chemical Society* **2000**, *122*, 12523-12529.

(179) Powers, E. T.; Yang, S. I.; Lieber, C. M.; Kelly, J. W. *Angewandte Chemie-International Edition* **2002**, *41*, 127-130.

(180) Wittmann, J. C.; Smith, P. *Nature* **1991**, *352*, 414-417.

(181) Butoi, C. I.; Mackie, N. M.; Gamble, L. J.; Castner, D. G.; Barnd, J.; Miller, A. M.; Fisher, E. R. *Chemistry of Materials* **2000**, *12*, 2014-2024.

(182) Castner, D. G.; Lewis, K. B.; Fischer, D. A.; Ratner, B. D.; Gland, J. L. *Langmuir* **1993**, *9*, 537-542.

(183) Toney, M. F.; Russell, T. P.; Logan, J. A.; Kikuchi, H.; Sands, J. M.; Kumar, S. K. *Nature* **1995**, *374*, 709-711.

(184) Stohr, J.; Samant, M. G.; Luning, J.; Callegari, A. C.; Chaudhari, P.; Doyle, J. P.; Lacey, J. A.; Lien, S. A.; Purushothaman, S.; Speidell, J. L. *Science* **2001**, *292*, 2299-2302.

(185) Singh, B. R. *Infrared Analysis of Peptides and Proteins Principles and Applications*; Oxford University Press: Washington, DC, 2000; Vol. 750.

(186) Wang, J.; Buck, S. M.; Even, M. A.; Chen, Z. *Journal of the American Chemical Society* **2002**, *124*, 13302-13305.

(187) Kim, G.; Gurau, M. C.; Lim, S. M.; Cremer, P. S. *Journal of Physical Chemistry B* **2003**, *107*, 1403-1409.

(188) Buck, M.; Himmelhaus, M. *Journal of Vacuum Science & Technology a-Vacuum Surfaces and Films* **2001**, *19*, 2717-2736.

(189) Kim, J.; Kim, G.; Cremer, P. S. *Journal of the American Chemical Society* **2002**, *124*, 8751-8756.

(190) Garrison, M. D.; Luginbuhl, R.; Overney, R. M.; Ratner, B. D. *Thin Solid Films* **1999**, *352*, 13-21.

(191) Iler, R. K. In *The Chemistry of Silica*; Wiley: New York, 1979; pp 622-729.

(192) Ong, S. W.; Zhao, X. L.; Eisenthal, K. B. *Chemical Physics Letters* **1992**, *191*, 327-335.

(193) Gragson, D. E.; McCarty, B. M.; Richmond, G. L. *Journal of the American Chemical Society* **1997**, *119*, 6144-6152.

(194) Samuel, N. T.; McCrea, K. R.; Gamble, L. J.; Ward, R. S.; Stayton, P. S.; Somorjai, G. A.; Castner, D. G. *to be submitted* **2005**.

(195) Samuel, N. T.; Gamble, L. J.; Fischer, D. A.; Castner, D. G. *to be submitted* **2005**.

(196) Roke, S.; Schins, J.; Muller, M.; Bonn, M. *Physical Review Letters* **2003**, *90*.

(197) Lu, R.; Gan, W.; Wu, B. H.; Chen, H.; Wang, H. F. *Journal of Physical Chemistry B* **2004**, *108*, 7297-7306.

(198) Paszti, Z.; Wang, J.; Clarke, M. L.; Chen, Z. *Journal of Physical Chemistry B* **2004**, *108*, 7779-7787.

(199) Wernet, P.; Nordlund, D.; Bergmann, U.; Cavalleri, M.; Odelius, M.; Ogasawara, H.; Naslund, L. A.; Hirsch, T. K.; Ojamae, L.; Glatzel, P.; Pettersson, L. G. M.; Nilsson, A. *Science* **2004**, *304*, 995-999.

(200) Richmond, G. L. *Chemical Reviews* **2002**, *102*, 2693-2724.

(201) Becraft, K. A.; Richmond, G. L. *Journal of Physical Chemistry B* **2005**, *109*, 5108-5117.

(202) Wang, J.; Chen, X. Y.; Clarke, M. L.; Chen, Z. *Proceedings of the National Academy of Sciences of the United States of America* **2005**, *102*, 4978-4983.

(203) Chen, X. Y.; Wang, J.; Sniadecki, J. J.; Even, M. A.; Chen, Z. *Langmuir* **2005**, *21*, 2662-2664.

(204) Beattie, D. A.; Haydock, S.; Bain, C. D. *Vibrational Spectroscopy* **2000**, *24*, 109-123.

(205) Williams, C. T.; Yang, Y.; Bain, C. D. *Langmuir* **2000**, *16*, 2343-2350.

(206) Kweskin, S. J.; Komvopoulos, K.; Somorjai, G. A. *Langmuir* **2005**, *21*, 3647-3652.

Appendix 1 : Electrospray Ionization Mass Spectrometry (ESI-MS) data of the various synthesized peptides

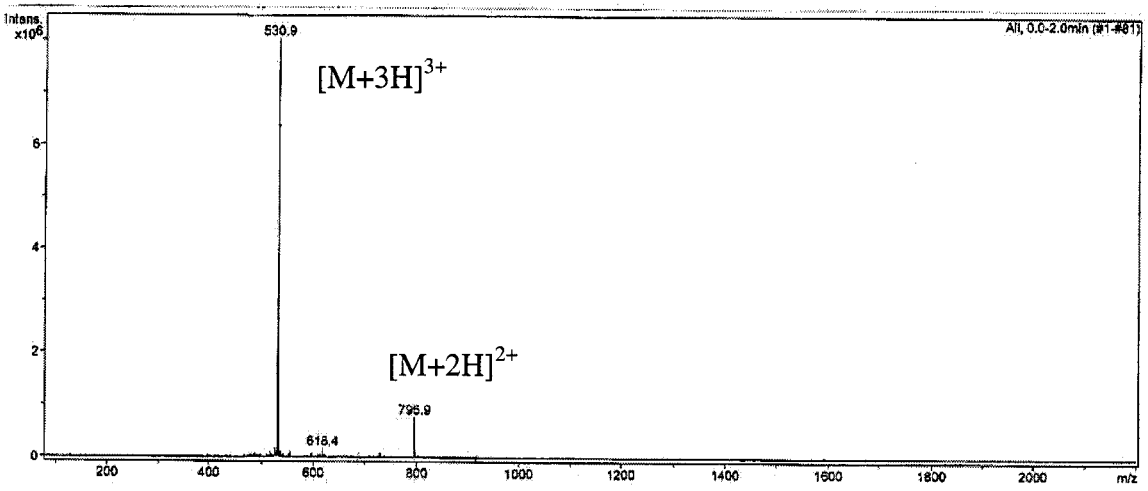

ESI-MS data of HPLC purified LK 310 peptide (unlabeled)
(calculated mol. wt. = 1590.2Da)

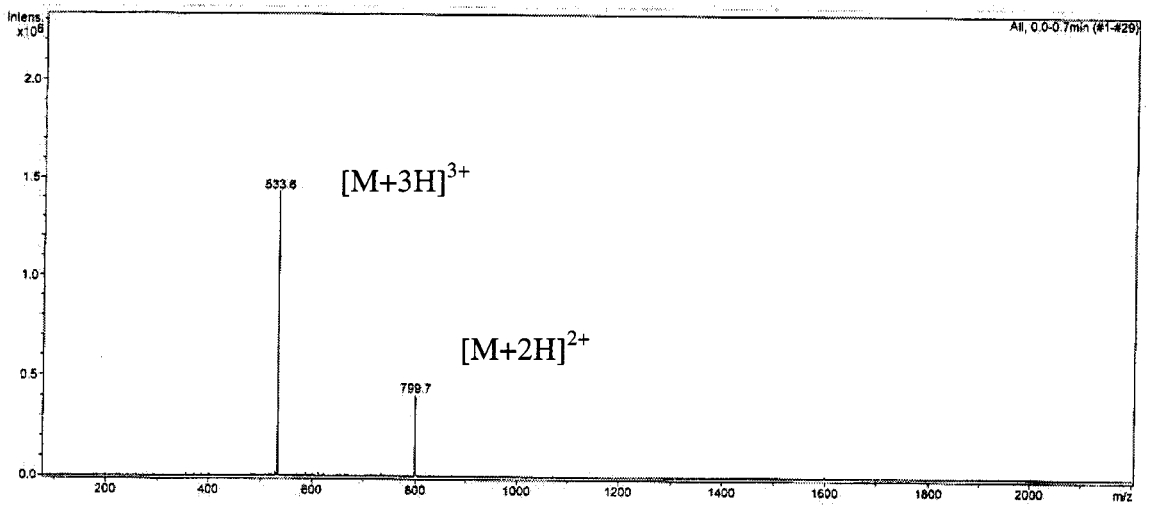

ESI-MS data of HPLC purified LK310Lab1 peptide (one deuterium labelled leucine)
(calculated mol. wt. = 1597.2Da)

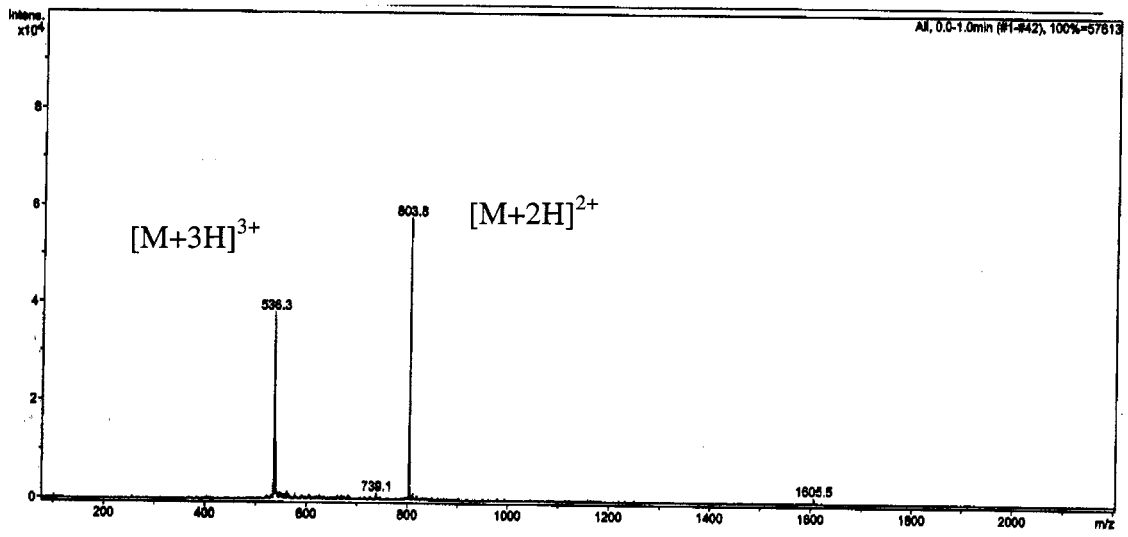

ESI-MS data of the LK310Lab2 peptide (2 deuterium labeled leucine)
(calculated mol. wt. = 1605.3Da)

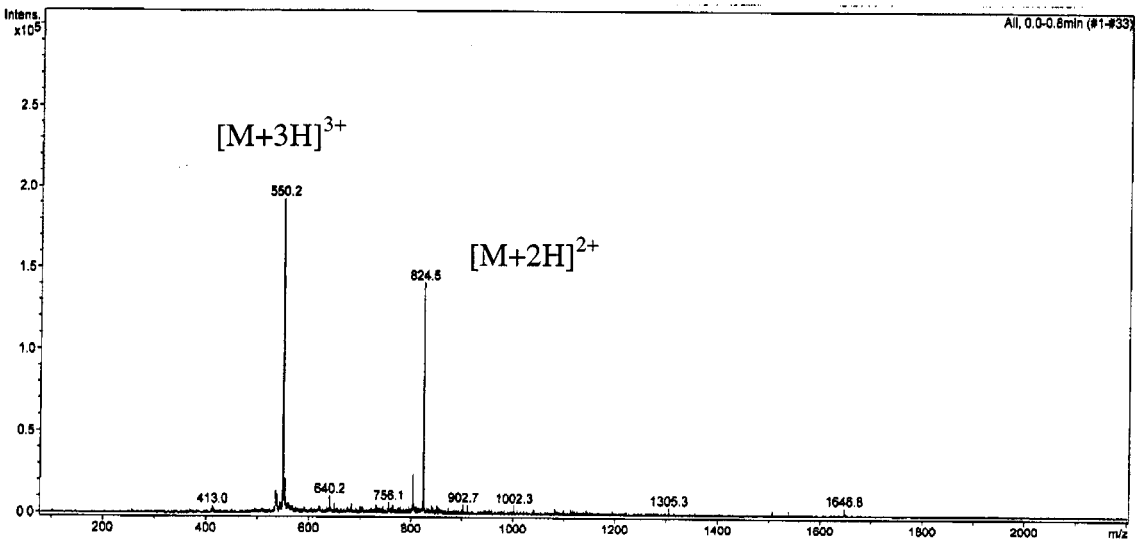

ESI-MS data of the LK310Lab8 peptide (8 deuterium labeled leucine)
(calculated mol. wt. = 1646.5Da)

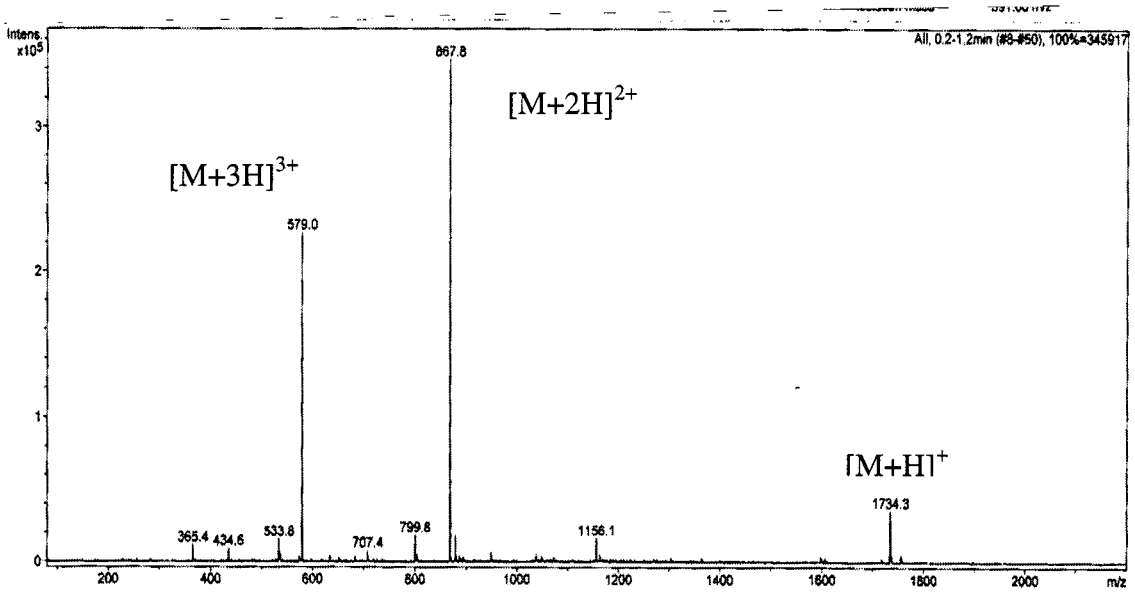

ESI-MS data of the LK α peptide
(calculated mol. wt. = 1733.4Da)

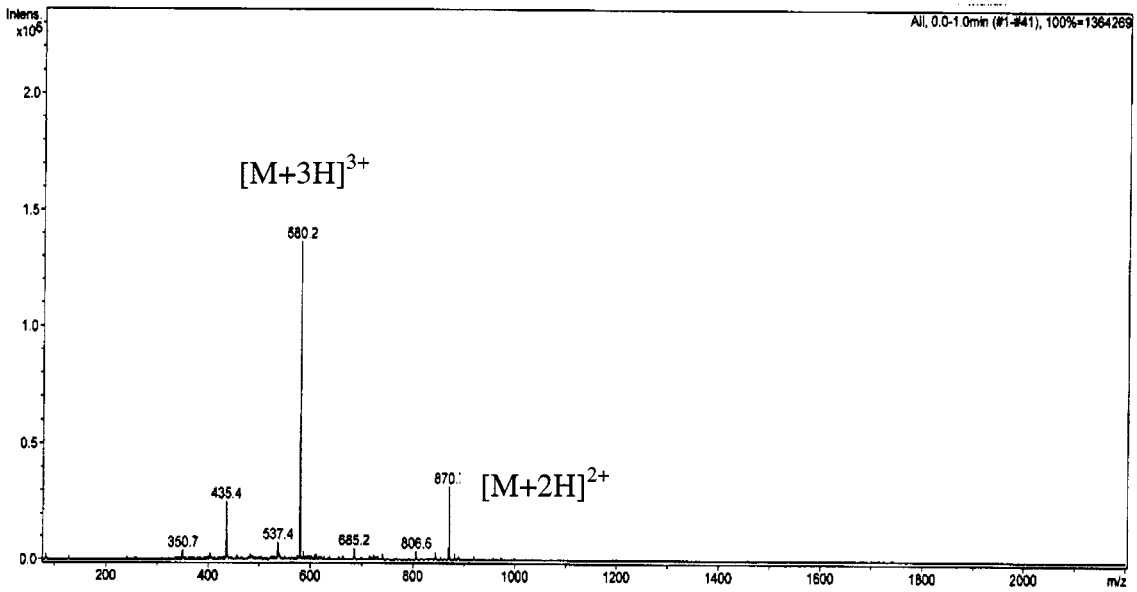

ESI-MS data of the LKα peptide (one deuterium labelled leucine)
(calculated mol. wt. = 1740.4Da)

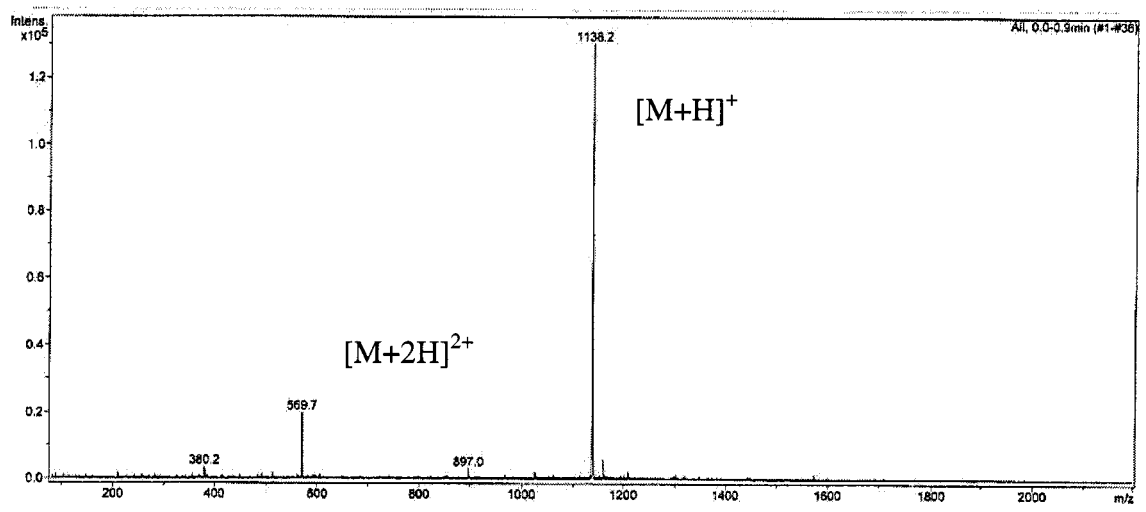

ESI-MS data of the LK β peptide (9mer)
(calculated mol. wt. = 1137.5Da)

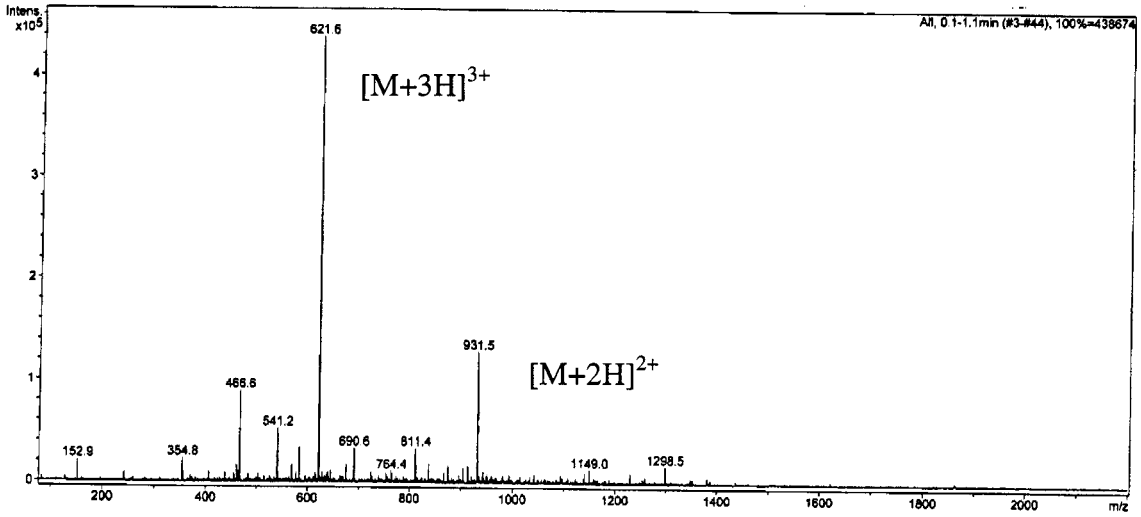

ESI-MS data of the LK β peptide (15mer)
(calculated mol. wt. = 1861.5Da)

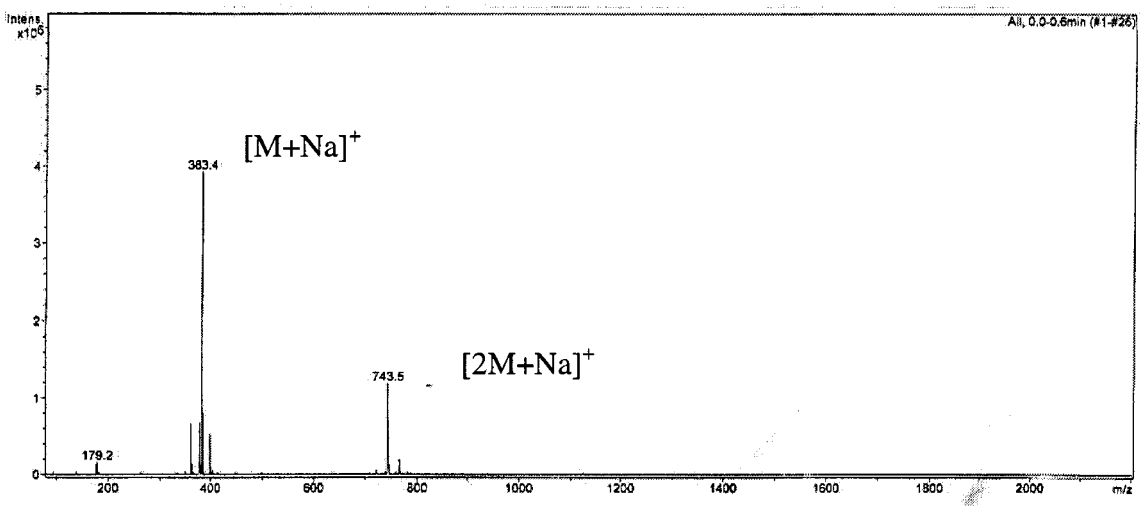

ESI-MS data of the synthesized FMOC labeled deuterated-leucine
(Calculated mol. wt. = 360.4Da)

Vita

Newton Samuel obtained his Bachelor of Technology in Chemical Engineering from Anna University (Chennai, India) in May, 2000. In September, 2000, he joined University of Washington (Seattle, WA) to pursue his graduate studies in Chemical Engineering. He joined Prof. Castner's research group in December, 2000, to investigate the structure of adsorbed peptides on surfaces with high-resolution surface analytical tools. In August, 2005, he earned his Ph.D. degree in Chemical Engineering from University of Washington. He will be starting his career as a Postdoctoral researcher working for Ethicon, Inc.